Elucidation of Dysregulated Immune Profiles via Vaccine-Induced Transcriptomics

BY

YISHIN CHANG
B.S.E., Duke University, 2011
M.S., University of California in San Francisco, 2013

THESIS

Submitted as partial fulfillment of the requirements
for the degree of Doctor of Philosophy in Bioengineering
in the Graduate College of the
University of Illinois at Chicago, 2024

Chicago, Illinois

Defense Committee:

David Perkins, Chair and Advisor
Patricia Finn, Medicine, Advisor
Yang Dai
Jalees Rehman, Pharmacology
Alex Leow
Beatriz Penalver Bernabe

Contribution of Authors

The authors who contributed to this dissertation are listed with their respective contributions under each work.

1. **Chang YS**, Turturice B, Schott C, Finn P, Perkins D. Immune network dysregulation precedes clinical diagnosis of asthma. Sci Rep. 2020 Jul 30;10(1):12784. doi: 10.1038/s41598-020-69494-x. PMID: 32732938; PMCID: PMC7393349.

   YSC, BT, CS, PWF, DLP designed study. YC analyzed data. YC, DLP, and PWF wrote the manuscript.

2. Vagts CL, **Chang YS**, Ascoli C, Lee JM, Huang K, Huang Y, Cherian RA, Sarup N, Warpecha SR, Edafetanure-Ibeh R, Amin MR, Sultana T, Ghassemie T, Sweiss NJ, Novak R, Perkins DL, Finn PW. Trimer IgG and Neutralizing Antibody Response to COVID-19 mRNA Vaccination in Individuals with Sarcoidosis. ERJ Open Research. *Under Revision.*

   Conception and study design, Vagts CL, Chang YS, Ascoli C, Perkins DL., and Finn PW. Participant recruitment, sample collection, and sample processing, Vagts CL, Chang YS, Lee JM, Huang K, Ascoli C, Huang Y, Sarup N, Warpecha SR, Cherian RA, R. Edafetanure-Ibeh, and Sweiss NJ. Experiments, Vagts CL, Chang YS, Lee JM, Sarup N., R Cherian, Amin M, T. Sultana, Ghassemi M, R. Novak. Analysis and interpretation, Vagts CL, Chang YS, Ascoli C, and Sweiss N. Drafting the manuscript for important intellectual content, Vagts CL, Chang YS, Huang K, Huang Y, Ascoli C, Sweiss NJ, and Finn PW. Vagts CLacts as the the guarantor of the paper.

3. To be submitted for publication as: **Chang YS**, Huang K, Lee JM, Vagts CL, Ascoli C, Huang Y, Cherian RA, Sarup N, Warpecha SR, Edafetanure-Ibeh R, Amin MR, Ghassemi M, Novak R, Lora CM, Perkins DL, Finn PW. Altered transcriptomic immune response of maintenance hemodialysis patients to the Covid-19 mRNA vaccine.

   Conception and study design, Chang YS, Huang K, Ascoli C, Vagts CL, Perkins DL, and Finn PW. Participant recruitment, sample collection, and sample processing, Chang YS, Huang K, Lee JM, Huang Y, Sarup N, Warpecha SR, Cherian RA, R. Edafetanure-Ibeh. Experiments, Chang YS, Huang K, Lee JM, Amin M, Ghassemi M, Novak R. Analysis and interpretation, Chang YS, Huang K, Lee JM, Vagts CL. Drafting the manuscript for important intellectual content, Chang YS, Huang K, Lee JM, Vagts CL, Ascoli C.

4. To be submitted for publication as: **Chang YS**, Lee JM, Huang K, Vagts CL, Ascoli C, Perkins DL, Finn PW. Altered transcriptomic immune response of maintenance hemodialysis patients to the Covid-19 mRNA vaccine.

   Conception and study design, Chang YS, Lee JM, Ascoli C, Vagts CL, Perkins DL, and Finn PW. Participant recruitment, sample collection, and sample processing, Chang YS, Lee JM, Huang K. Experiments, Chang YS, Lee JM, Amin M, Ghassemi M, Novak R. Analysis and interpretation, Chang YS, Lee JM, Huang K. Drafting the manuscript for important intellectual content, Chang YS, Lee JM, Vagts CL.

Table of Contents

List of Tables

List of Figures

List of Abbreviations

APC	Antigen presenting cell
BTM	Blood transcription module
CR	Cockroach extract
DC	Dendritic cell
DEG	Differentially expressed gene
DGE	Differential gene expression
DMR	Differentially methylated region
ESRD	End stage renal disease
HAT	Histone acetyltransferase
HD	Hemodialysis
HDAC	Histone deacetylase
ID50	50% inhibitory dilution
IFN	Interferon
Ig	Immunoglobulin
IL	Interleukin
LFC	Log fold change
LPS	Lipopolysaccharide
MHC	Major histocompatibility complex
nAb	Neutralizing antibody
NK	Natural killer (cell)
PBMC	Peripheral blood mononuclear cell
TF	Transcription factor
Th	Helper T (cell)
TLR	Toll-like receptor
Treg	Regulatory T cell
TT	Tetanus toxoid
WBC	White blood cell

Summary

Systems vaccinology involves the measurement of genome-wide expression (transcriptomics) in peripheral blood to identify early predictors of vaccine efficacy and to gain mechanistic insight into the biological actions of effective vaccines. Prediction of the degree and duration of immune protection conferred by vaccines is accomplished by identifying patterns of gene expression induced rapidly after vaccination that correlate with downstream antibody or T cell production. These methods were first applied to define molecular signatures of the yellow fever vaccine, YF-17D, and have most recently been applied to study the Covid-19 mRNA vaccines. These studies have demonstrated the value of systems vaccinology in elucidating the biological underpinnings of vaccine-induced immune recruitment and in predicting protective immune responses.

While traditional transcriptomic studies have utilized differential gene expression analyses to identify key genes that associate with immune phenotypes, there is growing evidence of the importance of studying the regulatory processes that govern gene expression. This is particularly relevant in the study of the immune system due to its vast, inter-connected system of activating and inhibitory loops that finely tune immunogenic versus tolerogenic balance. Gene networks can thus provide a more holistic characterization of the relationships within this system. In fact, regulatory alterations can define immune phenotypes, even in instances where key regulators do not exhibit differential gene expression levels

Due to the dependence of gene network construction on gene expression variance across samples, a natural extension of this approach is to stimulate and then characterize

the resultant networks to enable more sensitive measurement of regulatory interactions. We posited that the widespread gene expression perturbations induced by vaccination can elucidate patterns of immune dysregulation in disease. Thus, we investigated immune-mediated disease using two different systems vaccinology approaches; one in which we characterized vaccine-conferred immune protection and identified transcriptomic correlates of this protection, and one in which we investigated the broader structure and dynamics of gene dysregulation in immune-mediated disease using vaccination as an *in vivo* stimulus. We applied these approaches to publicly available RNA sequencing data in children at risk for developing asthma, and peripheral blood samples that we collected from healthy controls and immunocompromised patient populations at multiple time points surrounding Covid-19 mRNA vaccination. First, we showed non-allergen-specific immune network dysregulation in peripheral blood mononuclear cells (PBMCs) of children who later developed a clinical diagnosis of allergic asthma. Next, we characterized the BNT162b2 SARS-CoV-2 mRNA vaccine-conferred immune protection from Covid-19 in sarcoidosis and end stage renal disease (ESRD), two immunocompromised patient populations, compared to controls. Finally, we elucidated decreased coupling between immune system components in ESRD, and identified dysregulated blood transcription modules and genes that underlie these altered relationships.

1. Background

High-throughput sequencing technologies have created enormous potential for the characterization of biological processes using systems biological approaches. While traditional biological investigation isolates a given component of a biological system such as a gene, a protein, or a cell and study it in isolation, high throughput data allow us to study the structure and dynamics of the entire system (Kitano 2002). Systems biology thus capitalizes on the -omics technologies including genomics to identify global differences of genetic polymorphisms, transcriptomics to characterize genome-wide expression, and epigenomics to profile genome-wide methylation, DNA-protein interactions, and chromatin accessibility. These approaches gained traction in the early 2000s using transcriptomics and proteomics to identify diagnostic and prognostic biomarkers in cancer (Quackenbush 2006). Since then, systems biology has been applied to study of the immune system to characterize the mechanisms of innate and adaptive immunity (Aderem and Hood 2001), and the pathophysiology of immune-mediated diseases such as systemic lupus erythematosus, multiple sclerosis (Chaussabel et al. 2008), and asthma (Bunyavanich and Schadt 2015).

Systems vaccinology includes the application of transcriptomics in peripheral blood to identify early predictors of vaccine efficacy and to gain biological insights into the mechanisms of action of effective vaccines. While systems biological investigation of cancer profiles gene expression of the cancer cells themselves for diagnosis and prognosis, systems vaccinology profiles gene expression of peripheral blood. This enables the investigation of many immune cell lineages, including recent emigrants of peripheral vaccination sites (Pulendran, Li, and Nakaya

2010). Furthermore, immune cells are highly sensitive to perturbation, with vaccination leading to differential expression of thousands of genes in circulating immune cells (Querec et al. 2009).

Prediction of the degree and duration of immune protection conferred by vaccines is accomplished by identifying patterns of gene expression induced rapidly after vaccination that correlate with downstream antibody or T cell production. This may be useful for vaccine development, enabling quick iteration through different formulations to identify those that will induce the most protective immune response. Pulendran et al. (Pulendran, Li, and Nakaya 2010) envisioned the development of a vaccine chip to facilitate screening of vaccines to predict different facets of immunogenicity such as induction of long-lived plasma cells that produce highly specific antibodies, or polyfunctional T cells that produce multiple cytokines. This could be particularly relevant to predict immunogenicity of vaccines for various immunocompromised patient populations that demonstrate impairments of selective facets of the immune system. This is additionally valuable for identifying populations who may benefit from altered vaccine dosing, formulations, or adjuvants.

The first applications of systems vaccinology identified early molecular signatures induced by the yellow fever vaccine YF-17D (Gaucher et al. 2008; Querec et al. 2009). YF-17D, a live attenuated vaccine, confers seroconversion in more than 90% of vaccinees (Gotuzzo, Yactayo, and Córdova 2013) with duration of protection lasting as long as 40 years in 80% of vaccinees (Monath et al. 2002), making it one of the most successful vaccines ever developed. It was thus of interest to characterize the immunological mechanisms contributing to this high efficacy. In response to vaccination, peripheral blood mononuclear cells (PBMCs) produced a gene expression signature of innate sensing of viruses and antiviral immunity (Querec et al. 2009). This

signature was distinct from one that was predictive of the magnitude of CD8+ T cell responses, which included genes involved in the integrated stress response pathway. The gene signature predictive of antibody response included TNFRSF17a, a receptor for the B cell growth factor BAFF known to play a key role in B cell differentiation. This demonstrates the potential utility of these different signatures for predicting various facets of immune protection and consequently for vaccine design.

Systems vaccinology has recently been applied to study the COVID-19 mRNA-based vaccines, BNT162b2 and mRNA-1273, which were rapidly developed and disseminated in response to the COVID-19 pandemic. These vaccines have proven efficacious, with initial reports showing 95% and 94.1% reduction of COVID-19 disease in recipients (Baden et al. 2021; Polack et al. 2020). Bulk RNA sequencing of whole blood from healthy vaccinees demonstrated that both doses of the BNT162b2 stimulated antiviral and interferon responses one day after each dose, but the second dose additionally led to upregulation of dendritic cell activation, Toll-like receptor signaling, monocyte, and neutrophil modules (Arunachalam et al. 2021). Using single-cell RNA sequencing, Arunachalam et al. further identified a cluster of myeloid cells (monocytes and dendritic cells) that was uniquely induced in response to mRNA vaccination as compared to natural infection. They demonstrated that IFN gamma induced expression of this cluster and suggested a role of increased chromatin accessibility at interferon-stimulated genes. This demonstrates the power of systems vaccinology approaches to elucidate the mechanistic underpinnings of vaccine-induced immune recruitment.

While traditional transcriptomic studies have utilized differential gene expression analyses to identify key genes that associate with immune phenotypes, there is growing evidence

of the importance of studying the regulatory processes that govern these phenotypes (Weighill et al. 2021). This can be accomplished through the construction of gene networks, which represent the relationships between genes rather than the state of individual genes themselves. This is particularly relevant in the study of the immune system, with its vastly complex, inter-connected system of feedback and feed-forward loops between various subsets of innate immune cells, antigen presenting cells, T cells, and B cells (Rahman et al. 2018). To add further complexity, evidence suggests that immune cells may not differentiate into a limited number of discrete cell phenotypes, but rather a continuum of cell fates (Eizenberg-Magar et al. 2017). As the immunogenic versus tolerogenic response of the immune system depends on a complex interplay of these regulatory loops, gene networks can provide a more holistic characterization of the relationships within this system. In fact, regulatory alterations can define immune phenotypes, even in instances where key regulators do not exhibit differential gene expression levels (Ettou et al. 2020; Carnesecchi et al. 2020; Mikhaylova et al. 2013a). For example, a prior study in a murine model of asthma found minimal gene expression differences in dendritic cells from asthma-at-risk neonates compared to control mice, despite the presence of extensive genome-wide methylation differences. Substantial differential gene expression became evident only upon allergen sensitization, primarily among transcripts that showed epigenetic alterations at birth (Mikhaylova et al. 2013a).

Computational methods have been developed to capture regulatory relationships of genes and transcription factors (TFs). PANDA (Passing Messages between Networks for Data assimilation) is an algorithm for gene regulatory network construction that integrates information from multiple types of data (Glass et al. 2013). The three inputs to this algorithm are

(1) an initial transcription factor (TF)–gene adjacency matrix with edge weights calculated based upon sequence motif data, (2) a protein–protein interaction matrix based upon physical interactions between proteins, and (3) a gene expression adjacency matrix (Glass et al. 2013). These networks are iteratively updated using a message-passing algorithm, based upon the assumptions that (1) two genes that are co-expressed are more likely to be co-regulated by a similar set of TFs, and (2) two TFs that physically interact are more likely to co-regulate the expression of their target genes. PANDA has been shown to accurately predict TF binding using chromatin immunoprecipitation sequencing (ChIP-seq) and has been used to investigate gene regulatory relationships in several disease contexts, including asthma (Qiu et al. 2018), ovarian cancer (Glass et al. 2015), and colorectal cancer (Vargas, Quackenbush, and Glass 2016). Using PANDA, Qiu et al. (Qiu et al. 2018) constructed gene regulatory networks in asthma that differentiated treatment response of children to inhaled corticosteroids. They further identified and validated multiple TFs influencing differential response. Sonawana et al. (Sonawane et al. 2017)constructed gene regulatory networks for 38 different tissues and identified tissue-specific targeting patterns that were largely independent of TF expression.

Due the reliance of gene network construction on variance of gene expression, it seems natural to perturb the network to enable more sensitive measurement of regulatory interactions. We posit that the widespread gene expression perturbations induced by vaccination can elucidate patterns of immune dysregulation in disease. We further posit that this vaccine-induced network perturbation may enable the direct construction of single-subject gene networks through transcriptomic measurements of a given subject across multiple time points surrounding vaccination. Thus, this thesis applies systems vaccinology and gene network methods to (1)

characterize immune dysregulation that predisposes towards the allergic phenotype of asthma, (2) determine level of immune protection conferred by Covid-19 vaccination in two conditions of immunocompromise, sarcoidosis and end stage renal disease, (3) identify transcriptomic predictors of immune protection after Covid-19 vaccination in end stage renal disease (ESRD), and (4) characterize underlying immune dysregulation in ESRD utilizing the BNT162b2 mRNA COVID-19 vaccine as a stimulus.

2. Immune network dysregulation precedes clinical diagnosis of asthma

Previously published as: **Chang YS**, Turturice B, Schott C, Finn P, Perkins D. Immune network dysregulation precedes clinical diagnosis of asthma. Sci Rep. 2020 Jul 30;10(1):12784. doi: 10.1038/s41598-020-69494-x. PMID: 32732938; PMCID: PMC7393349.

2.1. Introduction

Childhood asthma is a disease of high prevalence (Akinbami, Simon, and Rossen 2016; Asher et al. 2006) that eludes early diagnosis (Ducharme, Tse, and Chauhan 2014). Diagnosis in young children is challenging due to the lack of specificity in the early clinical presentation of atopy and wheeze. While nearly half of the population will experience at least one wheezing episode in early childhood, most individuals will not go on to develop asthma (Ducharme, Tse, and Chauhan 2014; Martinez et al. 1995). Spirometry, which is the gold standard for asthma diagnosis, is typically not utilized in children under the age of 6. It is thus important to characterize early immune states that predispose toward clinical diagnosis of asthma in order to facilitate identification of individuals that are poised to develop disease.

The prototypic immune alteration in allergic asthma is that of dominant T-helper 2 cell (Th2) activation without adequate counter-regulation by T-helper 1 (Th1) and regulatory (Treg) cells (Barnes 2008). The process of allergic sensitization involves differentiation of these effector T-cell populations and re-shaping of their cytokine profiles (Smale and Fisher 2002). Less is known regarding the differential basal immune states that predispose towards allergic sensitization and disease development, “asthmatic poise.” Our laboratory has previously reported altered Th2 cytokine elaboration in response to common aeroallergens in the cord blood mononuclear cells of neonates with differing *in utero* microbial exposures (Turturice et al. 2017). These differential immune signatures can be probed as early as birth.

Genome-wide association studies (GWAS) have identified genetic polymorphisms associated with asthma and other atopic phenotypes, but, to date, explain only a small percentage of disease heritability (Ducharme, Tse, and Chauhan 2014). Explanations for the "missing heritability" include risk from copy number variation, gene-gene interactions, and gene-environment interactions which are not generally assessed in GWAS (Barnes 2008). Findings of epigenetic alterations in asthma suggest a strong mediatory effect of epigenetic modifications to disease susceptibility (Ducharme, Tse, and Chauhan 2014). For example, the ratio of histone deacetylase (HDAC) to histone acetylase (HAT) is known to be perturbed by environmental agents such as tobacco smoke (Smale and Fisher 2002), and to correlate with asthmatic status and disease severity (Biswas and Lopez-Collazo 2009; Foster, Hargreaves, and Medzhitov 2007; Gunawardhana et al. 2014; Cosío et al. 2004; K. Ito et al. 2002; Su et al. 2009). The HDAC/HAT ratio has further been shown to influence the Th1/Th2 balance (Su et al. 2009; Gunawardhana et al. 2014; Cosío et al. 2004; K. Ito et al. 2002; Su et al. 2008). Genome-wide methylation changes have been demonstrated in response to environmental agents (Breton et al. 2009), and were identified in a meta-analysis of children who develop asthma (Reese et al. 2018).

Investigation of genome-wide expression networks and gene regulatory networks prior to the development of asthma may provide clues of altered gene-gene interactions and epigenetic effects that underlie allergic predisposition. In a prior study, German cockroach extract (CR) stimulation of peripheral blood mononuclear cells (PBMCs) increased natural killer cell-type gene expression in 2-year-olds who developed aeroallergen sensitization by age 3 and clinical asthma by the age of 7 (Altman et al. 2018). These differentially expressed genes were only found in children with both CR sensitization and asthma by the age of 7. Similar to our

findings in a prior study, immune signatures correlated with home allergen levels (CR) (Turturice et al. 2017). We posit that these differential transcriptomic responses represent early pathways of sensitization to CR. In order to identify non-allergen-specific biomarkers of asthma and to characterize underlying immune states of asthmatic predisposition, in this study we analyze the tetanus toxoid (TT) -stimulated PBMCs from the same study cohort using a network-centric approach. TT stimulation elicits an unbiased and broad immune recall response, since all the children received tetanus vaccination in infancy. It therefore provides a useful immune perturbation, allowing for characterization of more subtly altered immune networks in asthmatic poise prior to clinically diagnosable disease. We elucidate differences of gene expression networks and gene regulatory networks, and infer epigenetic changes, in children at the age of 2 who develop asthma by age 7 compared to those who do not.

2.2. Methods

2.2.1. Data

Gene expression data was downloaded from the Gene Expression Omnibus database (GSE96783), and consisted of RNAseq data from children enrolled in the Urban Environment and Childhood Asthma (URECA) study, in which subjects have parental history of allergic disease and live in low-income urban areas (Gern et al. 2009; Altman et al. 2018). In this prior study, RNA sequencing was performed on peripheral blood mononuclear cells (PBMCs) from the children at the age of 2, incubated with either German cockroach extract (CR) or dust mite extracts, tetanus toxoid (TT), or media alone (no stimulation). For this study, we utilize RNAseq data from the CR-stimulated, TT-stimulated, and un-stimulated PBMCs, with in-depth analysis of gene expression networks and gene regulatory networks from TT-stimulated data. We compare TT-stimulated

networks of children at the age of 2 who developed aeroallergen sensitizations (including CR, dust mite, or both) by the age of 3 and clinical asthma by the age of 7 (asthma, n=19 with TT data) versus matched subjects who did not have any aeroallergen sensitizations or asthma at age 7 (control, n=30). Asthma at 7 years of age was defined by a pre-specified algorithm including use of asthma medications in the previous year, spirometry with reversibility, and bronchial hyperresponsiveness assessed using a methacholine challenge. The case group demonstrated a higher incidence of wheezing illnesses and symptoms of atopic dermatitis in the first year of life compared to controls. More details about these subjects and samples including demographic data, home allergen exposure, clinical data, IgE levels, case criteria, and PBMC stimulation and processing are available at the URECA study (Gern et al. 2009) and Altman et al. (Altman et al. 2018).

2.2.2. Differential gene expression with CR and TT stimulation

DESeq2 was used to obtain variance stabilized transformations of raw RNAseq count data (Love, Huber, and Anders 2014), and to perform differential expression analysis. Wald's test was used to identify genes that changed expression after CR stimulation (compared to no stimulation) and after TT stimulation, separately for controls (n=30) and asthma (n=19). Wald's test was also used to assess for interactions between group and stimulation. Significance of differential expression was assessed at $p<0.05$ with false discovery rate (FDR) correction.

2.2.3. Gene expression modules

For the 5667 genes that were determined to be perturbed by TT stimulation ($q<0.05$) in either asthma or controls, weighted gene correlation network analysis (WGCNA) (Langfelder and

Horvath 2008) was used to identify modules of highly correlated genes. WGCNA was performed with a soft thresholding power of 12 to produce scale-free network topology, a signed network and topology overlap matrix, the default minimum module size of 30 genes, and a cut height of 0.15. Gene ontology enrichment analysis was performed using the PANTHER classification system (Thomas et al. 2003; Mi et al. 2010) and MsigDB (Subramanian et al. 2005; Liberzon et al. 2015) to characterize the biological processes captured by each gene expression module. Downstream analyses of gene expression modules were performed on the modules which had significant functional enrichments.

Module eigengenes (first principal component) were calculated for each module for the control expression data with no stimulation and with TT stimulation, and for asthma expression data with no stimulation and with TT stimulation. Two-way ANOVAs with repeated measures were used to identify group x TT-stimulation interaction effects of each module eigengene.

To identify high centrality genes in the WGCNA modules, a protein-protein interaction network was constructed for each module based on the STRING database (http://string-db.org). Default parameters were used to construct the gene interaction networks, and the *igraph* package in R was used to calculate centrality for each gene in the network.

2.2.4. Network connectivity of gene expression modules

Pairwise connectivity of WGCNA modules was calculated using Pearson correlations of module eigengenes, separately for controls and asthma. Statistically significant associations were assessed at $p<0.05$ separately for each group with FDR correction.

2.2.5. Regulatory network construction using PANDA

To examine regulatory differences that might give rise to altered WGCNA module connectivity, PANDA (Passing Attributes between Networks for Data Assimilation) (Glass et al. 2013) was used to construct regulatory networks separately for the control and asthma group, and the no-stimulation and TT stimulation condition (four networks total). For each PANDA model, the transcriptomic matrix included the expression data from genes that were included in the WGCNA analysis, as well as expression of transcription factors with binding profiles in the JASPAR (Sandelin et al. 2004) database (n=338). In order to obtain an initial regulatory network, we used a motif-based transcription factor (TF) mapping to genes included in our transcriptomic matrix. TF position frequency matrices (PFMs) were obtained from JASPAR, and were mapped to the promoter regions of each gene from 1000 base pairs upstream of the transcriptional start site to 200 base pairs downstream. A motif match of 80% maximum accuracy was counted as a TF-target "hit," and the number of hits of each TF with each target was used an initial input regulatory network to PANDA. The initial protein-protein interaction network was derived from the STRING database interaction scores between all TFs used in our initial regulatory network.

2.2.6. Patterns of TF regulatory shifts

Regulatory strength (z scores outputted from PANDA in the regulatory network) of each TF was compared between asthma and controls. Due to the observation that most TFs demonstrated a combination of stronger and weaker target regulation depending upon target module membership, regulatory shift was calculated for each TF with each module. For example, the regulatory shift of GATA3 on CREM, one of its targets in the Th2 module, is simply $z_{asthma,GATA3}$

$_{\text{-> CREM}} - z_{\text{control,GATA3 -> CREM}}$. The regulatory shift of GATA3 on Th2, then, was calculated as the median shift of GATA3 across all of its gene targets in the Th2 module. TFs with at least one target in each module were then clustered using k-means based upon regulatory shift across WGCNA modules. A Euclidean distance metric was used, with number of clusters ranging from 2 to 10, each time calculating mean Silhouette score of the clustering result in order to assess clustering quality and to obtain the optimal number of TF clusters. The TF clusters obtained from this analysis are subsequently referred to as TF regulatory clusters.

2.2.7. Binding locations of TFs in differentially methylated regions

The proximity of binding locations between TFs (based on motif data) was assessed in differentially methylated regions (DMRs) identified from a separate meta-analysis. In this prior meta-analysis of cord blood mononuclear cells (CBMCs) from neonates who are eventually diagnosed with asthma, 35 DMRs were identified (Reese et al. 2018). Of these 35 DMRs, ten were in genes that changed expression with TT stimulation in our cohort. We assessed the similarity of binding locations in these 10 DMRs of TFs within the same regulatory cluster compared to TFs in different regulatory clusters. The specific methodology is described below.

For each of the 10 DMRs, binding locations of TFs on DMRs were identified in the same manner as described for the PANDA analysis above, with motif-based TF mapping. The similarity of binding location within versus between TF regulatory clusters was then assessed by computing a distance matrix of binding distances between every pair of TFs, and then calculating Silhouette score based upon TF regulatory cluster membership. This procedure was executed as described in the following steps:

1. The binding level of TF_i is represented as a vector of length n_{DMR}, where n_{DMR} = the # of bp in

the DMR, i = 1:m_{DMR}, m_{DMR} = # of TFs that bind on the DMR

2. For each location along the DMR with the binding motif for TF_i, a Gaussian distribution of 21-bp width and 5-bp standard deviation is placed.

3. The TF_i binding vector is normalized to sum to 1.

4. Distance between every TF that binds in the DMR is calculated as the absolute value of the difference between every pair of TF binding vectors. This yields a distance matrix of size m_{DMR} x n_{DMR}

5. In order to ensure that results are not biased by TFs that share the same binding motifs or exact same binding locations, TFs are eliminated such that there are no pairs with distance < 0.1. Specifically, in an iterative process, all pairs of TFs with distance < 0.1 are identified. Then one pair is randomly selected, and one of the TFs in the pair is completely eliminated from the distance matrix. This process is repeated until no pairs of TFs have distance < 0.1.

6. Silhouette score (SS) is computed for the distance matrix using TF regulatory cluster memberships.

7. Significance of SS is determined through a permutation test. Specifically, the TF regulatory clustering labels are permuted 10,000 times, each time calculating the corresponding S. P value is determined as: [# permutations with SS > actual SS]/10,000.

2.3. Results

2.3.1. Stimulated gene expression with tetanus toxoid (TT) and German cockroach extract (CR)

TT stimulation perturbed expression of thousands of genes, with 5051 genes perturbed

in the control group (n=30) and 3328 genes perturbed in the asthmatic group (n=19). The discrepancy between number of genes altered in controls vs asthma can be explained by difference in sample size. The genes perturbed in each group were largely overlapping, with 5667 genes total perturbed in at least one group. Specifically, out of 22426 genes with non-zero read counts for controls, 2539 (11%) were upregulated after TT stimulation and 2512 (11%) were downregulated. In the asthma group (n=19), out of 22424 genes with non-zero read counts, 1845 (8.2%) were upregulated after TT stimulation and 1483 (6.6%) were downregulated. These results are summarized in **Figure 1.**

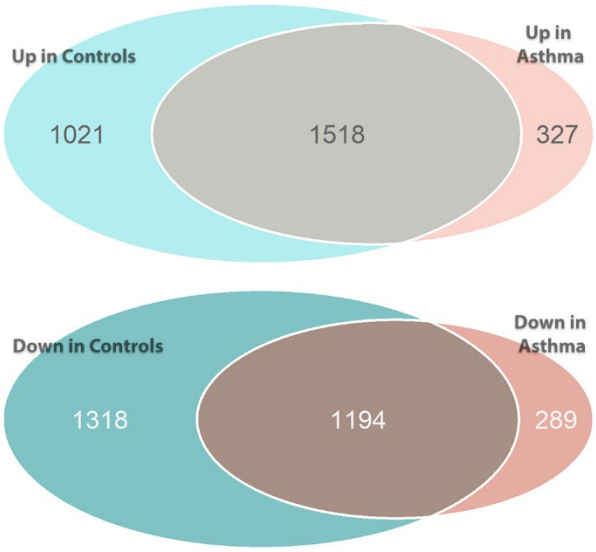

Figure 1. Stimulation of peripheral blood mononuclear cells (PBMCs) with tetanus toxoid (TT) perturbs expression of thousands of genes both in controls and asthma.
The number of genes that increase expression (upper venn diagram) and decrease expression (lower venn diagram) with TT stimulation are shown for the controls (n=30) and asthma (n=19). *DESeq2* was used to perform differential gene expression analysis with FDR-corrected $p<0.05$.

Compared to TT stimulation, a much smaller set of genes changed expression with CR stimulation; in the control group (n=30), 184 (0.8%) were upregulated after CR stimulation and 102 (0.5%) were downregulated. In the asthma group (n=19), 502 (2.2%) were upregulated after

CR stimulation and 304 (1.4%) were downregulated. As previously reported, there were extensive significant interaction effects of group (asthma vs controls) with CR stimulation on gene expression (Altman et al. 2018). However, there were no genes with significant interaction effects of group with TT stimulation of PBMCs at age 2.

The genes perturbed by CR stimulation were functionally enriched for biological pathways involved in the allergic response; negative regulation of regulatory T cell differentiation, positive regulation of humoral immune response mediated by circulating immunoglobulin, negative regulation of T-helper Type 1 immune response, T-helper 17 cell lineage commitment. While there was no significant differential gene expression in the children who developed asthma compared to controls in response to TT, this antigen perturbed expression of a much larger set of genes than CR. Our downstream analysis thus aims to characterize immune network changes that may precede the development of asthmatic phenotypes, using TT-elicited gene expression patterns.

2.3.2. Gene expression modules

WGCNA of the 5667 genes with perturbed expression after TT stimulation in either the control or asthma group yielded 18 gene expression modules. Using Panther gene list analysis, 13 of these modules demonstrate significant pathway enrichment, with a majority of these representing immune pathways. These include an IL1 response pathway, two MHC Class 1 (MHC1) presentation pathways, an immunoglobulin somatic recombination and diversification pathway, a Th2 pathway, two myeloid-mediated immune pathways, and two interferon response pathways. The labels by which we refer to these modules going forward, along with some of their significant GO annotations and the highest centrality genes in each module, are delineated in

Table 1. Subsequent analysis was performed only on the 13 modules demonstrating significant enrichments.

Table 1. WGCNA modules from tetanus toxoid-stimulated gene expression, with associated Gene Ontology (GO) annotations and high centrality genes

Module	GO annotations	Genes with high centrality in STRING PPI network
Mitos-1	Mitotic nuclear division sister chromatid segregation	CDC20, CDK2, BIRC5, PLK1, AURKA
IL1	Cellular response to IL-1 IL-1-mediated signaling Protein modification by small protein removal	HSP90AA1, BCL2, CASP3, UBE2N, CHUK
Mitos-2	DNA replication Chromosome segregation Cell cycle checkpoint	CDK1 , PRKCB, PCNA, TOP2A, BRCA1
Ig_rec	Somatic recombination of immunoglobulin genes involved in immune response Somatic diversification of immunoglobulins involved in immune response DNA-dependent DNA replication	PARP1, MCM5, MCM7, POLA2, H2AFX
MHCI-1	Antigen processing and presentation of exogenous peptide antigen via MHC class I Tumor necrosis factor-mediated signaling pathway Regulation of hematopoietic stem cell differentiation	ACTA2, SF3B3, UBC, TUBG1, BCL3
LPS	Response to LPS Response to molecule of bacterial origin Positive regulation of VEGF production	IL6, IL1B, LEP, SOCS3, IL1A
MHCI-2	Antigen processing and presentation of peptide antigen via MHC class I Positive regulation of NFkB signaling	STAT3, RUNX3, STAP2, AMER1, PIM2
Th2	Humoral immune response mediated by circulating immunoglobulin B cell mediated immunity Adaptive immune response	PDGFB , ITGB3, MMP1, NBEAL2, CCL13
Myel-1	Neutrophil activation involved in immune response Positive regulation of macrophage derived from foam cell differentiation Positive regulation of monocyte chemotaxis Receptor-mediated endocytosis	CAT, LPL, TLR4, HSD17B4, ACSL1

Ifn-1	Response to type 1 interferon Defense response to virus	OAS1, ISG15, OASL, MX2, IRF7
Metab	Lipid catabolic process	INSR, HSPA5, SDC2, PPARG, APOE
Myel-2	Myeloid cell activation involved in immune response Neutrophil degranulation Neutrophil activation	TSPO, RHOA, JUN, RAC1, ICAM1
Ifn-2	Defense response to virus Response to interferon-beta Regulation of interferon-alpha production	DDX58, IFIH1, HERC5, STAT1, IFIT1

As expected, all 13 modules demonstrated statistically significant effects of stimulation using two-way ANOVA with repeated measures ($p<0.01$), with all exhibiting increased eigengene expression except for Myel-1, Metab, and Myel-2, which showed decreased expression with TT stimulation (**Figure 2**). None of the modules demonstrated significant interaction effects of group (controls vs asthma) with TT stimulation ($p<0.05$).

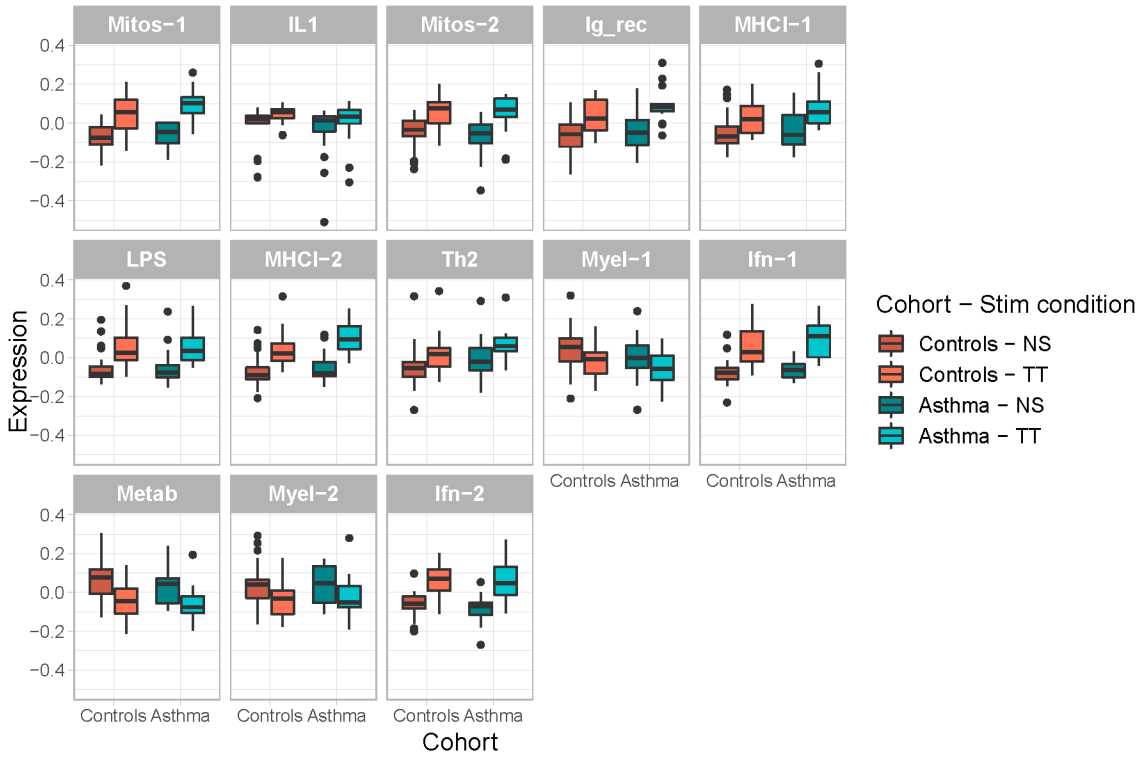

Figure 2. Module eigengenes change significantly with tetanus toxoid (TT) stimulation of peripheral blood mononuclear cells, but demonstrate no group effects.
Eigengene expression is displayed for each WGCNA module, separately for controls and asthma, with no stimulation (NS) and TT stimulation of PBMCs. Every module demonstrates a significant effect of stimulation ($p<0.01$), but none demonstrate a significant group x stimulation effect ($p<0.05$).

2.3.3. Network connectivity of gene expression modules

Both the control and asthma gene expression network demonstrate extensive co-regulation between WGCNA gene expression modules (**Figure 3**). The control and asthma networks demonstrate similar overall network structure (the majority of significant edges in each group are shared by both groups). However, there is extensive gain of negative co-regulation in the asthma network compared to the control network, and to a lesser degree, loss of positive co-regulation (**Figure 3; Figure 4**).

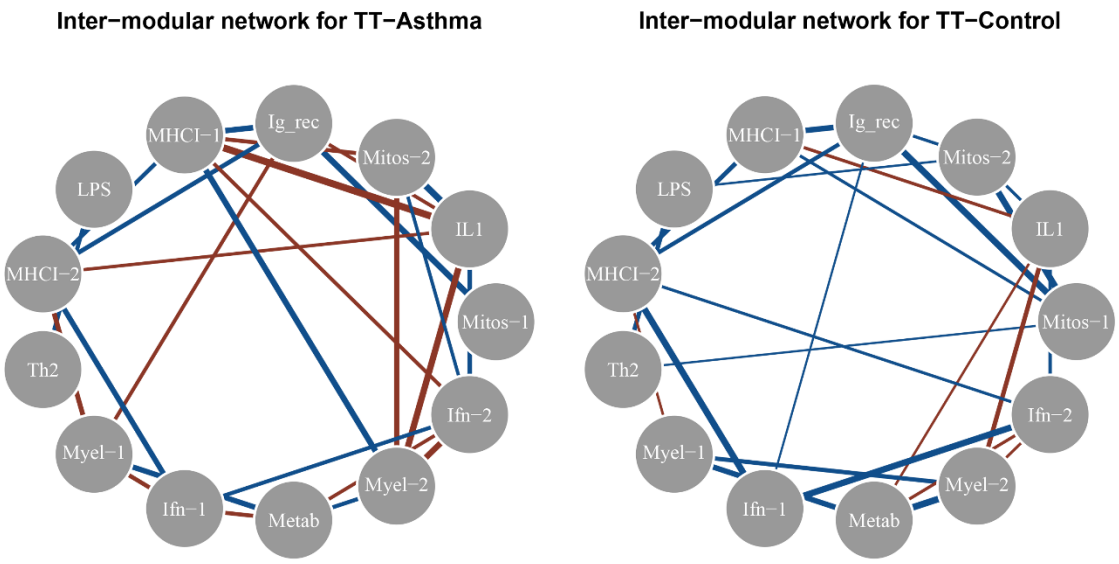

Figure 3. Gene module network differences in asthma are characterized primarily by aberrant negative co-regulation.

All significantly positively co-regulated modules (q<0.05, FDR corrected) are connected with blue edges, while negatively co-regulated modules are connected with red edges. Edge thickness corresponds to strength of correlation.

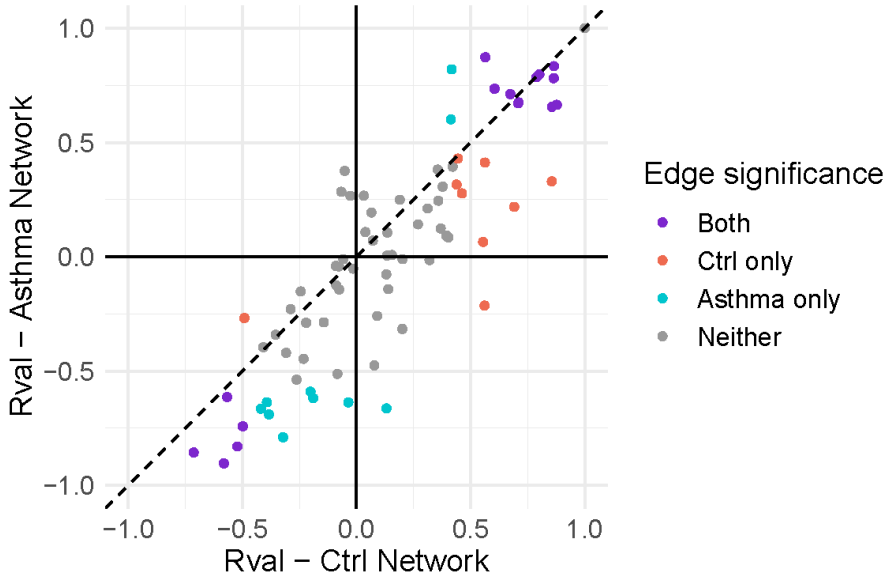

Figure 4. The asthma gene module network demonstrates several aberrant negatively co-regulated modules.

R values from Pearson correlations between the eigengenes of every pair of modules are displayed for the asthma network on the y axis, and control network on the x axis. Points are colored by statistical significance of the correlations, with FDR correction across all pairs of tested

modules. The solid line is y=x, representing the line of equal edge strengths between controls and asthma, and the dotted line is a linear regression with 95% confidence interval shading.

2.3.4. Regulatory Network Alterations

Extensive regulatory differences were found between the TT-stimulated asthma and control networks using PANDA, with the majority of transcription factors (TFs) demonstrating altered regulation after FDR correction (284 out of 338) (**Figure 5**). Of the 284 TFs with altered regulation, 135 show weakened regulation, and 149 show strengthened regulation. The magnitude and direction of regulatory shift not only varies by TF, but also varies for a given TF by the WGCNA module membership of the gene targets. Examples of this are shown in Figure 5 for several representative TFs - GATA3, T-bet, FOXP3, STAT1, STAT4, and STAT6. Two representative WGCNA modules are displayed for demonstrative purposes - MHCI_1, which demonstrated extensive differences of co-regulation in the expression network, and IL1, which demonstrated stronger negative co-regulation with MHCI_1 in the asthma network. GATA3 demonstrates stronger regulation of its targets in the MHCI_1 module in asthma, but weaker regulation of its targets in the IL1 module. FOXP3 and STAT6 demonstrate a similar pattern of altered target regulation, with FOXP3 demonstrating an even more amplified difference between regulation of its targets in these two modules, and STAT6 demonstrating a more subtle difference. In comparison, T-bet, STAT1, and STAT4 regulation of their targets do not appear to significantly differ between the MHCI_1 and IL1 modules (the points lie along the y=x line). This indicates that certain TFs exhibit simultaneous strengthened and weakened regulation of gene targets, and that the direction of regulatory shift depends systematically on target WGCNA module membership.

The two top TFs with the largest median regulatory shift across modules were KDM5B and ARID3A, which have been shown to be important regulators of the epigenome.

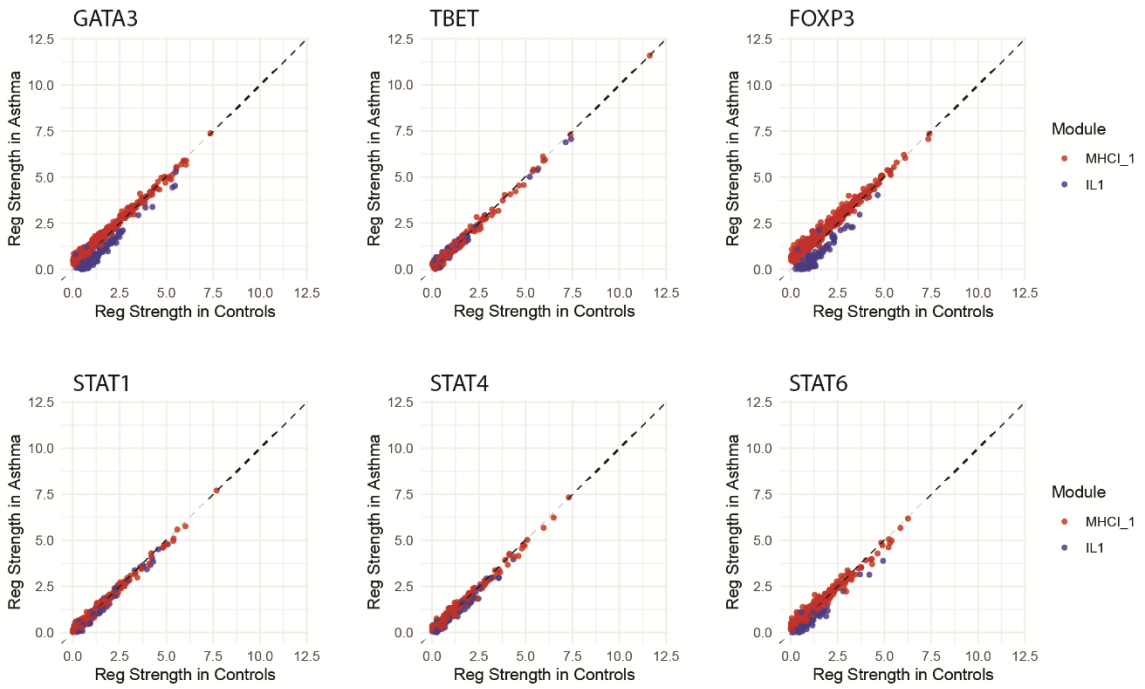

Figure 5. Asthma regulatory networks demonstrate extensive alterations, with both increased and decreased transcription factor (TF) regulation strength.
Regulatory strengths outputted from PANDA are displayed for several example TFs in two representative WGCNA modules (MHCI_1 and IL1). The y axis represents regulatory strength in the asthma network while the x axis represents regulatory strength in the control network. Each individual point represents the regulatory strength of the given TF on each of its gene targets in the representative modules. Points above and below the y=x line respectively indicate stronger regulation in asthma relative to controls, and controls relative to asthma.

2.3.5. Transcription factor clustering by patterns of regulatory shift

Due to the recognized role of epigenetics in asthma, we hypothesized that broad alterations of the epigenetic landscape might drive the differential transcriptomic and regulatory networks that control the predisposition to disease. TFs bind to regulatory regions of their respective gene targets to activate or repress transcription. Thus, TFs with proximal binding sites on their gene targets will likely be similarly altered by epigenetic alterations of genomic accessibility (i.e. DNA methylation) in these regulatory regions. The presence of broad alterations to the epigenetic landscape could therefore cause shared patterns of “regulatory shift” of TFs

that bind at similar locations.

A heatmap of median regulatory shift per TF with each WGCNA module reveals community structure of TFs, where communities of TFs demonstrate shared patterns of regulatory shift across WGCNA modules (**Figure 6**). For example, certain TFs show predominantly weaker regulation of targets in Ifn-2, Mitos-2, IL1, and Myel-1 in asthma compared to controls, but stronger regulation of targets in the remaining modules. In contrast, TFs labeled by the green bar on the y axis show an inverse pattern of dysregulation; these TFs show predominantly stronger regulation of targets in Ifn-2, Mitos-2, IL1, and Myel-1 in asthma compared to controls, but weaker regulation of targets in the remaining modules. Hierarchical clustering of TFs based on these median shifts per module yields an optimal cluster number of two TF groups based on the maximum silhouette score.

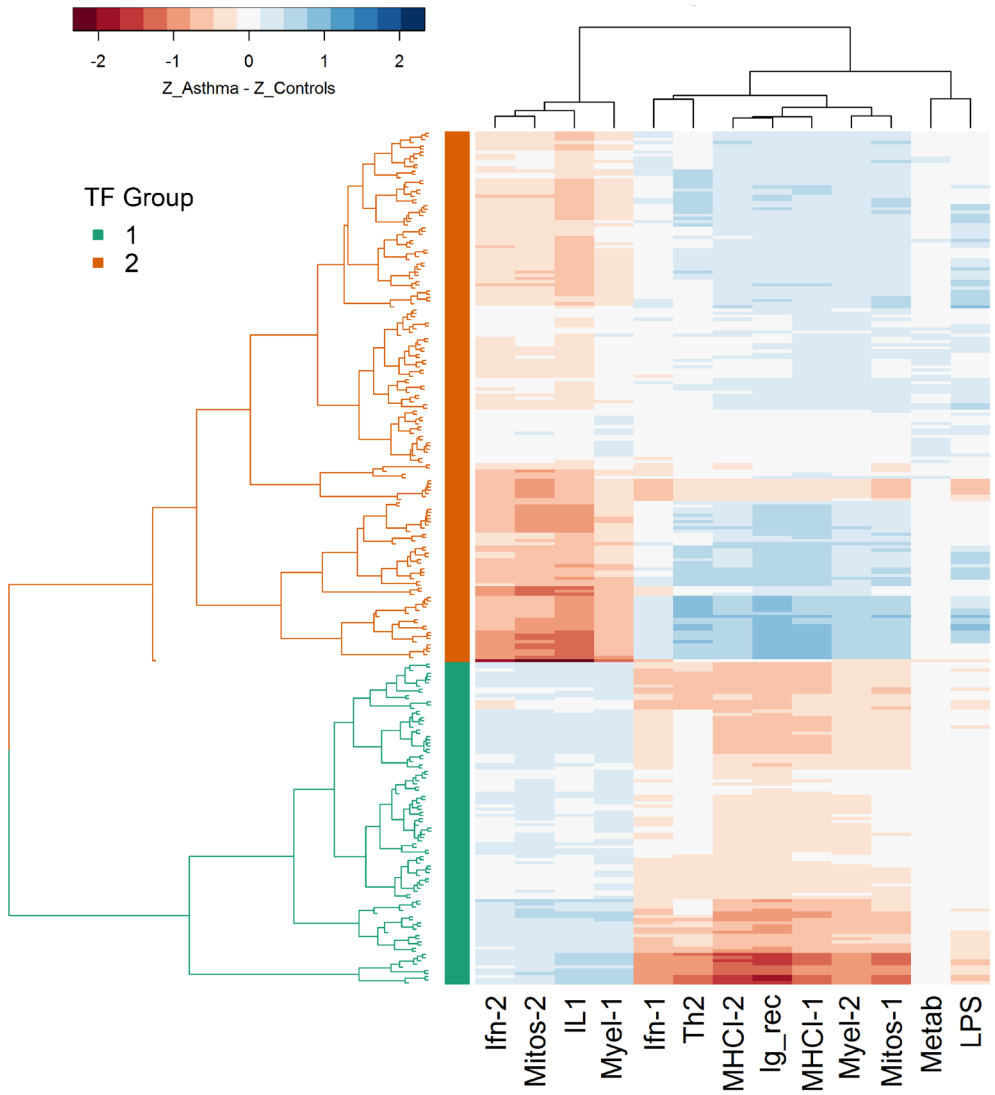

Figure 6. Transcription factors (TFs) cluster into groups based upon the pattern of their regulatory alteration across gene expression modules.

A heatmap of the median regulatory shift of targets within each gene expression module (for a given TF: median value of z_{Asthma}-$z_{Control}$ across targets within a module). The x axis represents different WGCNA modules, while TFs are represented on the y axis, with branches colored by TF communities from hierarchical clustering. Blue/positive values represent stronger regulatory control in asthma, while red/negative values represent strong regulatory control in controls.

2.3.6. Binding locations of transcription factor groups

TFs that cluster into the same communities based upon regulatory shift tend to have proximal binding locations to one another in DMRs (**Figure 7,8**). Binding locations of TFs with motifs in a differentially methylated region of TNFSF13B (encodes B-cell activating factor (Baff)) are shown to illustrate the proximal binding of TFs within the same communities (**Figure 7**). The TFs are separated based upon their regulatory community. TFs within the same community bind more closely to one another than TFs between regulatory communities. The similarity of binding locations within communities suggests that shared patterns of dysregulation may be driven by permissive or repressive epigenetic changes at the level of the target genes.

The mean SS from the binding location distance matrix using TF regulatory cluster memberships is displayed for all 10 DMRs (**Figure 8**). For the majority of DMRs, the mean SS is significantly higher ($p<0.001$) than the null distribution of silhouette scores (SS) generated from permutation of TF regulatory cluster labels. Thus, regulatory communities of TFs cluster based upon their binding distances within DMRs.

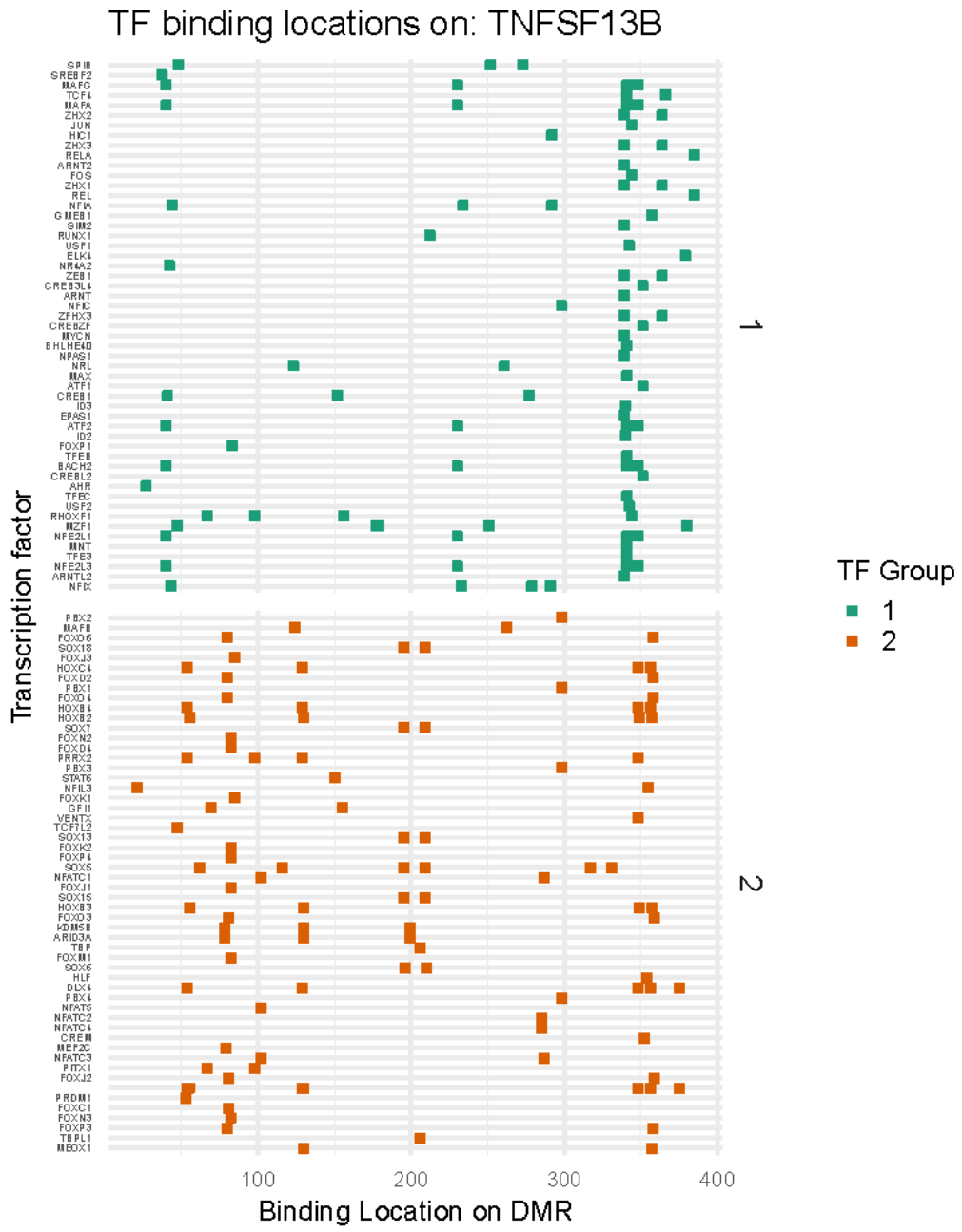

Figure 7. Transcription factors (TFs) within the same regulatory communities bind in similar locations on differentially methylated regions (DMRs).
Binding locations of TFs with binding motifs (based on 80% of maximum confidence) in a DMR in TNFSF13B. The TFs are separated based upon their regulatory cluster memberships as defined in Figure 5.

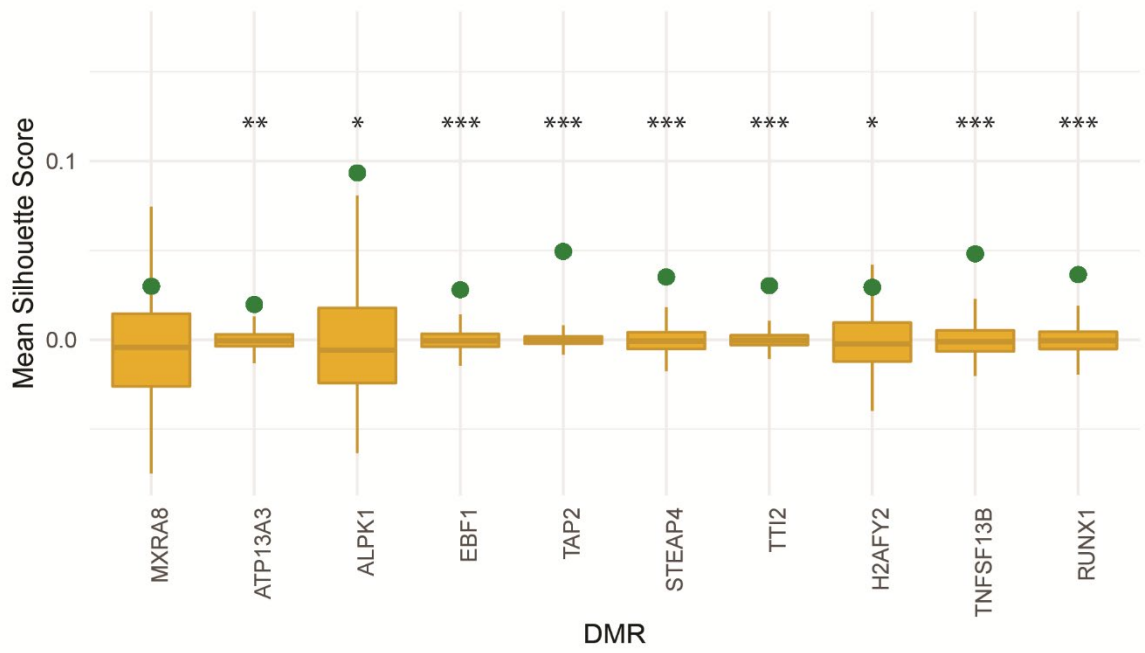

Figure 8. Regulatory communities of transcription factors (TFs) exhibit significant clustering based on binding distances within differentially methylated regions (DMRs).
The genes on the X axis represent all DMRs from the Reese et al. meta-analysis of CBMCs, which demonstrated perturbation of expression from tetanus toxoid (TT) stimulation. The green dot represents the mean silhouette score (SS) calculated from the binding location distance matrix with TF regulatory clusters. The gold points and density plots represent the null distribution of mean SS from each of 10,000 permutations of the regulatory cluster labels. Asterisks represent statistical significance *p<0.05, **p<0.01, ***p<0.001

2.4. Discussion

We characterize asthmatic poise by probing gene-gene interactions and inferring epigenetic alterations. Specifically, we identify significantly altered interactions in our gene expression networks. We also demonstrate that these altered expression networks can be explained by regulatory differences, and provide evidence that broad epigenetic alterations cause the downstream disruption of these networks. In summary, gene network investigation powered by associations of stimulated gene expression across subjects allows us to uncover

immune imbalances that precede clinical diagnosis of asthma.

The differential gene networks elucidated with tetanus toxoid (TT) stimulation suggest that broad immune imbalances prime allergic sensitization. Prior transcriptomic studies of childhood asthma have investigated subjects who already have a disease diagnosis, and have primarily investigated differential gene expression as opposed to differential gene interactions. Significant differential gene expression in response to German cockroach extract (CR), but not TT, was previously reported in this cohort (Altman et al. 2018). However, this was only found in children with both CR sensitization and asthma by the age of 7, and not in children without CR sensitization. We posit that the differential response to CR, which perturbs a much more limited set of genes (~800 for asthma and ~300 for controls, versus ~5000 for TT stimulation in both groups), represents an allergic response to CR. In contrast, TT elicits more widespread non-allergen-specific stimulation of immune responses in both groups, allowing us to uncover network states poised for allergic sensitization. Since allergic asthma can be triggered by diverse allergens depending on individual exposure, it is valuable to identify non-exposure-dependent differential immune responses (i.e. to TT) that characterize allergic predisposition.

While we expected to find regulatory network alterations, the unexpected findings here are the uncovered patterns of dysregulation. It is particularly interesting that a given TF can exhibit strengthened regulation of some targets in the asthma group compared to controls, but weakened regulation of other targets. Even more striking, the direction and magnitude of change varies systematically depending upon the WGCNA module membership of the target gene. This finding, combined with the demonstrated shared patterns of dysregulation amongst communities of TFs (**Figure 6**) and proximal binding locations of TFs with the same community,

support the idea that broad epigenetic alterations perturb regulatory and expression networks. The absence of statistically detectable differential gene expression, concurrent with regulatory network alterations, is consistent with previously indicated epigenetic mechanisms of asthmatic poise. A prior study in a murine model of asthma found minimal gene expression differences in dendritic cells from asthma-at-risk neonates compared to control mice, despite the presence of extensive genome-wide methylation differences (Mikhaylova et al. 2013b). Substantial differential gene expression became evident only upon allergen sensitization, primarily among transcripts that showed epigenetic alterations at birth. Taken together, these suggest a paradigm in which subtle but widespread changes to the epigenetic landscape poise the immune system for allergic sensitization. Subsequently, allergic sensitization leads to enhanced epigenetic modifications, differential gene expression and cytokine elaboration, and phenotypic disease manifestation.

This paradigm is further supported by the TFs that we found to demonstrate the most altered regulation across modules; ARID3A and KDM5B have both been implicated as important players in epigenetic control. ARID3A is required for hematopoietic stem cell differentiation and B cell development, and has been shown to suppress somatic cell reprogramming (Popowski et al. 2014). ARID3A also activates transcription of the immunoglobulin heavy chain (IgH) by altering chromatin accessibility to the IgH enhancer (Lin et al. 2007). KDM5B is a histone demethylase, a critical regulator of genome stability required for efficient DNA double-strand break repair, and has been shown to be enriched at DNA-damage sites after ionizing radiation and endonuclease treatment (X. Li et al. 2014). It represses expression of genes involved in immune cell proliferation and migration, and may cooperate with histone deacetylase in repression of gene expression

(Klein et al. 2014; Wu et al. 2018).

There is evidence of epigenetic differences in asthmatics, with genome-wide methylation studies demonstrating predominantly permissive methylation differences as early as birth (Reese et al. 2018). However, results of epigenetic studies have not established robust associations with downstream gene expression. These prior studies have focused on DNA methylation, and thus do not capture the full landscape of epigenetic alterations (Vercelli 2016). Studies investigating histone modifications have provided more mechanistic insight into epigenetic changes in asthma. The ratio of histone deacetylase to histone acetylase is lower in lung samples of asthmatics, correlates with disease severity, and corrects with treatment (Su et al. 2009; Gunawardhana et al. 2014; Cosío et al. 2004; K. Ito et al. 2002). Further, HDAC inhibition in *ex vivo* memory T cells results in strongly elevated Th2 cytokine production and reduced Th1 cytokine production during immune recall response (Su et al. 2008). Interestingly, this shift in Th2/Th1 cytokine responses is driven by elevation of the master Th2 regulator GATA3, without change in the expression level of the corresponding Th1 regulator T-bet. These findings are consistent with our finding of strong regulatory differences in GATA3 but not T-bet as a function of gene module membership (**Figure 4**). GATA3 interacts with HDACs and methyltransferases to produce suppressive changes at Th1 loci, and with HAT to create permissive changes at Th2 loci (Zeng 2013; Hosokawa et al. 2013; Chang and Aune 2007). It binds to its own regulatory elements, positively regulating its own expression (Ouyang et al. 2000). These findings further expand upon epigenetic theories of early atopic predisposition, in which positive feedback mechanisms progressively destabilize immune balance, ultimately producing measurable differential gene expression and asthmatic phenotypes.

This study is limited by lack of epigenetic data to validate the inferred alterations, as well as by the pooled cell populations, which make it challenging to identify key cellular players in the altered gene interactions. Future investigation will benefit from simultaneous collection of transcriptomic and epigenomic data from separated cell populations or single cell analyses. Collection of epigenomic data using a method such as Assay for Transposase-Accessible Chromatin using sequencing (ATAC-Seq) will facilitate validation and complementary characterization of regulatory relationships. Additionally, it may allow for diagnosis or prognosis of individual subjects using epigenomic fingerprints of altered accessibility at regulatory regions of DNA. Our present transcriptomic network analyses allow us to identify group-level network differences. However, it would be challenging to perform individual diagnosis based upon this framework, since construction of subject-level networks would require several datasets per subject, or would rely on unstable statistical inference methods. It will also be of interest in the future to determine whether altered expression and regulatory networks can be discerned even earlier in life (e.g. by studying cord blood mononuclear cells (CBMCs)), as epigenetic influences begin *in utero*.

In conclusion, we have described a novel framework to characterize transcriptomic network alterations, shown that gene network dysregulation can be detected in atopically predisposed individuals long before clinical asthma diagnosis, and provided evidence that these atopically primed networks are a result of widespread alterations of the epigenetic landscape. Our approach indicates the potential to identify development of allergic disease including asthma prior to clinical diagnosis.

3. Trimer IgG and Neutralizing Antibody Response to COVID-19 mRNA Vaccination in Individuals with Sarcoidosis

Published as: Vagts CL, Chang YS, Ascoli C, Lee JM, Huang K, Huang Y, Cherian RA, Sarup N, Warpecha SR, Edafetanure-Ibeh R, Amin MR, Sultana T, Ghassemie T, Sweiss NJ, Novak R, Perkins DL, Finn PW. Trimer IgG and Neutralizing Antibody Response to COVID-19 mRNA Vaccination in Individuals with Sarcoidosis. ERJ Open Research 2022 Jan; 9(1): 00025-2022.

3.1. Introduction

Since the start of the COVID-19 pandemic, the development of effective treatments to diminish COVID-19 disease severity has been an international priority. Vaccines were developed at record speed and offer a life changing opportunity for disease mitigation and prevention. Initial studies demonstrated the mRNA-based COVID-19 vaccines, BNT162b2 and mRNA-1273, were efficacious in preventing up to 95% and 94.1% of COVID-19 disease in recipients, respectively (Baden et al. 2021; Polack et al. 2020). However, vaccine response in vulnerable populations remains ill defined.

Sarcoidosis is a multisystem disease of unknown etiology characterized by granulomatous inflammation and subsequent organ dysfunction. This inflammation is believed to stem from maladaptive immune responses, resulting from chronic immune stimulation with subsequent risk of lymphocyte anergy, exhaustion, and depletion (Ascoli et al. 2018; Sweiss et al. 2010; Hawkins et al. 2017). Data supports sarcoidosis subjects as having increased risk of infection (Dureault et al. 2017; Ungprasert, Crowson, and Matteson 2017), though the overall risk of SARS-CoV-2 is unclear (Baughman et al. 2020). Beyond immune susceptibility conferred by underlying disease pathology, nearly one-fourth of all sarcoidosis patients require treatment with immunosuppressive agents which further contributes to infectious risk (Baughman et al. 2016). Primary infection prevention with vaccination in this population is therefore of great

importance.

Literature regarding how individuals with sarcoidosis respond to vaccines is limited and indicate varying responses. A study of tetanus vaccination in sarcoidosis patients found 50% had an insufficient increase in antibody titers regardless of sarcoid disease state, stage, or duration, and independent of treatment (Seyhan et al. 2012). A separate study of a 3-dose series of the hepatitis B vaccine found that none of the 16 sarcoidosis subjects had detectable antibody levels at one month follow up (Mert et al. 2000). In contrast, a study of the 2008-2009 trivalent influenza vaccine showed sarcoidosis and control subjects had a comparable serological response (Tavana et al. 2012). In addition, existing literature explores quantitative assessment of antibody response through measurement of immunoglobulin titers however these titers may not assure conferred protective immunity. While developed antibodies may target any viral epitope, neutralizing antibodies (nAb) bind to the virus in such a way that it inhibits cell entry and/or viral replication therefore blocking infection from propagating (Payne and Ebook Central Academic 2017). Post vaccination nAb assays provide insight into the functional protection allocated by the vaccine and to our knowledge there are no current studies evaluating nAb in sarcoidosis.

In regards to immunosuppression, data assessing the effect of immunosuppressive medication on vaccine efficacy in sarcoidosis is limited and recommendations are extrapolated from studies of other immune related disoders. Use of various immunosuppressive medications is associated with decreased antibody response to multiple types of vaccinations, including the mRNA COVID vaccines (Friedman, Curtis, and Winthrop 2021; Mahil et al. 2021; Ruddy et al. 2021; Subesinghe et al. 2018). Regardless of a potential insufficient response, vaccination is strongly recommended in sarcoidosis to protect against various community acquired infections to include

COVID-19 (Manansala et al. 2021; Syed et al. 2020).

We postulate that subjects with sarcoidosis will have a deficient immune response to COVID-19 vaccination. This study aims to characterize the antibody response to COVID-19 vaccination in subjects with and without sarcoidosis through quantitative assessment of binding antibodies and correlation to functional assessment of nAb. Our findings may direct vaccination guidelines, inform the need for further booster vaccines, and extrapolate further information about the immune dysregulation underlying sarcoidosis pathology.

3.2. Methods

3.2.1. Study population and sample acquisition

Study approval was obtained through the University of Illinois at Chicago (UIC) IRB Ethics Review Committee, Approval #2018-1038.

Subjects with biopsy-proven sarcoidosis, diagnosed in accordance with ATS/ERS/WASOG criteria (Hunninghake et al. 1999), and who were undergoing vaccination with the BNT162b2 mRNA COVID-19 vaccination were recruited. All subjects were older than 18 years of age and receive their sarcoidosis care in the Bernie Mac Sarcoidosis Translational Advanced Research (STAR) Center at UIC. Demographic and clinical data was extracted from the electronic medical record and included sex, race, age, body mass index (BMI), sarcoidosis organ involvement, as well as treatment with immunosuppressive therapy (systemic steroids and/or disease modifying anti-sarcoid drugs i.e. DMASDs). Peripheral lymphocyte counts in the preceding 6 month were also recorded. Age and gender matched self-reported-immunocompetent control subjects consisted of University of Illinois Hospital employees who were undergoing vaccination at UIC.

Demographic and clinical data were collected using a questionnaire and included race, sex, age, height and weight, medication use, and existing medical problems. Any subject who self-reported a personal history of COVID-19 infection was excluded.

Blood samples were collected at baseline (just prior to 1st vaccine dose, timepoint V1D0), 4 weeks (i.e. 7 days after the booster dose, timepoint V2D7), and 6 months after the 1st vaccine dose (time point M6). Serum was extracted within two hours of sample collection and stored at -80°C.

3.2.2. Anti-Spike (Trimer) IgG Titer Quantification

The Human SARS-CoV-2 Spike Trimer IgG ELISA Kit from Invitrogen was used to quantitate serum IgG levels of each subject at each timepoint, per the manufacturer's protocol. All samples were diluted 1:100 and assayed in duplicate with 2-fold serial dilution of the 150,000 units/mL standard control for relative quantification. Absorbance at 450 nm was quantified using a Spark® multimode microplate reader. Samples that produced signals greater than the upper limit of the standard curve were reassayed at 1:1000 dilution. IgG concentration was calculated by fitting 5-parameter logistic curves to the standard controls. The average concentration of duplicates was utilized for analysis. Inter-assay variability was addressed utilizing the ELISAtools package in R (version 4.0.4) which to account for batch-effect (Feng et al. 2019).

3.2.3. Antibody Neutralization Assays

Neutralization activity against SARS-2-CoV was measured in a single-round-of-infection assay using pseudotyped viruses (Nie et al. 2020). Briefly, 293T ACE cells were infected with modified vesicular stomatitis virus (VSV), which lacks a gene vital for VSV replication and instead carries a

firefly luciferase reporter gene that allows for chemiluminescence. The cells are also transfected with plasmids encoding full length SARS-CoV-2 spike (S) protein, which is a surface protein responsible for binding the host cell receptor, ACE2, to mediate viral entry during SARS-CoV-2 infection (SARS-CoV-2 Spike-pseudotyped lentiviral particle kit, BEI # NR-53816). The pseudotyped virus therefore contains the SARS-CoV-2 S protein to simulate viral entry, and VSV, which provides the structural genes for viral packaging without the ability to replicate. The 50% tissue culture infectious dose (TCID50) of the pseudotyped virus, which indicates the amount of virus required to quash 50% of the inoculated cells, was calculated according to the Reed-Muench method.

Serial dilutions of each subject's serum were incubated for 1hr at 37 °C with 1000 TCID50/ mL of the pseudotyped virus (virus plus antibody) then added to monolayers of ACE2-overexpressing 293T cells in quadruplicate on a 96-well plate. Controls consisted of pseudotyped virus and 293T cells without added serum sample (virus-only). The plate was incubated for 65-72 hours in the cell culture incubator at 37 °C and 5% (vol/vol) CO2 after which 50 µL of luciferase substrate was added to stimulate chemiluminescence. The amount of chemiluminescence, determined by a plate reader, directly correlates with the amount of pseudotyped virus that has entered and "infected" the cells. The amount of nAbs, which inhibit viral entry into the 293T cell, is therefore inversely correlated with the chemiluminescence signal intensity. Neutralizing antibody titers are reported as the 50% inhibitory dilution (ID50), calculated using the Reed-Muench method, which refers to the dilution fold required to achieve 50% neutralization (Nie et al. 2020; Ferrara and Temperton 2018). Higher ID50 correlates to increased potency of nAb within the serum sample.

3.2.4. Statistical Analysis

Demographic data was tested for significance between groups utilizing the Mann-Whitney U (MWU) testing for nonparametric continuous data, or Fisher's exact test for categorical data, as appropriate. Statistical differences between groups of time from vaccination to sample collection were assessed using the student's T test. The primary outcome measures were post vaccination Trimer IgG titers and nAb titers at both V2D7 and M6. Antibody titers for all time points were log transformed and z-scores were calculated to identify outliers (z score ≥2.5). Titers were tested for significance using the MWU test separately for each time point. Subgroup analysis was performed to assess the role of immunosuppressive therapy, with differences tested using the Kruskal-Wallis test with Dunn's post hoc test and Benjamini-Hochberg correction for multiple comparisons. Univariate correlation analysis was performed by calculating Pearson's coefficients for log transformed antibody titers. Multivariate regression models were then constructed separately for Trimer IgG and nAb to determine the relative effect of significant baseline variables on short term (V2D7) and long term (M6) results. P values <0.05 were considered significant. All analyses were performed in R version 4.0.4 (https://www.R-project.org/). Kruskal-Wallis and Dunn tests were implemented using the Dunn.test package. T testing, MWU, and Fisher's exact testing was implemented using the stats package. Pearsons coefficients were calculated using the corr.test function of the psych package.

3.3. Results

3.3.1. Demographics

Fourteen sarcoidosis subjects and 27 control subjects were recruited. Group characteristics

are highlighted in **Table 2**. Nearly all subjects received the BNT162b2 mRNA COVID-19 vaccine and booster at the recommended time interval of 21 days (mean 21.15 days; st. dev 0.57, range 20-24 days). All subjects had blood samples collected just prior to the first vaccine dose administration (V1D0) and 7 days after the booster dose at time point V2D7 (mean 6.91 days; st. dev 0.28, range 6-7 days) . All recruited subjects had available samples for Trimer IgG analysis at V1D0 and V2D7; of whom, 17 control samples and all 14 sarcoidosis samples were included in nAb analysis. Due to attrition, 22 control subjects and 11 sarcoidosis subjects were available for blood samples at the 6-month time point (mean 184.8 days from first vaccine, st dev 12.2, range 170-214 days) and included in Trimer IgG analysis at M6, of whom 11 control subjects and all 11 sarcoidosis subjects were included in nAb analysis.

Table 2. Demographics of control and sarcoidosis groups

	Control Subjects	**Subjects with Sarcoid**	*P-value*
Total Subjects, n	27	14	
Age, median (years)	53.0	60.5	*0.3355*
Sex, n **Female** **Male**	 10 17	 10 4	*0.7337*
Race, n **Black** **White** **Asian** **Other**	 2 18 1 6	 9 5 0 0	*0.0005*
Body Mass Index, median (kg/m^2)	26.1	31.84	*0.0319*
Days between Vaccine Dose, mean	21.3	20.9	*0.0793*
Days Between 1st Vaccine and V2D7, mean	6.9	6.9	*0.4939*
Days Between 1st Vaccine and M6, mean	180.9	192.6	*0.0575*
V2D7 = 7 days after vaccine dose 2 (4 weeks after 1st dose) M6 = month 6 time point			

The sarcoidosis group was comprised of 13 subjects with pulmonary manifestations and 6 with extrapulmonary involvement. Six subjects were not on any treatment and 8 were treated with

immunosuppressive therapy. Specifics regarding sarcoidosis phenotypes and treatment regimens for each subject are described in **Table 3**. Absolute peripheral lymphocyte values were available for 12 sarcoidosis subjects and had a group median of 1.8 x 10^9 cells/liter. Four subjects had medication titration within this 6 month pre-vaccination time interval.

Table 3. Clinical details regarding sarcoidosis chronicity, organ involvement, and treatment for each of the fourteen subjects in the sarcoidosis group.

Subject	Years Since Diagnosis	Organ Involvement	Treatment	Prednisone Equivalent (mg)	Abs Lymphocyte (10^9 cells / L)
1*	26	Pulmonary	Steroids, anti-metabolite, anti-TNF, IVIG	10	0.9
2	2	Lymph Node	Steroids, HCQ	7.5	1.2
3	13	Pulmonary, Ocular	Steroids, anti-metabolite	2.5	3.0
4	8	Pulmonary, Neurologic	Steroids	5	NA
5*	12	Pulmonary, Cardiac	None	0	1.2
6	24	Pulmonary	None	0	2.0
7	41	Pulmonary	None	0	1.7
8*	11	Pulmonary	Steroids, anti-TNF, IVIG	15	3.1
9	10	Pulmonary, Neurologic, Hepatic	Steroids, anti-metabolite, anti-TNF	10	1.6
10	6	Pulmonary	HCQ	0	1.7
11	8	Pulmonary	None	0	2.9
12	7	Pulmonary, Ocular	Anti-metabolite, anti-TNF	0	1.9
13	30	Pulmonary	None	0	NA
14	7	Pulmonary	None	0	2.0
*6 month time point not available					

3.3.2. Anti-Spike Protein Trimer IgG Titer and Neutralizing Antibody Analysis

Trimer IgG titers for each group across all three time points are illustrated in **Figure 9**. There were no outliers detected at either time point. While sarcoidosis subjects had a higher median baseline IgG titer than the control group (*MWU p-val* <0.001), both groups demonstrated a significant increase in IgG titers at V2D7 compared to their respective baselines (sarcoidosis:

MWU p-val <0.001; control: *MWU p-val* <0.001) with comparable titers at V2D7 between groups (*MWU p-val* =0.3680). IgG titers in both groups significantly decreased at the M6 time point from their respective V2D7 titers (sarcoidosis: *MWU p-val* <0.001; control: *MWU p-val* <0.001); however, M6 IgG titers in the sarcoidosis group fell to levels comparable to sarcoidosis V1D0 titers (*MWU p-val* =0.9786) and were significantly less than M6 control IgG titers (*MWU p-val* =0.0237). M6 IgG titers in the control group remained significantly higher than baseline values (*MWU p-val* <0.001). Overall, this trend indicates a robust initial IgG response in both groups that diminishes over time, returning to baseline in the sarcoidosis group and raising the concern for more transient antibody protection.

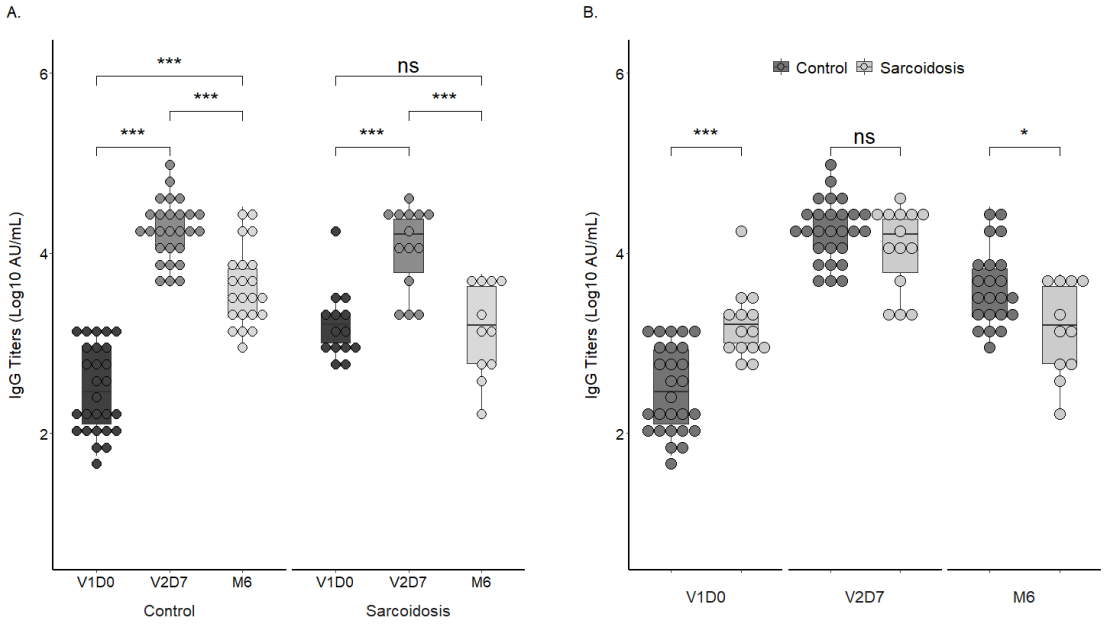

Figure 9. Trimer IgG titers for control and sarcoidosis groups are shown.
(a) log transformed titers for comparison between time points for each group and (b) log transformed titers for comparison between groups at each time point. ns: p > 0.05; *: p <= 0.05; **: p <= 0.01; ***: p <= 0.001

Functional nAb assays were performed to better determine protection conferred from

vaccination. The ID50 for each group across all three time points (V1D0, V2D7, and M6) are illustrated in **Figure 10**. Both control and sarcoidosis groups had a significant increase in nAb titers from baseline to V2D7 suggesting robust nAb formation after 1st and 2nd vaccination doses (sarcoidosis: *MWU p-val* <0.001; controls: *MWU p-val* <0.001), similar to what was observed for IgG trends. However, median ID50 for both groups at M6 were not significantly changed from their respective V2D7 values (sarcoidosis: *MWU p-val* =0.2250; controls: *MWU p-val* =0.0894) and remained significantly higher than baseline (sarcoidosis: *MWU p-val* <0.001; controls: *MWU p-val* <0.001) suggesting persistent immunity. Finally, median ID50 for sarcoidosis subjects were comparable to those of controls at all time points (V1D0 *MWU p-val* =0.5879; V2D7 *MWU p-val* =0.5740; M6 *MWU p-val* =0.7409) indicating similar levels of nAb present.

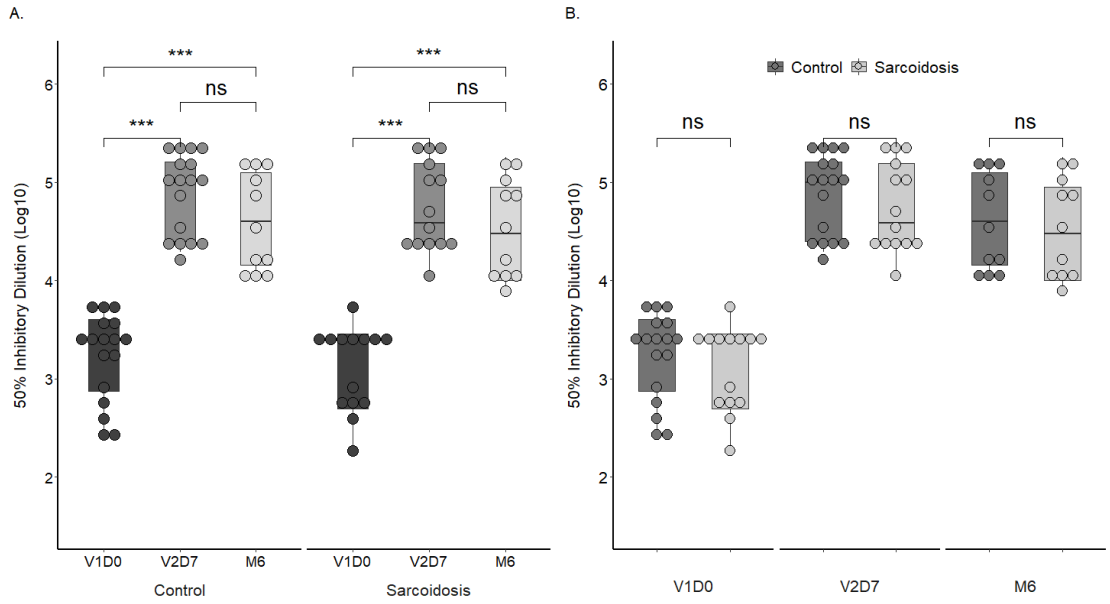

Figure 10. Neutralizing titers (50% Inhibitory Dilution) for control and sarcoidosis groups are shown.
(a) log transformed titers for comparison between time points for each group and (b) log transformed titers for comparison between groups at each time point. ns: p > 0.05; *: p <= 0.05; **: p <= 0.01; ***: p <= 0.001

Trends in IgG and nAb were further evaluated across sarcoidosis treatment groups (**Figure 11**). Pairwise comparisons using Dunn's test indicated sarcoidosis subjects on and off immunosuppression had comparable V2D7 IgG titers to controls (immunosuppression vs. control *BH adj p val* =0.3197, no treatment vs. control *BH adj p-val* =0.4514) as well as comparable nAb titers to controls (immunosuppression vs. control *BH adj p val* =0.4904, no treatment vs. control *BH adj p-val* =0.9333) indicating a robust initial antibody response regardless of immunosuppression. At M6, sarcoidosis subjects on immunosuppression had significantly decreased IgG titers compared to controls (*BH adj p-val* =0.0162), however nAb titers remained comparable (controls (*BH adj p-val* =0.3688) suggesting preserved protection.

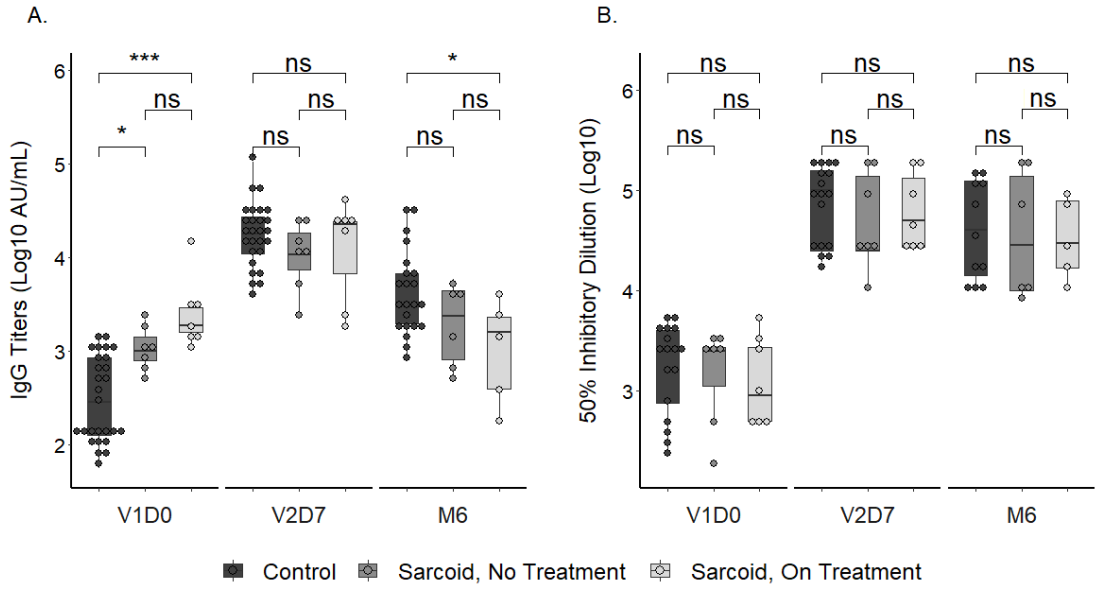

Figure 11. Antibody titers for Sarcoidosis subjects separated by treatment status and controls. (a) log transformed trimer spike-protein IgG titers are shown. Sarcoidosis subjects not on treatment had significantly higher V1D0 titers than controls and comparable titers at V2D7. M6 IgG titers were significantly lower in the sarcoidosis group than controls. (b) log transformed neutralizing titers (50% inhibitory dilution). Values were comparable across all groups at each time point. ns: p > 0.05; *: p <= 0.05; **: p <= 0.01; ***: p <= 0.001

3.3.3. Regression Analysis

Given variation in Trimer IgG and nAb trends, a univariate linear regression model was constructed to characterize the relationship between IgG and nAb titers across all time points. Correlation coefficients for control and sarcoidosis group are shown in **Figure 12**. IgG titers were significantly and directly associated with nAb titers in both groups, with a strong correlation for the control group (R =0.7715, *p-val* <0.001) and a weak correlation for sarcoidosis group (R =0.3905, *p-val* 0.0140). IgG titers in the sarcoidosis group were overall determined to be less predictive of nAb (R^2 =0.1525) than in the control group (R^2 =0.5952). With such low variance explained by IgG titers in the sarcoidosis group, a multivariate linear regression model was subsequently constructed to delineate which, if any, variables independently predict short term (V2D7) and long term (M6) nAb titers. Regression models for each outcome are shown in **Figure 13**. The overall regression was not statistically significant for either group. Additional regression models for M6 for each group were constructed with the addition of V2D7 and M6 IgG titers, also with interdependencies accounted for, and yielded similar results. None of the additional independent variables were significantly predictive of nAb though analysis may be underpowered to detect significance.

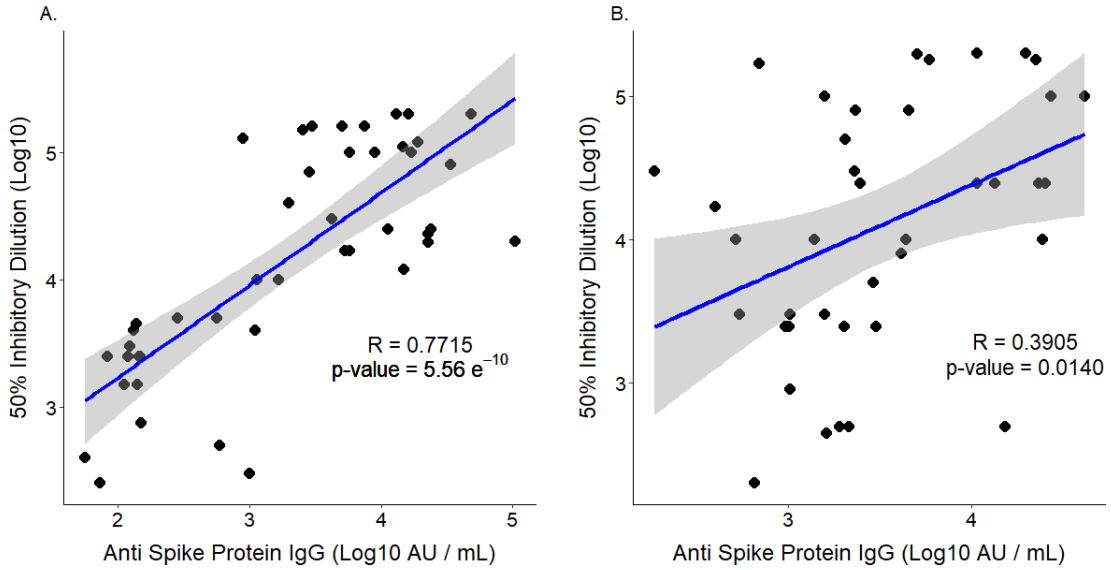

Figure 12. Univariate linear regression analysis illustrating the relationship between log transformed Trimer IgG titers and log transformed 50% inhibitory dilution across all time points.

(a) Control group showing a significant and strong correlation, and (b) Sarcoidosis group showing a significant yet weak correlation.

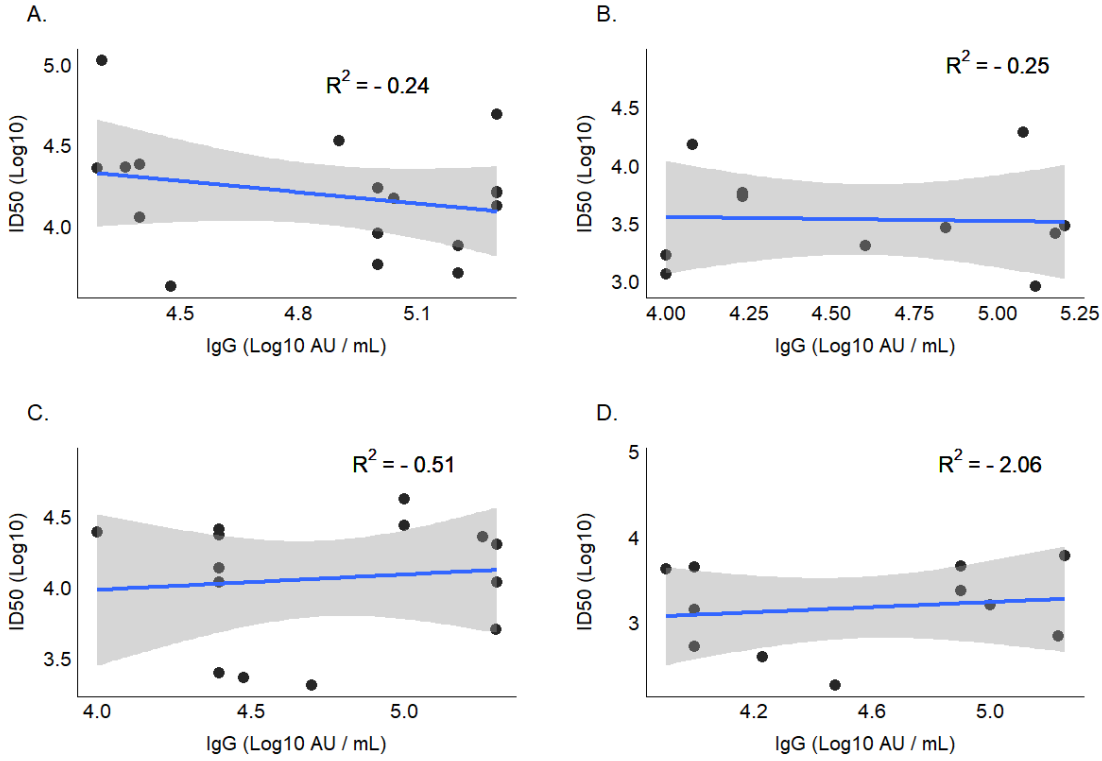

Figure 13. Multivariate regression analysis to assess independent predictors of 50% inhibitory

dilution (ID50) by group (top row: controls; bottom row: sarcoidosis) and outcome time points (left column: V2D7; right column: M6).
Axes are log transformed. (a) V2D7 ID50 for control group. Model: Log10 V2D7 ID50 ~ Log10 V2D7 Trimer IgG * Log10 V1D0 Trimer IgG + Race + BMI. (b) M6 ID50 for the control group. Model: Log10 V2D7 ID50 ~ Log10 V2D7 Trimer IgG * Log10 V1D0 Trimer IgG + Log10 V2D7 Trimer IgG * Log10 M6 V2D7 IgG + Race + BMI. (c) V2D7 ID50 for the sarcoidosis group. Model: Log10 V2D7 ID50 ~ Log10 V2D7 Trimer IgG * Log10 V1D0 Trimer IgG + Race + BMI + Treatment Group. (d) M6 ID50 for the sarcoidosis group. Log10 V2D7 ID50 ~ Log10 V2D7 Trimer IgG * Log10 V1D0 Trimer IgG + Log10 V2D7 Trimer IgG * Log10 M6 V2D7 IgG + Race + BMI + Treatment Group. The overall regression was not statistically significant for either group at both time points.

3.4. Interpretation

We present a single center analysis of the quantitative and qualitative antibody response to vaccination with the BNT162b2 mRNA COVID-19 vaccine in infection naïve subjects with and without sarcoidosis. Our data indicates that sarcoidosis subjects mount a robust initial Trimer IgG antibody response to vaccination with subsequent quantitative decline by 6 months, driven by those on immunosuppression. Despite the decline in binding antibodies, sarcoidosis subjects develop and maintain functional immunity regardless of immunosuppressive treatment. With this discrepancy between IgG and nAb titers, it is not surprising that IgG antibodies weakly correlated with nAb and were not significantly predictive of nAb titers at any timepoint. While this study is of a single vaccine type, it sheds light on the clinical protection vaccination provides individuals with sarcoidosis despite IgG titers that may suggest otherwise.

The SARS-CoV-2 is an enveloped virus with numerous structural proteins vital for the viral life cycle. The S protein, which is composed a S1 subunit, S2 subunit, N-terminal domain, and receptor-binding domain (RBD), is responsible for viral entry into the host cell specifically through binding of the RBD. Antibodies to SARS-CoV-2 consist of IgM, IgG, and/or IgA antibodies and may target any subdomain of the S protein (Klingler et al. 2020; Sterlin et al. 2021; Ma et al. 2020;

Salvagno et al. 2021). Upon viral binding to ACE2, conformational changes of surface glycoproteins result in the formation of an S protein trimer (Walls et al. 2020), which is the target of the IgG antibodies quantified in this study. Despite a wide array of antibodies produced, nAb confer protection by preventing viral entry, receptor mediated infection and infection propagation. Numerous studies support a strong correlation between various antibody titers and neutralization; however, the strength of correlation may vary with different tested antibody targets as well as with time from SARS-CoV-2 exposure (Mazzini et al. 2021; Maeda et al. 2021; Volkova 1974). Our findings reveal a strong correlation in controls between Trimeric anti-spike IgG levels and neutralization, which aligns with a similar study of this antibody type in healthy individuals after BNT162b2 vaccine (Matusali et al. 2022). The sarcoidosis group, however, had a weak correlation between IgG levels and neutralization which was otherwise not explained by group differences. Neutralization in this group is therefore likely explained by the presence of non-IgG antibodies or antibodies to other spike protein subdomains not measured in our study, though further analyses are needed to assess this.

Sarcoidosis is a T cell mediated disease characterized by local CD4+ T lymphocyte inflammation and peripheral lymphocyte depletion in severe or active disease, as well as anergy and exhaustion in progressive disease (Sweiss et al. 2010; Hawkins et al. 2017; Grunewald et al. 2019; Vagts et al. 2021). Defects within humoral immunity have also been described and include evidence of B cell hyperactivation, autoantibody production, decreased circulating memory B cells, as well as previously mentioned impaired serologic responses to Tetanus and Hepatitis vaccines (Seyhan et al. 2012; Mert et al. 2000; Hunninghake et al. 1999; Hashemzadeh et al. 2021; Kudryavtsev et al. 2020; Musaelyan et al. 2018; Saussine et al. 2012). Despite these defects, vaccine induced

development and persistence of neutralization antibodies in sarcoidosis subjects is a particularly important and reassuring finding. However it is worth noting the median peripheral absolute lymphocyte count (1.8 x 10^9 cells/liter) in our cohort is greater than previously described thresholds of significant sarcoidosis-related lymphopenia (Vagts et al. 2021). This suggests lymphopenia is unlikely to be a significant disease manifestation in this cohort and therefore may explain the preserved nAb activity. Treatment was also uptitrated in four sarcoidosis individuals; despite this, neutralization was seemingly unaffected.

Limitations of this study include heterogeneity within the sarcoidosis group, limited sample size, and attrition rate at 6 months. Data regarding lymphocyte subsets in the sarcoidosis group were largely unavailable and may have allowed further interpretation of the immunity stimulated by vaccination if obtained concurrently. Only IgG antibody was quantified, and despite strong correlation to nAb among control subjects, further assessment of preserved immunity in sarcoidosis was limited. Future studies in the field should focus on inclusion of specific sarcoidosis phenotypes as well as direct assessment of cellular and humoral activity. In addition, only one mRNA COVID-19 vaccine was studied, thus conclusions should be cautiously applied to other COVID-19 vaccines.

Despite these limitations, we conclude that Trimer IgG levels in sarcoidosis subjects are poor predictors of nAb, which are an important mechanism in preventing infection While further analysis is needed to determine clinical outcomes from vaccination in this vulnerable population, particularly among those on immunosuppression, knowledge gained from our study suggests that vaccination may provide at least partial protection from COVID-19 infection in sarcoidosis. Additional studies of immune response stimulated by the BNT162b2 vaccine, which induces

robust cellular and humoral immunity (Fotin-Mleczek et al. 2011), may offer mechanistic insights into the pathogenesis of sarcoidosis.

4. Altered transcriptomic immune responses of maintenance hemodialysis patients to the Covid-19 mRNA vaccine

Modified from publication: **Chang YS**, Huang K, Lee JM, Vagts CL, Ascoli C, Huang Y, Cherian RA, Sarup N, Warpecha SR, Edafetanure-Ibeh R, Amin MR, Ghassemi M, Novak R, Lora CM, Perkins DL, Finn PW. Altered transcriptomic immune response of maintenance hemodialysis patients to the Covid-19 mRNA vaccine. medRxiv. Preprint. 2023 Jan 19.

4.1. Introduction

The rapid development and dissemination of coronavirus disease 2019 (COVID-19) vaccines in response to the COVID-19 pandemic has necessitated the characterization of immune protection conferred by these vaccines across various populations. The COVID-19 mRNA-based vaccines, BNT162b2 and mRNA-1273, have proven to be efficacious, with initial reports showing 95% and 94.1% reduction of COVID-19 disease in recipients (Baden et al. 2021; Polack et al. 2020). However, certain immunosuppressed populations remain at risk of infection. Given the widespread transmission of COVID-19, detailed assessments of degree, duration, and determinants of immune protection conferred by these vaccines are vitally needed in immunocompromised patient populations including those with end-stage renal disease.

End-stage renal disease (ESRD) is the most advanced stage of chronic kidney disease (CKD), with prevalence in the U.S. reaching 809,000 in 2019 (Johansen et al. 2022) . The most used form of renal replacement therapy for ESRD patients in the U.S. is hemodialysis (HD). Despite significant improvements in hemodialysis technology, the mortality rate in ESRD patients is still as high as 20% annually (Williams et al. 2004), with infections being the most common cause of hospitalization and mortality after cardiovascular disease (Kato et al. 2008). The immunocompromised state of ESRD is characterized by simultaneous immunodepression due to the impact of uremic milieu on immunocompetent cells and immunoactivation due to the

accumulation of proinflammatory cytokines (Kato et al. 2008). There are alterations to both innate and adaptive immunity, including elevated levels of mannose-binding lectin (Satomura et al. 2002), impaired maturation of monocytes and dendritic cells (Lim et al. 2007; Satomura et al. 2002), increased B cell apoptosis (Fernández-Fresnedo et al. 2000), and decreased T-cell proliferation with elevated Th1/Th2 ratio (Stenvinkel et al. 2005). This immune compromise leads to higher susceptibility to infection and lower response to vaccination (Ghadiani et al. 2012). For example, while more than 90% of patients without CKD develop protective antibodies against HBV after vaccination, only 50-60% of patients with ESRD seroconvert. There have also been higher vaccination failure rates demonstrated against influenza virus, Clostridium tetani, and Corynebacterium diphtheriae in ESRD (Eleftheriadis et al. 2007).

Studies of genome-wide expression (i.e. transcriptome) profiles of peripheral blood mononuclear cells in ESRD demonstrate a complex picture of immune alterations. One study found upregulation of genes involved in the complement and oxidative metabolism pathways, and downregulation of genes associated with the clathrin-coated vesicle endosomal pathway and T-cell receptor signaling (Scherer et al. 2013). Two other studies have demonstrated impaired expression of genes involved in oxidative phosphorylation and mitochondrial function (Granata et al. 2009; Liu, Fiskum, and Schubert 2002). A study identifying a group of inflammatory genes playing a causative role in oxidative stress in dialysis patients showed unique gene expression alterations in maintenance HD patients compared to un-dialyzed CKD patients and compared to patients undergoing peritoneal dialysis (Zaza et al. 2008). These studies indicate a range of immune pathways that may impair vaccination response, and further suggest that dialysis leads to unique immune profile alterations.

While recent studies of the SARS-CoV-2 BTN162b2 vaccine in HD demonstrate high levels of seroconversion ranging from 84-96% (Anand et al. 2021; Attias et al. 2021; Grupper et al. 2021; Jahn et al. 2021), they also demonstrate quantitatively reduced SARS-CoV-2 IgG antibodies. We posit that characterization of the transcriptomic underpinnings of antibody titer development on a continuous scale may identify biomarkers for weaker or less durable immune protection in this population. Furthermore, transcriptomic analyses may identify targets for the development of new, effective vaccines against other infectious diseases for this population. Thus, we characterized the immune response of the HD population to the COVID-19 mRNA-based BNT162b2 vaccine using RNA sequencing, antibody ELISA and neutralization titers across multiple time points. We additionally identified transcriptomic and clinical determinants of the humoral immune response in HD patients.

4.2. Methods

4.2.1. Study population and sample acquisition

The study was approved by the University of Illinois at Chicago IRB (#2018-1038) Ethics Review Committee. Maintenance HD patients undergoing vaccination with the BNT162b2 mRNA COVID-19 vaccine in February 2021 were recruited from the outpatient HD unit at the University of Illinois Hospital (UIH) in Chicago, IL. Control subjects consisted of UIH employees undergoing BNT162b2 mRNA COVID-19 vaccination at UIH from December 2020 to January 2021 with no self-reported history of kidney disease or immune disorders. A subset of control subjects matched for age, gender, and COVID-19 history was also analyzed for this study. Blood was collected at 0 – 48 hours prior to and at multiple time points after both the first (V1) and second

vaccination doses (V2), which were administered three weeks apart. Control samples were collected prior to each vaccination dose (D0) and at one day (D1) and seven days (D7) after each dose, corresponding to six time points: V1D0, V1D1, V1D7, V2D0, V2D1, V2D7. Blood was collected from HD subjects prior to each vaccination dose and at two days (D2) and seven days after each dose, corresponding to six time points: V1D0, V1D2, V1D7, V2D0, V2D2, V2D7. A final blood sample was drawn six months after initial vaccination (M6) for measurement of antibody titers, prior to additional vaccination doses. Serum and peripheral blood mononuclear cells (PBMCs) were extracted within two hours of blood collection, then stored at -80°C. PBMCs were extracted using density gradient centrifugation at 400g with Ficoll-Paque PLUS. The extracted buffy coat was stored in RNAlater (Invitrogen).

4.2.2. Clinical and Demographic Characterization

Demographic and clinical data was collected from the electronic health record (EHR) for HD subjects, including medical diagnoses, medications, and laboratory values. Laboratory values included monthly SARS-CoV-2 test results, as well as urea reduction ratio (URR, a measure of dialysis adequacy), hemoglobin (Hgb), ferritin, transferrin saturation, albumin levels, white blood cell (WBC) count and WBC differential counts obtained during standard of care monthly blood draws for the three months preceding vaccination. Within our analyses, ferritin was coded as either low risk (200ng/ml – 1200 ng/ml) or high risk (<200 ng/ml or >1200 ng/ml), since ferritin levels 200ng/ml – 1200 ng/ml have been shown to be associated with lowest all-cause mortality in HD patients (Kalantar-Zadeh et al., 2005). Baseline clinical lab values were calculated as the median of three lab values across the three months prior to vaccination. Demographic and clinical data was collected from a medical questionnaire at time of consent for control subjects, and

included medical history, medications, and self-reported prior SARS-CoV-2 positive test results.

4.2.3. RNA extraction and RNA Sequencing (RNAseq)

RNA sequencing was performed on PBMCs at all V1 and V2 time points for all subjects for whom RNA libraries were successfully built at ≥ 5 time points. PBMCs stored in RNAlater were thawed and diluted 1:1 with 1X phosphate buffered saline. The mixture was then pelleted and RNA was extracted using the PureLink RNA Mini kit (Invitrogen). DNase treatment to remove genomic DNA contamination was performed using either the PureLink DNase kit or DNA-free kit DNA Removal Kit (Invitrogen). Purified RNA in sterile water was stored at -80°C. Each RNA sample was quantified using the Qubit RNA High Sensitivity kit (Invitrogen) and Bioanalyzer RNA Pico kit (Agilent) with RIN>=8.

For library construction, 50ng of RNA from each sample was aliquoted in 96 well plates. Libraries were generated using the NEBNext Ultra II Directional RNA Library Prep Kit for Illumina with the optional NEBNext Poly(A) mRNA Magnetic Isolation Module (New England BioLabs). Each individual sample library was barcoded during PCR amplification using unique dual indexed i5 and i7 primers from the NEBNext Multiplex Oligos for Illumina kit. Each sample library was quantified using the Qubit DNA High Sensitivity kit and Bioanalyzer DNA High Sensitivity kit. Samples were then pooled and sequenced using the MiSeq Nano V2 kit (Illumina) to check read proportions between samples. Samples with lower-than-expected percentage of reads detected were supplemented with an additional spike-in of sample library to the main pool. The supplemented pooled library was sequenced again using the MiSeq Nano V2 kit to verify adequate adjustment. The finalized library was sequenced using a NovaSeq S2 flow cell configured for 75bp paired end output.

4.2.4. Differential Gene Expression Analysis

Raw demultiplexed reads were filtered using fastp to remove adapters and short reads (Chen et al. 2018). Trimmed reads were then quantified using the Salmon pipeline with an hg38 reference transcriptome index (Patro et al. 2017). Quantified data was imported into R using the tximeta package (Love et al. 2020) to convert Salmon quantification and index data to a count matrix. Transcript names were extracted and matched using Entrez IDs with the AnnotationHub package (Love et al. 2020). This finalized count matrix was then imported into a DESeqDataset object and normalized using the variance stabilizing transformation in DESeq2.

The *DESeq2* R package was used to identify genes that were differentially expressed at each time point after vaccination for each subject group. Specifically, we implemented a design incorporating group-specific condition effects with individual subjects nested within groups. We performed the classical *Deseq2* workflow of estimation of size factors, estimation of dispersion, and negative binomial GLM fitting for β_i and Wald statistics, increasing the maximum number of iterations for estimation of the negative binomial distribution to 500. We then generated contrasts to obtain differentially expressed genes for controls at V1D1 and V1D7 (compared to V1D0), and at V2D1 and V2D7 (compared to V2D0). Differentially expressed genes for HD were similarly obtained at V1D2 and V1D7 (compared to V1D0), and at V2D2 and V2D7 (compared to V2D0). We also directly compared gene expression between controls and HD at V1D7 and at V2D7. The significance threshold to determine differential expression was FDR-adjusted ($p < 0.05$).

4.2.5. Anti-Spike (trimer) IgG Titer Quantification

The Human SARS-CoV-2 Spike (Trimer) IgG ELISA Kit from Invitrogen was used to

quantitate IgG to the SARS-CoV-2 spike protein in serum samples at V1D0, V2D7, and M6 time points. All samples were initially diluted 1:100 (in addition to the 1:10 assay buffer dilution on the 96-well plate) and assayed in duplicate, with two-fold serial dilution of the 150,000 units/mL standard control in duplicate for relative quantification. Absorbance at 450 nm was quantified using a *Spark*® multimode microplate reader. Samples that produced signals greater than the upper limit of the standard curve were diluted 1:2000 and assayed again. IgG concentration was calculated by fitting four-parameter logistic curves to the standard controls and taking the average concentrations of duplicates.

4.2.6. Antibody Neutralization Assays

Neutralization assays were performed on serum samples from V1D0 and V2D7 using SARS-CoV-2 pseudotyped virus (pseudovirus). To produce pseudoviruses, an expression plasmid bearing codon-optimized SARS-CoV-2 full length S plasmid was co-transfected into HEK293T cells using the SARS-CoV-2 Spike-pseudotyped lentiviral particle Kit (BEI # R-52948). The cell supernatants were collected 72h after transfection, divided into aliquots and cryopreserved at −80 °C.

To titrate the pseudovirus, $5x10^3$ 293T-ACE2 cells were seeded per well in a 96-well plate in DMEM containing 10% FBS and 1% penicillin streptomycin. Twenty-four hours later, the pseudovirus was diluted 1:10, followed by five-fold serial dilutions for a total of nine dilutions, with each dilution performed in six replicate wells. After incubation at 37 °C and 5% (vol/vol) CO2 for 72h, the luciferase substrate was added to the 96-well plate for chemiluminescence detection. The 50% tissue culture infectious dose (TCID50) of the pseudovirus was calculated according to the Reed-Muench method in the titration macro template (MATUMOTO 1949).

Neutralization activity against SARS-2-CoV was measured in a single-round-of-infection assay with pseudoviruses as previously described (Nie et al. 2020). $5x10^3$ 293T-ACE2 cells were seeded per well in a 96-well plate. Twenty-four hours later, serial dilutions of the serum samples were performed, incubated for one hour at 37 °C with ~1000 TCID50/ml of pseudovirus, then added to monolayers of ACE2-overexpressing 293T cells in quadruplicate. The cell control with cells alone and the virus control (VC) with pseudovirus were set up in each plate. The target cells were incubated for 65h-72h at 37 °C and 5% (vol/vol) CO2. Fifty µL of Bright-Glo, reconstituted following manufacturer's instructions, was added to each well of the 96-well plate and incubated for five minutes at room temperature. The 96-well plate was read by a 96-well luminescence plate reader (Tecan Genius Pro plate reader) (Ferrara and Temperton 2018). Percent neutralization was calculated as 100*([Virus-only control] – [Virus plus serum])/[Virus-only control], and neutralizing titer levels are reported as the serum dilution required to achieve 50% neutralization (50% inhibitory dilution [ID50]) (Pegu et al. 2021). The input dilution of serum was 1:20, thus 20 is the lower limit of quantification.

4.2.7. BTM module enrichment analysis

Gene set enrichment analysis was performed for each contrast generated in the DESeq2 analysis above using blood transcription module (BTMs) gene sets (S. Li et al. 2014). BTMs with FDR-adjusted $p < 0.05$ were considered significantly enriched. Enriched BTMs were further characterized using the distribution of Wald statistics of membership genes from DESeq2. To summarize BTM analyses, BTMs were categorized into different families: B cells, cell cycle, dendritic cell/antigen presentation, type I interferon (IFN type I), myeloid activity/inflammation/ T/NK cells, and "others" (Braun et al. 2018). The percentage of BTMs in each BTM family with

significant enrichment at each time point was then quantified over time.

4.2.8. Statistical analysis of antibody response

To determine the effect of vaccination on anti-spike IgG titers at V2D7 and M6, Kruskal-Wallis tests were performed separately for HD subjects and controls. For each group, anti-spike IgG titer levels were compared to assess for the significant effect of time (V1D0, V2D7, M6), and Wilcoxon rank sum tests were performed with FDR correction to assess significant differences between each pair of time points (V2D7 vs. V1D0, M6 vs. V1D0, M6 vs. V2D7). To determine the effect of vaccination on antibody neutralization activity (ID50) at V2D7, Wilcoxon rank sum tests were performed for each group to compare V2D7 vs. V1D0.

Linear models were constructed to establish the effect of prior SARS-CoV-2 infection and subject group on anti-spike IgG titer development at V2D7 and M6 and neutralization activity at V2D7. Specifically, log-transformed V2D7 anti-spike IgG titers or V2D7 neutralization activity (ID50) were modeled as the dependent variable, with subject group (HD or controls), log-transformed V1D0 anti-spike IgG titers or V1D0 neutralization activity (ID50), gender, age, race, and ethnicity as independent predictors. To determine predictors of anti-spike IgG at six months, a linear model was constructed with the log-transformed M6 anti-spike IgG titers as the dependent variable, and V2D7 anti-spike IgG titers, SARS-CoV-2 history, gender, age, race, and ethnicity as independent predictors.

4.2.9. Identification of BTM and clinical predictors of Ab response in HD

BTM predictors of antibody response in HD were identified by first calculating a representative expression level of each BTM per sample, which we will refer to as the eigengene.

Specifically, the first principal component of each BTM was calculated using DESeq2-derived variance-stabilized gene counts from each module's member genes across the HD V1 time points, and then across the HD V2 time points. Signs (positive or negative) were assigned to the eigengenes such that samples with higher expression of member genes in a BTM would be given a positive sign, while those with lower overall gene expression would be given a negative sign. This was accomplished for each BTM by (1) computing the median gene expression level across membership genes in a given BTM for each sample, (2) computing the Pearson correlation between the eigengene of the BTM and the median gene expression level across all samples, and (3) multiplying the eigengene of the BTM by -1 if the correlation was negative.

Subsequently, we constructed linear models with log-transformed anti-spike IgG at V2D7 as the dependent variable and change in BTM eigengene expression after vaccination as the independent variable, controlling for SARS-CoV-2 history. Separate models were constructed for each BTM that was enriched at each time point after vaccination in HD (V1D2 vs V1D0, V1D7 vs V1D0, V2D2 vs V2D0, V2D0 V2D7). Change in BTM expression was calculated as the BTM eigengene after vaccination minus the BTM eigengene before vaccination. P-values were FDR-adjusted across number of enriched BTMs per time point.

Additionally, baseline clinical laboratory values predictive of antibody response in the HD subjects were identified. Linear models were separately constructed using URR, ferritin (high risk vs low risk), transferrin saturation, hemoglobin, and WBC count to predict log-transformed anti-spike IgG at V2D7 and M6.

Finally, clinical laboratory values responding to vaccination that predicted antibody titer response in the HD subjects were identified. Linear models were separately constructed using

log-fold change (LFC) from baseline measurements of ferritin (continuous instead of binarized low- and high-risk), transferrin saturation, and WBC count to predict log-transformed anti-spike IgG titers at V2D7 and M6.

4.3. Results

4.3.1. Demographic and Clinical Characterization

Demographic and clinical data of the 20 maintenance hemodialysis (HD) and controls (HC) are summarized in **Table 4**. The racial distribution differed between cohorts with more Black/African American subjects in the HD cohort. The cohorts were otherwise demographically similar. The subjects within the HD cohort had significantly more comorbidities, most notable of which include type 2 diabetes mellitus (T2DM), hypertension (HTN), dyslipidemia, and other cardiovascular conditions. The most common causes of renal failure were T2DM and HTN, with a minority of cases attributed to anatomic defects (reflux uropathy) and autoimmune conditions (systemic lupus erythematous and idiopathic thrombocytopenic purpura).

Table 4. Demographic and clinical data for maintenance hemodialysis and control subjects.

	Hemodialysis	Control	P-val
Total # of subjects	20	20	
Gender			
Male	11	10	1.0
Female	9	10	1.0
Age (mean (sd))	54 (12)	54 (13)	0.98
Race/Ethnicity			
Black/African American	10	3	0.041
Asian/Pacific Islander	1	2	1.0
White/Caucasian	2	8	0.067
Hispanic/Latinx	7	6	1.0
Other	0	1	1.0
BMI, kg/m^2 (mean (sd))	27.8 (5.1)	28.7 (6.4)	0.61
Medical Hx			
Diabetes	11	1	0.0012

Hypertension	18	4	< 0.001
Other CV disease*	9	0	0.0012
Dyslipidemia	10	0	< 0.001
Autoimmune disease**	3	0	0.23
Immunosuppression***	1	0	1.0
Active Malignancy****	1	0	1.0
Positive COVID-19 Hx	8	5	0.5

* includes coronary artery disease (CAD), congestive heart failure (CHF), atrial fibrillation (AF), peripheral vascular disease (PVD), and cerebral vascular accent (CVA)
** includes systemic lupus erythematosus (SLE), immune thrombocytopenic purpura (ITP), microscopic polyangiitis (MPA)
*** hydroxychloroquine
**** defined as malignancy requiring treatment in the last six months; one patient with papillary thyroid cancer requiring thyroidectomy, no systemic treatment required

There were eight HD subjects who previously tested positive for SARS-CoV-2, with positive test dates ranging from 7 months to four weeks preceding vaccination. Five control subjects self-reported a prior positive SARS-CoV-2 test, with positive test dates ranging from 8 months to four weeks preceding vaccination. Detailed clinical characterization of HD subjects is summarized in **Table 5**. Notable laboratory data includes an elevated ferritin from normal (with high population variance), and anemia.

All subjects received two BTN162b2 vaccination doses with the second dose (V2) administered three weeks after the first (V1). Anti-spike IgG binding and neutralizing assay data were obtained for all subjects prior to V1 (V1D0) and seven days after V2 (V2D7). RNA sequencing data was obtained for all control subjects prior to each vaccination dose (D0), and at one day (D1) and seven days (D7) after each dose, corresponding to six time points: V1D0, V1D1, V1D7, V2D0, V2D1, V2D7. One control subject is missing V2D0 data, and one is missing V2D1 data. RNA sequencing data was obtained for 12 HD subjects prior to each vaccination dose, and at two days (D2) and seven days after each dose, corresponding to six time points: V1D0, V1D2, V1D7, V2D0,

V2D2, V2D7. Two HD subjects are missing V2D2 data. Sequencing data was not obtained for subjects with fewer than five time points of successfully constructed RNA libraries, due to time points without sample collection or failure to extract high quality mRNA from PBMCs. Six-month follow-up (M6) anti-Spike IgG binding titers were obtained for 15 HC subjects and 19 HD subjects. One HD subject tested positive for SARS-CoV-2 14 days after the second vaccination dose, demonstrating mild symptoms. None of the other subjects reported SARS-CoV-2 infection up to 6 months follow up after the second vaccination.

Table 5. Baseline clinical lab values for maintenance hemodialysis patients.

	Normal range	Mean (SD)
Kidney/HD status		
Urea Reduction Ratio (URR)	-	0.74 (0.052)
Months on HD	-	46 (44)
Iron		
Ferritin (ng/ml)	10 - 259	838 (550) *
% Transferrin saturation	25 - 50	38 (13)
Albumin	3.4 – 5	4.1 (0.40)
CBC		
WBCs (k/ul)	3.9 - 12	6.0 (2.1)
Hgb (g/dl)	13.2 – 18	10.5 (1.5) *
Lymphocytes (k/ul)	1.3 - 4.2	1.5 (0.7)
Neutrophils (k/ul)	1.3 - 7.5	3.7 (1.5)
Monocytes (k/ul)	0.4 - 1	0.5 (0.2)
Eosinophils (k/ul)	0.2 - 0.5	0.2 (0.2)

* indicates value outside of normal range

4.3.2. Differential Gene Expression Analysis

To characterize the molecular basis of immune responses to vaccination in HC and HD, we performed differential gene expression analyses of the PBMC RNA sequencing data. There are substantially more differentially expressed genes (DEGs) in response to V2 compared to V1, and at D1 and D2 post-vaccination compared to D7 (**Figure 14**). For HC, the largest number of

DEGs is found at V2D1, indicating the most transcriptional activity immediately after the 2nd vaccine dose, followed by V2D7, V1D1, and V1D7. HD follows a similar pattern, with the largest number of DEGs found at V2D2, followed by V2D7, V1D2, and V1D7. Notably, HD subjects with no SARS-CoV-2 history (n = 6) have substantially lower numbers of DEGs than HD subjects with positive SARS-CoV-2 history (n = 6) at each time point, and particularly at V2 time points.

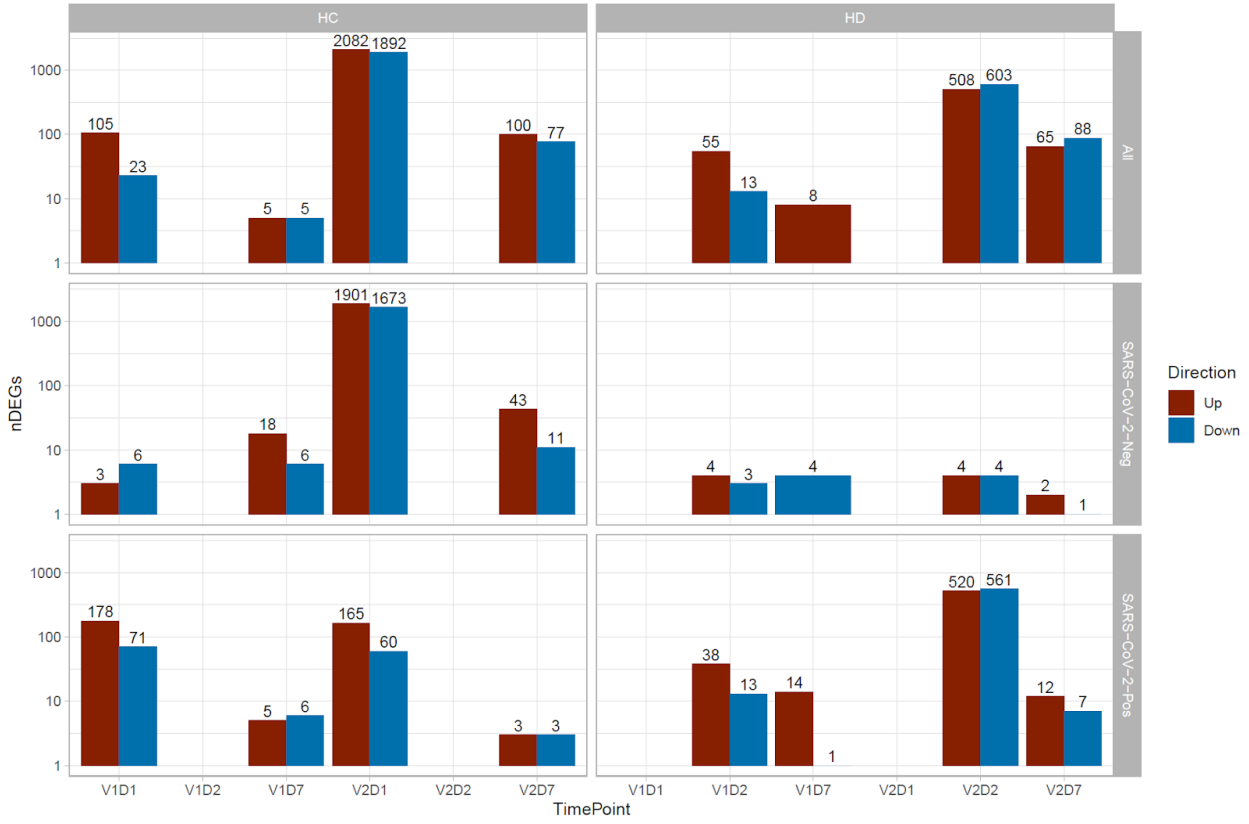

Figure 14. Differentially expressed genes (DEGs) increased after second vaccination dose compared to first, and at Day 1 and 2 (D1/D2) compared to Day 7 (D7) for both controls (HC) and maintenance hemodialysis (HD).
Number of DEGs at each time point is displayed on a log scale, with DEGs for HC shown for D1 and D7 compared to pre-vaccination time point (D0), and DEGs for HD shown for D2 and D7 compared to D0. DEGs are shown independently of SARS-CoV-2 history (Top), for analysis of only subjects with no prior SARS-CoV-2 history (Middle), and for analysis of only subjects with prior SARS-CoV-2 history (Bottom). The DESeq2 R package was used to identify genes that were differentially expressed at each time point after vaccination for each subject group ($p < 0.05$, FDR-adjusted).

Direct comparison of gene expression between HC and HD with no prior reported SARS-CoV-2 infection at V1D7 yielded five DEGs in HD versus HC including increased expression of chemokine CCL19 in HD ($p < 0.05$, FDR-corrected). Comparison of these same groups at V2D7 yielded 18 DEGs including increased expression in HD of TIA1, which encodes a granule-associated protein expressed in cytolytic lymphocytes (Anderson et al. 1990) and natural killer cells, and BH3, a pro-apoptotic Bcl-2 family member and mediator of lymphocyte apoptosis (Labi et al. 2008).

4.3.3. Blood Transcription Module (BTM) Enrichment

BTM enrichment analysis of subjects without SARS-CoV-2 history reveals the vaccine-induced progression of various immune processes at each time point after vaccination (Figure 2). Following V1, HC demonstrate early (V1D1) enrichment of 29 BTMs, with substantial upregulation of monocyte and antiviral IFN activity. The immune response transitions to V1D7 enrichment of four BTMs including significant T cell activation and downregulation of monocytes. Following V2, HC demonstrate early (V2D1) enrichment of 82 BTMs, with substantial upregulation of innate antiviral activity, similarly to V1D1. The immune response transitions to V2D7 enrichment of ten BTMs, with significant upregulation of plasma cells and immunoglobulins.

In contrast, HD demonstrate early (V1D2) enrichment of 12 BTMs after the first vaccination dose, most significantly involving upregulation of innate antiviral responses (**Figure 15**). The immune response transitions to V1D7 enrichment of 17 BTMs, with substantial upregulation of myeloid modules. The V1D7 positive enrichment of monocyte/myeloid modules

in HD contrast the negative enrichment of these modules in HC (**Figure 15**, **Figure 16**). Following the second vaccination dose, HD demonstrate early (V2D2) enrichment of 27 BTMs most significantly involving upregulation of dendritic cell activity and proinflammatory cytokines and chemokines. The immune response progresses to V2D7 enrichment of one BTM: PLK signaling events.

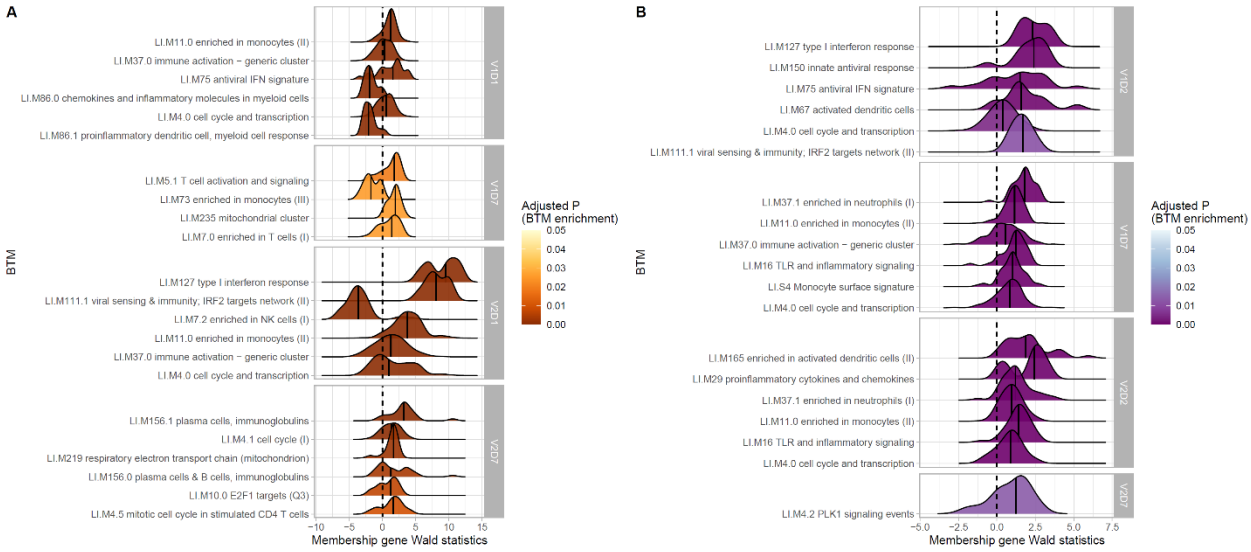

Figure 15. Controls (HC) and maintenance hemodialysis subjects (HD) with no SARS-CoV-2 history demonstrate differing longitudinal enrichments of blood transcription modules (BTMs). (A) The most significantly enriched BTMs are shown (up to six) for Day 1 (D1) and Day 7 (D7) after each vaccination dose (V1, V2) in HC with no prior infection with SARS-CoV-2 ($p < 0.05$, FDR-adjusted). Density plots for each BTM represent Wald statistics from DESeq2 analysis for each membership gene, thereby representing increased or decreased expression per gene at each time point compared to baseline (V1D0 or V2D0). (B) Similarly to (A), the most significantly enriched BTMs for Day 2 (D2) and Day 7 (D7) in HD are shown.

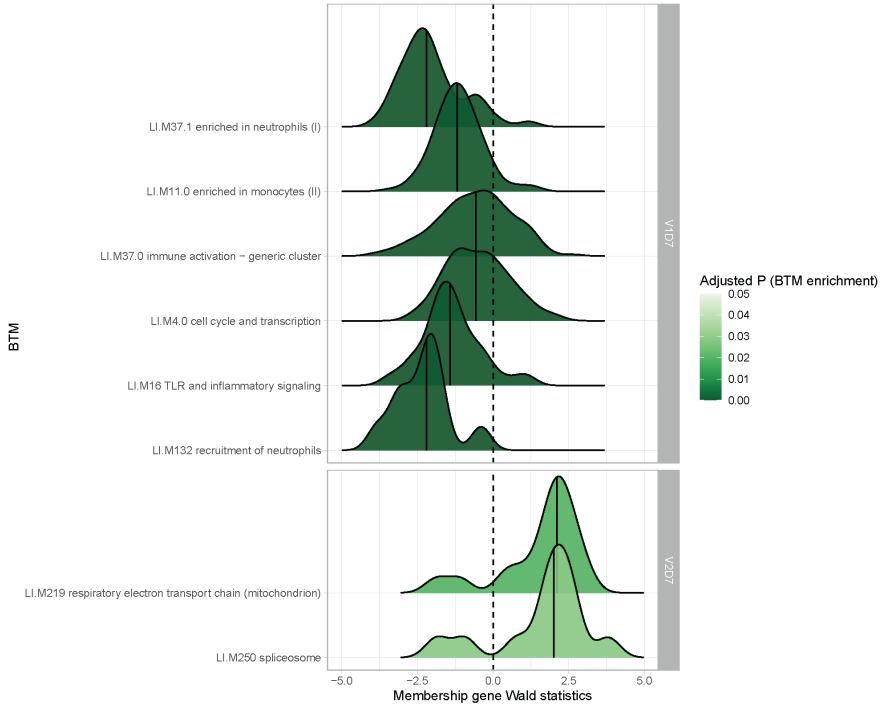

Figure 16. Hemodialysis patients (HD) without prior SARS-CoV-2 infection show increased myeloid activity at V1D7 and decreased metabolic activity at V2D7 compared to controls (HC). The most differentially enriched blood transcription modules (BTMs) between HC and HD with no prior infection with SARS-CoV-2 are shown ($p < 0.05$, FDR-adjusted) at V1D7 and at one week after second vaccination dose (V2D7). Density plots for each BTM represent Wald statistics from DESeq2 analysis for each membership gene per BTM, with positive Wald statistics indicating increased expression in HC compared to HD.

While there were no significant BTM enrichments in HC with positive SARS-CoV-2 Hx, most likely due to the insufficient number of subjects, BTM enrichments for HD with positive SARS-CoV-2 demonstrated notable upregulation of plasma cell activity at V1D7. This contrasts with V1D7 for HD with negative SARS-CoV-2, which show primary enrichment of myeloid BTMs (**Figure 15**). The remainder of these enrichments are shown in **Figure 17**.

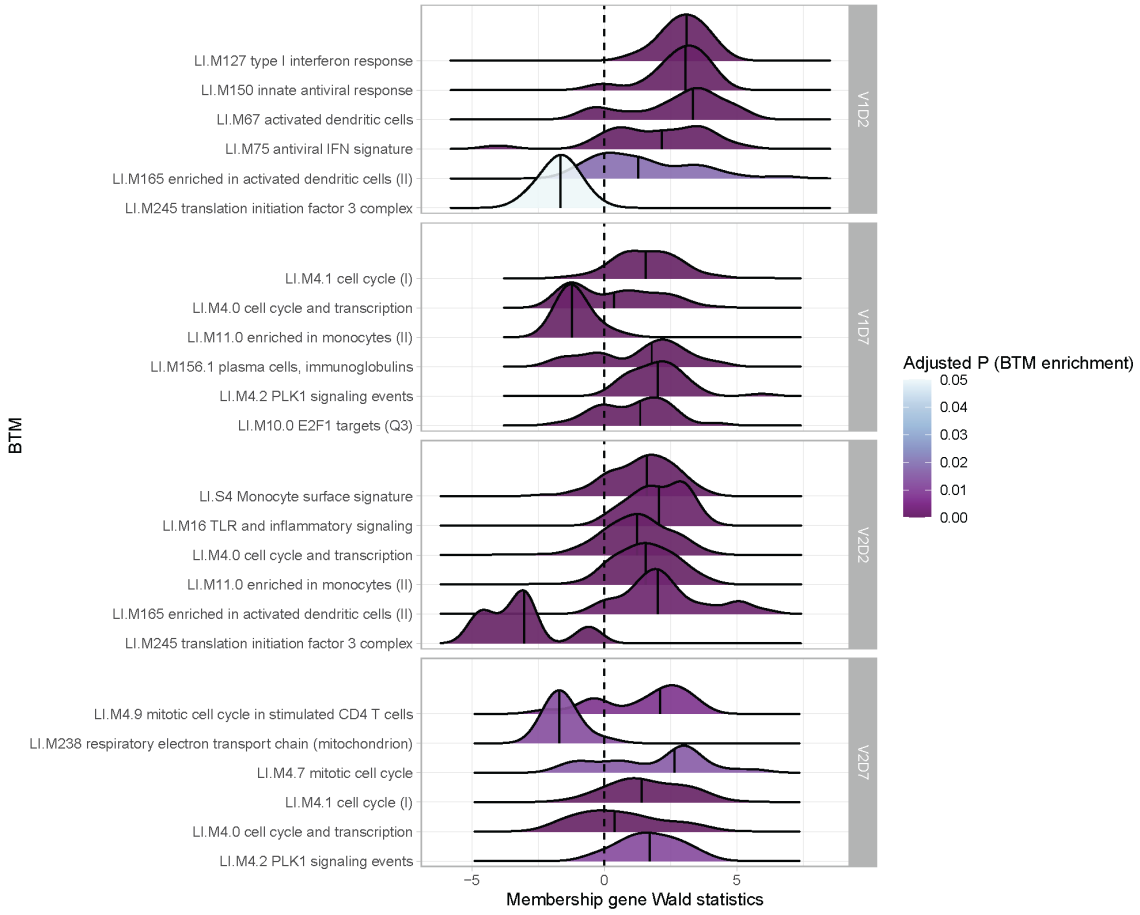

Figure 17. Hemodialysis patients (HD) with prior SARS-CoV-2 infection show increased expression of innate and adaptive immune blood transcription modules (BTMs) post-vaccination.

The most significantly enriched BTMs are shown (up to six) for Day 2 (D2) and Day 7 (D7) after each vaccination dose (V1, V2) in HD with prior infection with SARS-CoV-2 ($p < 0.05$, FDR-adjusted). Density plots for each BTM represent Wald statistics from DESeq2 analysis for each membership gene, thereby representing increased or decreased expression per gene at each time point compared to baseline (V1D0 or V2D0).

Summary enrichments using BTM families show many positive early V1 enrichments of Type 1 IFN activity that dissipate by V1D7 in both HC and HD (**Figure 18**). However, HC show early positive and negative enrichments of myeloid/inflammatory family activity that dissipate by V1D7, while HD show many early positive enrichments of myeloid/inflammatory family activity that persist and increase at V1D7. Following V2, HC show early predominance of dendritic cell

(DC)/antigen presenting cell (APC), IFN Type I, and myeloid/inflammatory family activity transitioning to B cell and cell cycle activity at V2D7, while HD show predominant early IFN type I family activity transitioning to just one detectable cell cycle module enrichment.

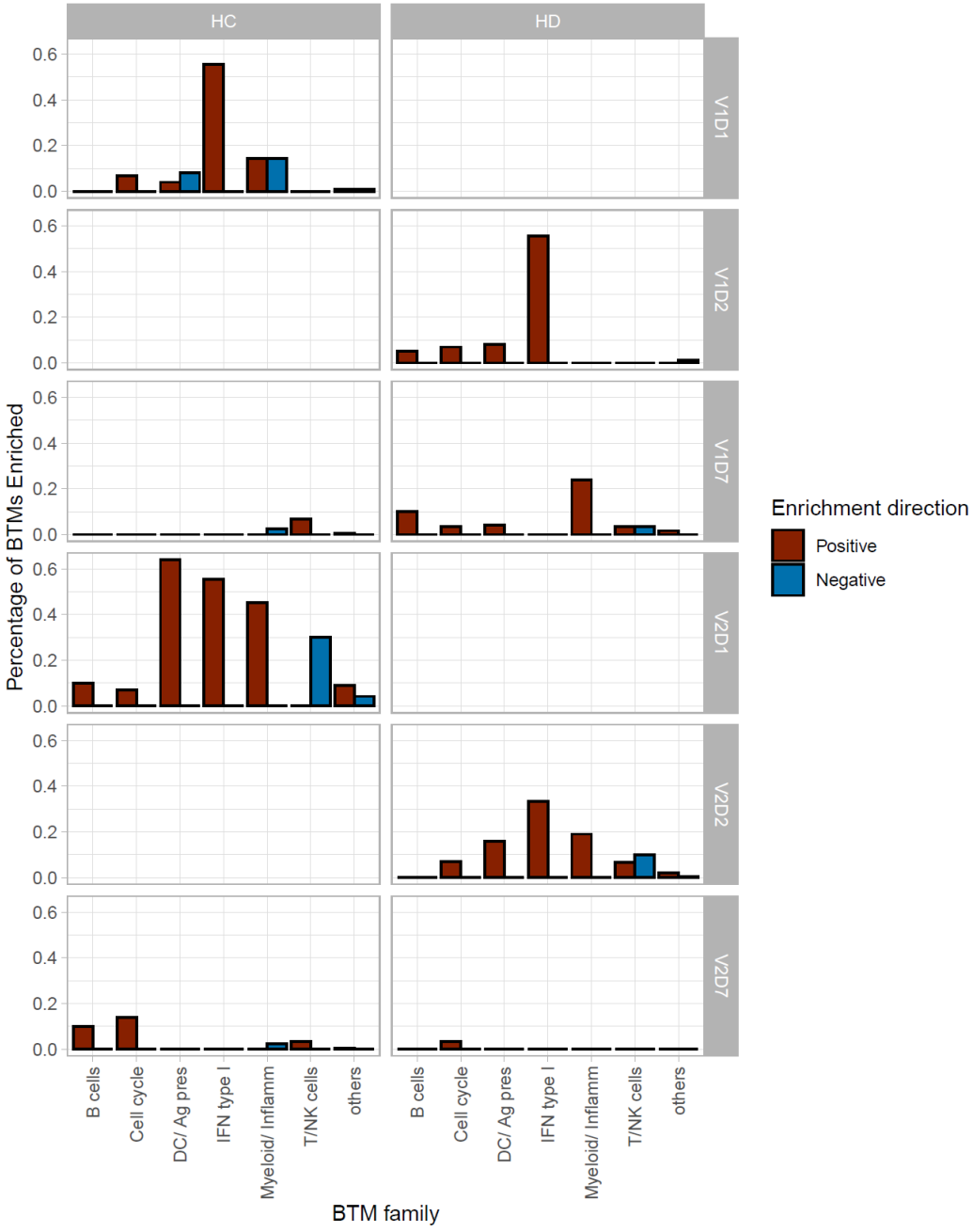

Figure 18. Controls (HC) and maintenance hemodialysis subjects (HD) demonstrate differing

time courses of blood transcription module (BTM) enrichment after each vaccination dose. Percentage of BTMs in each BTM family with significant enrichment at each time point after each vaccination dose (V1, V2) for Day 1 (D1) and Day 7 (D7) in HC, and Day 2 (D2) and D7 for HD in subjects with no prior infection with SARS-CoV-2 ($p < 0.05$, FDR-adjusted). Direction of enrichment was determined using the median Wald statistic from DESeq2 analysis for each BTM membership gene, thereby representing overall increased or decreased expression of membership genes at each time point compared to baseline (V1D0 or V2D0).

4.3.4. Antibody Binding and Neutralization Assay Response

We next aimed to assess immune protection conferred by the vaccine through quantification of anti- spike IgG antibodies and functional assessment of neutralizing antibodies. All subjects demonstrated an increase in anti-spike IgG at V2D7, with titers for all subjects except one still elevated above baseline at six months. The exception was one HD subject with prior SARS-CoV-2 infection who demonstrated the highest baseline titers of all subjects prior to vaccination. Both HC and HD subjects demonstrated a statistically significant increase in anti-spike IgG and neutralization activity (ID50) from V1D0 to V2D7 ($p < 0.001$), followed by an expected decrease at M6 from V2D7 levels ($p < 0.001$) (**Figure 19**). Despite this decrease, M6 titers were still increased compared to baseline ($p< 0.001$).

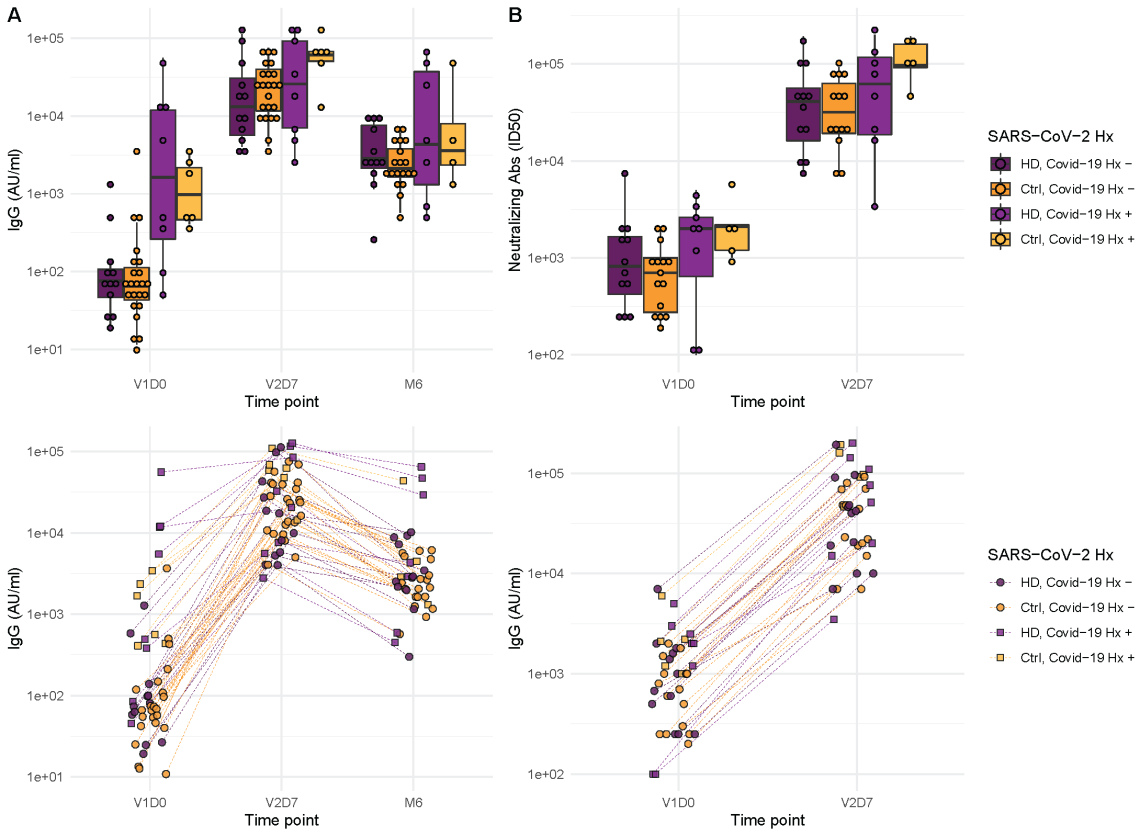

Figure 19. Antibodies significantly increased_in controls and maintenance hemodialysis (HD) one week after the second vaccination dose ($p < 0.001$) and six months after initial vaccination ($p < 0.001$) with the BNT162b2 mRNA COVID-19 vaccine.

(A) Anti-spike IgG levels in controls and HD subjects with and without prior SARS-CoV-2 history before vaccination (V1D0), one week after second vaccination dose (V2D7), and six months after initial vaccination (M6). (B) Antibody neutralization activity (ID50) in controls and HD subjects with and without prior SARS-CoV-2 history at V1D0 and V2D7.

Higher anti-spike IgG at V2D7 was significantly predicted by higher pre-vaccination anti-spike IgG, control group assignment, and younger age ($p < 0.01$, $p < 0.05$, $p < 0.05$, respectively), while gender, race, and ethnicity were not. Higher anti-spike IgG at M6 was significantly predicted by higher V2D7 anti-spike IgG ($p < 0.001$), with no additional predictive value conferred by SARS-CoV-2 history, subject group, age, gender, race, or ethnicity. Higher neutralization activity (ID50) at V2D7 was significantly predicted by higher pre-vaccination ID50, with no additional predictive value conferred by subject group, age, gender, race, and ethnicity.

4.3.5. Transcriptomic and clinical predictors of antibody binding response in HD

Linear models to predict anti-Spike IgG at V2D7 and at M6 in HD using enriched BTMs, controlling for SARS-CoV-2 history, identified BTM predictors at all time points except for V1D2. Of the 18 enriched BTMs at V1D7, increased expression (from V1D0) of "LI.M156.1 plasma cells, immunoglobulins" was predictive of higher anti-spike IgG at V2D7 ($p < 0.05$, FDR-corrected), controlling for SARS-CoV-2 history. Of the 30 enriched BTMs at V2D2, increased expression of 18 BTMs was predictive of higher anti-Spike IgG at V2D7 ($p < 0.05$, FDR-corrected). These include innate immune, antigen presentation, and T cell pathways (**Figure 20**). Increased expression of "LI.M4.2 PLK1 signaling events" at V2D7 compared to V2D0, which was the only enriched module at this time point for HD subjects with no SARS-CoV-2 history, was predictive of higher anti-spike IgG at both V2D7 and M6 ($p < 0.05$).

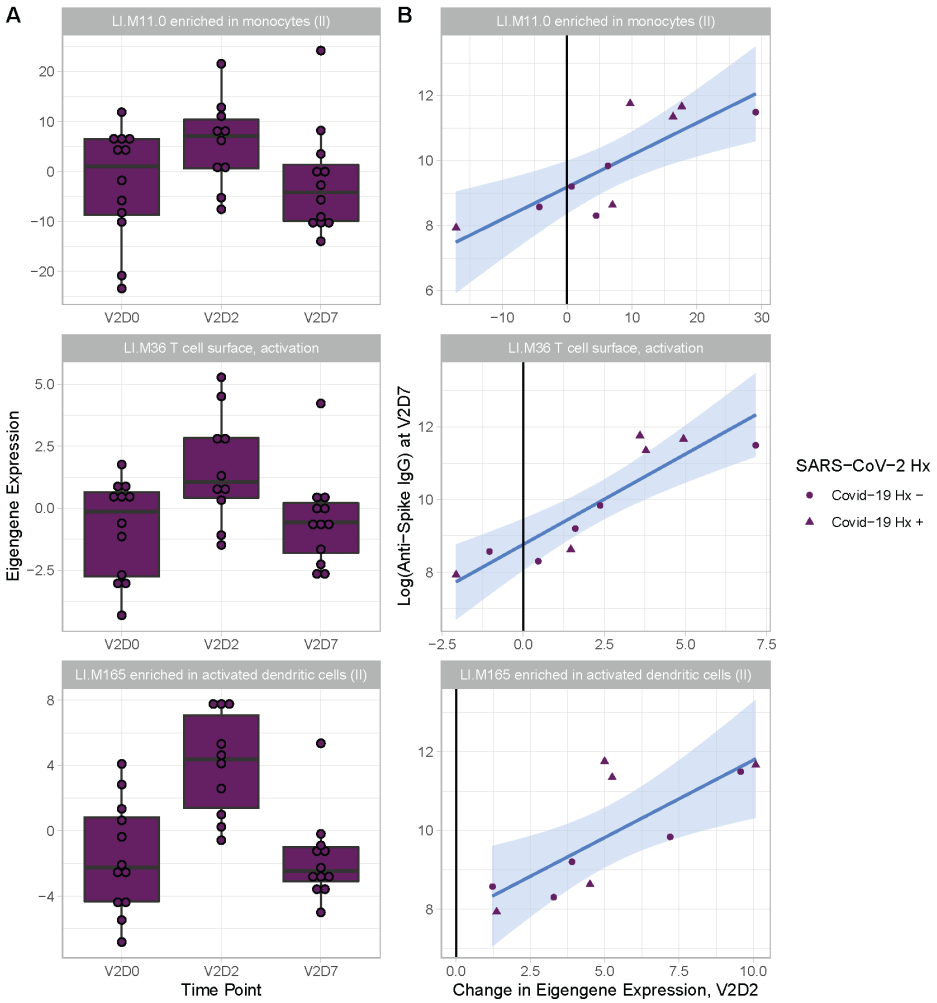

Figure 20. Increased expression of multiple Blood Transcription Modules (BTMs) at V2D2 is predictive of higher anti-spike IgG at V2D7.
Of 30 enriched BTMs at V2D2, increased expression of 18 BTMs is predictive of increased anti-spike IgG at V2D7 ($p < 0.05$, FDR-corrected), controlling for SARS-CoV-2 history. Predictive pathways include innate immune, antigen presentation, and T cell pathways. Three examples are shown.

Linear models to predict anti-Spike IgG at V2D7 and at M6 In HD using clinical predictors yielded significant baseline and post-vaccination predictors. Baseline ferritin levels in the intermediate range (200 – 2000 ng/ml) were associated with higher anti-spike IgG at V2D7 and M6 ($p < 0.01$, $p < 0.05$), controlling for history of SARS-CoV-2. URR, WBC counts, transferrin saturation, and hemoglobin were not significant predictors of antibody development. **Figure 21A**

shows anti-spike IgG at V2D7 as a function of baseline ferritin levels, identifying the intermediate range of ferritin which has previously been associated with lowest all-cause mortality (Kalantar-Zadeh et al., 2005)

The LFC of WBCs from baseline after the first vaccination dose was significantly predictive of antibody titer levels at both V2D7 ($p < 0.01$) and M6 ($p < 0.05$), controlling for SARS-CoV-2 history and number of days after vaccination that labs were collected (**Figure 21B**). The predictive value of LFC of WBCs is predominantly driven by increased lymphocyte counts; LFC of absolute lymphocyte counts was predictive of V2D7 ($p < 0.01$) and M6 (trend-level, $p = 0.056$) antibody titers, controlling for initial antibody titers and date of clinical labs.

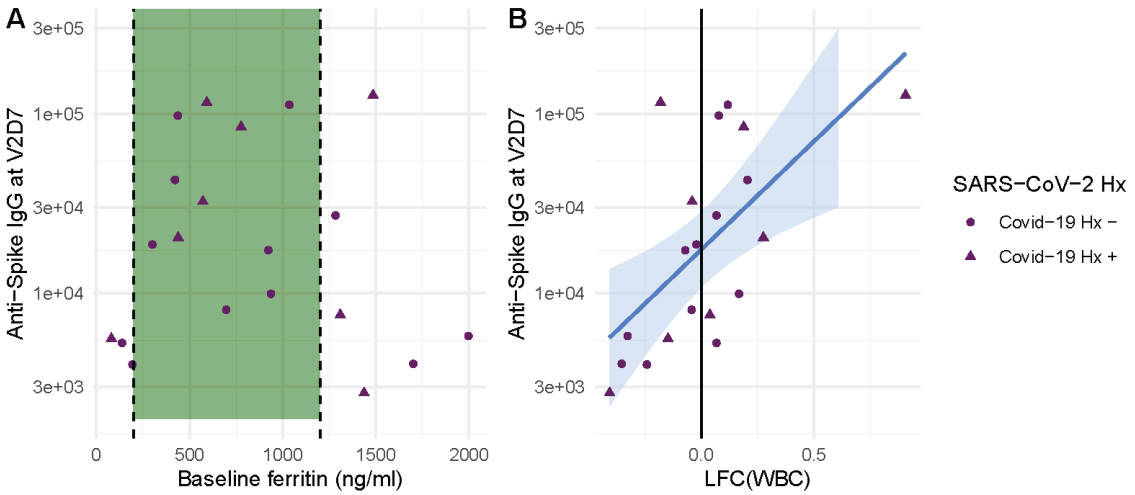

Figure 21. Baseline ferritin level and post-V1 white blood cell count (WBC) are clinical predictors of post-V2 antibody responses in maintenance hemodialysis patients (HD).
(A) Ferritin levels associated with lowest all-cause mortality predict the development of higher anti-spike IgG after vaccination at V2D7 ($p < 0.01$) and M6 (not shown, $p < 0.05$) in maintenance HD patients. Dashed vertical lines indicate the intermediate range of ferritin (200-1200 ng/ml) associated with lowest all-cause mortality (Kalantar-Zadeh et al., 2005). (B) Increased WBC after first vaccination dose is predictive of anti-spike IgG titers after vaccination at V2D7 ($p < 0.01$) and M6 (not shown, $p < 0.05$) in maintenance HD patients. Points with negative log-fold change of white blood cell counts (LFC(WBC)) and positive LFC(WBC) represent a decrease and increase, respectively, in WBC from baseline labs.

4.4. Discussion

Our results demonstrate differing expression of BTMs and differing time courses of immune responses to the BTN162b2 mRNA COVID-19 vaccination in maintenance hemodialysis subjects (HD) compared to controls. Controls demonstrated expected transitions from early Type I interferon and myeloid activity to T cell activity after the first vaccination dose (**Figure 15**, **Figure 18**). The predominant positive enrichment of T cell modules in controls at one week after the first vaccination dose (V1D7) was contrasted with predominant positive enrichment of myeloid modules in HD at V1D7. These results support prior evidence of decreased antigen presentation (Lim et al. 2007; Satomura et al. 2002) and decreased T cell proliferation (Stenvinkel et al. 2005) in end stage renal disease (ESRD). Interestingly, HD showed prolonged upregulation of myeloid activity at V1D7, while controls showed downregulation of these modules at V1D7 (**Figure 15**, **Figure 16**). Overall, these observations indicate prolonged myeloid responses but impaired or delayed progression to T cell responses in the HD cohort. Prior studies have shown alterations of all three classes of immune system pattern recognition receptors (PRR) (Kato et al. 2008); increased expression of mannose-binding lectin, a secreted PRR, and increased expression of major macrophage scavenger receptors SR-A and CD36 (Ando et al. 1996), but decreased expression of toll-like receptor 4 (TLR4) (Ando et al. 2006), a signaling PRR. Because TLRs are important for T-cell activation by antigen presenting cells (APCs) (Kato et al. 2008), and given impaired APC function in dialysis patients (Eleftheriadis et al. 2007), it is plausible that the pattern-recognition receptor alterations of ESRD impair APC-mediated activation of T cell responses while driving persistent myeloid cell activity.

Following the second vaccination dose, controls demonstrated prominent early dendritic

cell (DC)/antigen presentation cell (APC), myeloid, and IFN type I activity transitioning to B cell and cell cycle activity (**Figure 18**). HD demonstrated early DC/APC activity, but to a lesser degree than innate immune modules. At V2D7, metabolic activity was decreased in HD compared to controls. Interestingly, HD demonstrated increased V2D7 expression compared to controls of pro-apoptotic Bcl-2 family member BH3, a mediator of lymphocyte apoptosis. A prior study showed accelerated in vitro apoptosis of lymphocytes in uremia, with a particularly pronounced effect on B cells, mediated by dysregulation of Bcl-2. This suggests a potential role of lymphocyte apoptosis in diminished immune responses to vaccination in HD.

Our results demonstrate significant elevation of anti-spike IgG titers after two doses of BNT162b2 mRNA COVID-19 vaccination in both HD and controls. HD demonstrated only a slight decrease of IgG levels at V2D7 when controlling for SARS-CoV-2 history ($p < 0.05$) and no statistically significant difference at six months. Prior studies comparing short-term antibody response to BNT162b2 mRNA COVID-19 vaccination in HD versus controls find antibody response rates of 84-96% in HD after two vaccination doses, but with lower mean IgG levels compared to controls (Agur et al. 2021; Anand et al. 2021; Attias et al. 2021; Drakesmith et al. 2021; Grupper et al. 2021; Jahn et al. 2021; Longlune et al. 2021). Notably, the HD population studied here is younger and more racially and ethnically diverse. The average age of HD cohorts in prior studies was predominantly in the 60s, compared to an average age of 54 in our study. Jahn et al. found in a subset analysis that HD patients under 60 years of age responded equally to healthy controls, suggesting an interaction between increasing age and less effective antibody response in HD patients (Jahn et al. 2021).

HD subjects with documented SARS-CoV-2 infection prior to vaccination had wider

variance of antibody titers at all time points in this study, with two subjects demonstrating V1D0 antibody titer levels similar to that of uninfected subjects. These two subjects consistently had the lowest titer levels at V2D7 and M6 within the group of previously infected subjects and amongst the lowest titers across all subjects. One subject is the oldest enrolled patient, and both are diagnosed with hyperlipidemia.

Given previously and presently demonstrated the wider variance of protective immune responses in HD and altered interactions with risk factors including age, it is valuable to identify predictors of the strength of immune response to vaccination in this population. We identified both transcriptomic and clinical predictors of anti-spike IgG development at both V2D7 and six months after the second vaccination dose (M6). Increased gene expression of blood transcription modules (BTMs) including monocyte activity, dendritic cell and antigen presentation activity, IFN type I activity, and T cell activation two days after the second vaccination dose (V2D2) in HD were predictive of V2D7 anti-spike IgG. Additionally, increased expression of PLK1 signaling events, indicating increased cell cycle activity, at V2D7 was predictive of V2D7 and M6 anti-spike IgG. Clinically, serum ferritin values in the intermediate range at baseline predicted stronger anti-spike IgG development. A prior study of 58,058 maintenance HD subjects found serum ferritin levels between 200 and 1200 ng/ml to be associated with lower all-cause mortality, due to ferritin <200 ng/ml representing low iron status, and >1200 ng/ml representing a hyper-inflammatory state due to ferritin's status as an acute phase reactant (Kalantar-Zadeh et al. 2005). Iron deficiency has been linked to impaired immune response and vaccine efficacy in other infections, while inflammation induces macrophage release of the heavy chain component of ferritin, FTH, which has been reported to inhibit lymphocyte proliferation and function (Drakesmith et al. 2021;

Kernan and Carcillo 2017). Additionally, increased LFC in WBC count 1-3 weeks after vaccination was predictive of higher antibody titers.

Our study is limited by different early time points between controls and HD (Day 1 vs Day 2 after each vaccination dose) and by sample size, particularly when subdividing SARS-CoV-2 history. The smaller sample size additionally limits our ability to characterize differential immune pathways in clinical subsets of the dialysis population, such as those with low, medium, and high baseline ferritin levels. Future studies are needed for more comprehensive characterization of the immune pathway recruitment in response to the Covid-19 vaccinations in this population. The Covid-19 mRNA vaccines are proving more efficacious than other vaccines in the ESRD population; for example, while more than 90% of patients without chronic kidney disease develop protective antibodies against hepatitis B after vaccination, only 50-60% of patients with ESRD seroconvert (Eleftheriadis et al., 2007). One explanation is that, in mRNA vaccines, the mRNA both encodes the viral antigen and acts as an adjuvant due to its innate immunostimulatory properties; the mRNA is recognized by endosomal and cytosolic innate sensors upon cell entry, resulting in cellular activation and production of type I interferons and other inflammatory mediators (Teijaro and Farber 2021). This elevated innate immune stimulus could overcome immune desensitization in ESRD, evidenced by diminished TLR4 expression on monocytes (Koc et al. 2011) and downregulation of activating receptors on natural killer cells in this population (Nagai 2021). If so, the mRNA vaccine delivery vehicle could prove particularly valuable in vaccine development for ESRD and HD going forward.

Overall, we demonstrate differing time courses of immune responses to the BTN162b2 mRNA COVID-19 vaccination in maintenance hemodialysis subjects (HD) and identify

transcriptomic and clinical predictors of anti-Spike IgG titers in HD. Our results warrant further characterization of the immune dysregulation of ESRD and of immune biomarkers that underlie efficacious immune responses to vaccination in this population.

5. Elucidation of immune dysregulation in maintenance hemodialysis patients using vaccine-stimulated transcriptomics

Includes data and text from manuscript: **Chang YS**, Lee JM, Huang K, Vagts CL, Ascoli C, Perkins DL, Finn PW. Altered transcriptomic immune response of maintenance hemodialysis patients to the Covid-19 mRNA vaccine. medRxiv. Preprint. 2023 Jan 19.

5.1 Introduction

While the previous two chapters characterize the humoral immune response to vaccination and its transcriptomic correlates, this chapter investigates the broader underpinnings of immune dysregulation in end stage renal disease (ESRD). Examination of regulatory processes governing gene expression is particularly relevant in the study of the immune system in ESRD, which is characterized by a duality of (1) immune incompetence leading to increased susceptibility to infection co-existing with (2) immunoactivation which contributes to the progression of atherosclerotic lesions and vascular disease (Stenvinkel et al. 2005). This duality is further complicated by seemingly contradictory literature on ESRD. For example, one study has reported increased expression of toll-like receptor 4 (TLR4) on monocytes leading to increased production of inflammatory cytokines with LPS stimulation in chronic kidney disease (Gollapudi et al. 2010), while another has shown decreased expression of TLR4 with decreased LPS-induced cytokine production (Ando et al. 1996). Additionally, one study demonstrated accelerated apoptosis of B lymphocytes in ESRD accompanied by decreased expression of Bcl-2 (Fernández-Fresnedo et al. 2000), while another study showed no differences of B cell apoptosis, but in fact increased expression of two key B cell differentiation and survival factors IL-7 and BAFF (Pahl et al. 2010). Examination of co-expression and regulatory gene networks may thus yield insights into the complex immune dysregulation of ESRD.

Due the reliance of gene network construction on variance of gene expression, network

perturbation using vaccination as an *in vivo* stimulus will allow for sensitive measurement of altered regulatory interactions. We posit that this vaccine-induced network perturbation will further enable the direct construction of single-subject gene networks through transcriptomic measurements of a given subject across multiple time points surrounding vaccination. Thus, in this study, we characterize underlying gene co-expression networks and regulatory networks in ESRD compared to controls utilizing the BNT162b2 mRNA COVID-19 vaccine as a stimulus.

5.2. Methods

5.2.1. Group-level and single-subject blood transcription module (BTM) network construction

For BTM network construction, BTMs that demonstrated a significant effect of time point on eigengene expression were selected as candidate BTM nodes. Significance of time point was assessed using an ANOVA with main effects of group and time and random effect of subject. The p-values for the main effect of time point were FDR-corrected across BTMs. Candidate BTMs with significant membership gene overlap were excluded by the following criteria: if candidate BTMs overlapped with a Jaccard index greater than 0.2, then only the BTM with the larger number of membership genes was retained. Using this final set of BTMs, pairwise Pearson correlations were performed between all BTM eigengenes across subjects and V1D0, V1D7, V2D0, and V2D7 samples, separately for each subject group to generate one group HC co-expression network and one HD co-expression network.

To compare the HC network to the HD network, Fisher's Z transformation was applied to each network, and then the Z-transformed HC network was subtracted from the Z-transformed HD network to obtain a Z-score difference network. P values for the Z-score difference network,

calculated from a Z-score to p-value transformation, were FDR-adjusted across edges. Edges that were not significantly different between HD and HC after FDR correction were set to 0 in the Z-score difference network.

Single-subject co-expression networks were constructed in a similar fashion to the group networks, but with only four samples per network (V1D0, V1D7, V2D0, V2D7).

5.2.2. Group-level BTM co-expression network comparison

BTMs were categorized into different families: B cells, cell cycle, dendritic cell/antigen presentation, type I interferon (IFN type I), myeloid activity/inflammation/ T/NK cells, and "others" (Braun et al. 2018). In order to characterize differential co-expression (edge weight) of BTMs within each family (intra-family co-expression), we quantified the number of differentially co-expressed edges from the Z difference network that were (1) positively co-expressed in both HD and HC but weaker (less positive) in HD, (2) positively co-expressed in both HD and HC but stronger in HD, (3) negatively co-expressed in both HD and HC but weaker (less negative) in HD, (4) negatively co-expressed in both HD and HC but stronger in HD, (5) positively co-expressed in HD, but negative in HC, (6) negatively co-expressed in HD, but positive in HC.

These numbers of dysregulated edges were then divided by the total number of possible edges within the BTM family (n choose 2, where n is the number of nodes in the BTM family), yielding the percentage of edges within each family demonstrating each class of differential co-expression. A similar approach was used to characterize differential co-expression of BTMs between BTM families (inter-family co-expression). For each BTM family, percentages of dysregulated edges between BTMs within a given a family (first node) and BTMs outside of the family (second node) were quantified. Finally, percentages of dysregulated edges were quantified

pairwise between BTM families.

5.2.3. Single subject-level BTM co-expression network comparison

Edge weight (Fisher Z) distributions for single subject co-expression networks were compared between HD and HC both globally and for each BTM family. A global statistical comparison of edge weights was achieved by quantifying the median positive edge weight per subject, and then comparing these between HD and HC using a student's T-test. Global median negative edge comparisons were performed in the same way.

To characterize differential co-expression of intra-family BTMs, the median positive edge weight across all edges within a BTM family was calculated on a per-subject basis. These median edge weights were then compared between HD and HC using a student's T-test. Median intra-family negative edge weight within each BTM was compared in the same fashion.

A similar approach was used to characterize differential co-expression of inter-family BTMs. For each BTM family, the median positive edge weight across all edges between BTMs within a given family (first node) and BTMs outside of the family (second node) were quantified and then compared between HD and HC. Median inter-family negative co-expression was compared in the same fashion.

5.2.4. Gene regulatory network comparisons

To specifically characterize regulatory interactions underlying altered co-expression networks, gene regulatory networks were constructed separately for HD and HC using PANDA (Passing Messages between Networks for Data assimilation) analysis (Glass et al. 2013). The inputs to the PANDA algorithm are (1) an initial TF-gene regulatory matrix, (2) a protein-protein

interaction matrix, (3) a gene expression matrix. The TF-gene regulatory matrix was derived from the network on the Glass et al. website (https://sites.google.com/a/channing.harvard.edu/kimberlyglass/tools/resources), utilizing TFs present in our variance-stabilized gene expression matrix. The protein-protein interaction matrix was derived from the STRING database interaction scores between all TFs used in the initial TF-gene regulatory matrix.

The output regulatory network for HC was then subtracted from the output HD regulatory network, yielding a regulatory difference network. Gene set enrichment analysis was performed using the *clusterProfiler* R package with BTM gene sets and a list of gene targets ranked by most significant edge differences from the regulatory difference network. BTMs with FDR-adjusted $p < 0.05$ were considered significantly enriched. The core enrichment genes, representing those genes that contribute most to the enrichment signal of the BTM, were obtained for the most enriched BTMs.

5.3. Results

5.3.1. Blood Transcription Module (BTM) co-expression networks per subject group

The HD co-expression BTM network and HC co-expression BTM network demonstrated similar patterns of positive and negative co-expression, or edges (**Figure 22**). Of 3449 statistically significant edges in the across-group network ($p < 0.05$, FDR-corrected), 3149 (91%) were regulated in the same direction for HC and HD (1653 positive, 1496 negative) in both. 127 edges were positively coregulated for HC but negatively coregulated for HD, and 173 edges were positively coregulated for HD but negatively coregulated for HC. Despite these concordant patterns of regulation between the two groups, HD generally exhibited weaker regulation

compared to HC. Of the edges that were positively coregulated in both groups, 241 out of the 1653 (15%) exhibited weaker regulation in HD compared to HC ($p < 0.05$, FDR-adjusted), while only 90/1653 (5%) exhibited stronger positive regulation. Similarly, of the edges that were negatively coregulated in both groups, 236 out of 1496 (16%) edges exhibited weaker negative regulation in HD ($p < 0.05$, FDR-adjusted), while only 21/1496 (1%) exhibited stronger negative regulation in HD.

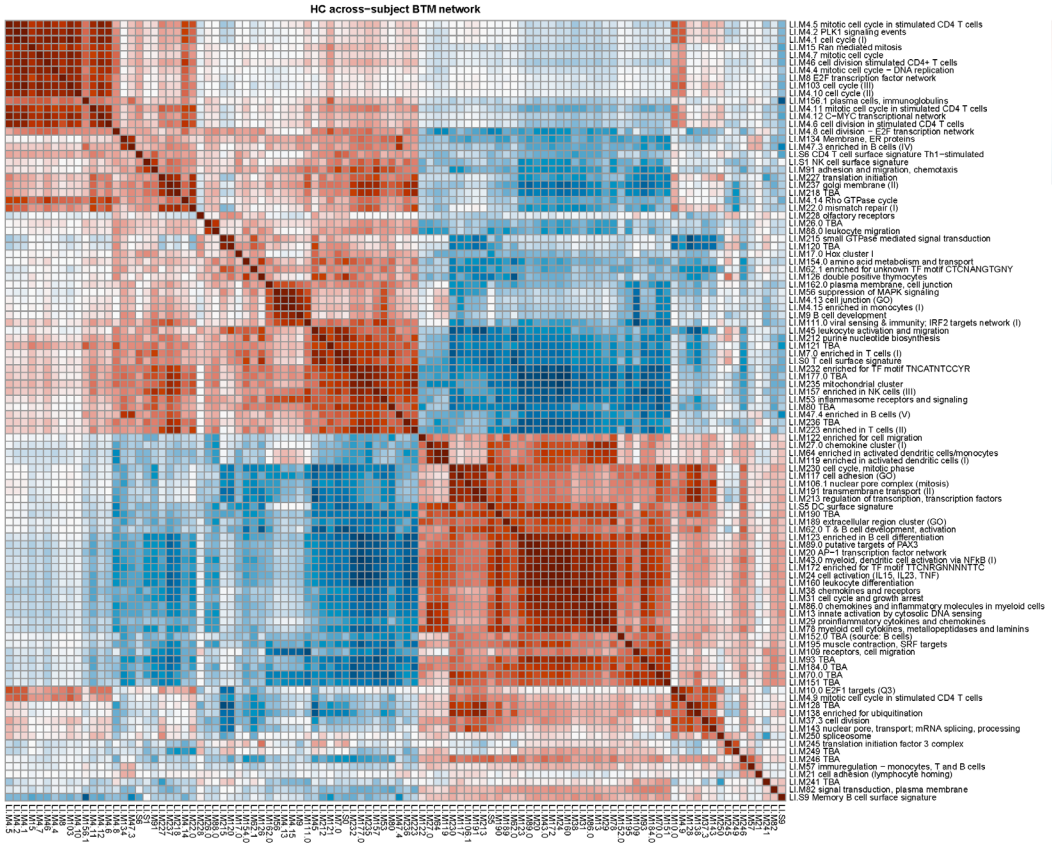
HC across−subject BTM network
LI.M4.5 mitotic cell cycle in stimulated CD4 T cells
LI.M4.2 PLK1 signaling events
LI.M4.1 cell cycle (I)
LI.M15 Ran mediated mitosis
LI.M4.7 mitotic cell cycle
LI.M46 cell division stimulated CD4+ T cells
LI.M4.4 mitotic cell cycle − DNA replication
LI.M6 E2F transcription factor network
LI.M103 cell cycle (III)
LI.M4.10 cell cycle (II)
LI.M156.1 plasma cells, immunoglobulins
LI.M4.11 mitotic cell cycle in stimulated CD4 T cells
LI.M4.12 C−MYC transcriptional network
LI.M4.6 cell division in stimulated CD4 T cells
LI.M4.8 cell division − E2F transcription network
LI.M134 Membrane, ER proteins
LI.M47.3 enriched in B cells (IV)
LI.S6 CD4 T cell surface signature Th1−stimulated
LI.S1 NK cell surface signature
LI.M91 adhesion and migration, chemotaxis
LI.M227 translation initiation
LI.M237 golgi membrane (II)
LI.M218 TBA
LI.M4.14 Rho GTPase cycle
LI.M22.0 mismatch repair (I)
LI.M229 olfactory receptors
LI.M26.0 TBA
LI.M88.0 leukocyte migration
LI.M215 small GTPase mediated signal transduction
LI.M120 TBA
LI.M17.0 Hox cluster I
LI.M154.0 amino acid metabolism and transport
LI.M62.1 enriched for unknown TF motif CTCNANGTGNY
LI.M126 double positive thymocytes
LI.M162.0 plasma membrane, cell junction
LI.M56 suppression of MAPK signaling
LI.M4.13 cell junction (GO)
LI.M4.15 enriched in monocytes (I)
LI.M9 B cell development
LI.M111.0 viral sensing & immunity; IRF2 targets network (I)
LI.M45 leukocyte activation and migration
LI.M212 purine nucleotide biosynthesis
LI.M121 TBA
LI.M7.0 enriched in T cells (I)
LI.S0 T cell surface signature
LI.M232 enriched for TF motif TNCATNTCCYR
LI.M177.0 TBA
LI.M235 mitochondrial cluster
LI.M157 enriched in NK cells (III)
LI.M53 inflammasome receptors and signaling
LI.M80 TBA
LI.M47.4 enriched in B cells (V)
LI.M236 TBA
LI.M223 enriched in T cells (II)
LI.M122 enriched for cell migration
LI.M27.0 chemokine cluster (I)
LI.M64 enriched in activated dendritic cells/monocytes
LI.M119 enriched in activated dendritic cells (I)
LI.M230 cell cycle, mitotic phase
LI.M117 cell adhesion (GO)
LI.M106.1 nuclear pore complex (mitosis)
LI.M191 transmembrane transport (II)
LI.M213 regulation of transcription, transcription factors
LI.S5 DC surface signature
LI.M190 TBA
LI.M189 extracellular region cluster (GO)
LI.M62.0 T & B cell development, activation
LI.M123 enriched in B cell differentiation
LI.M89.0 putative targets of PAX3
LI.M20 AP−1 transcription factor network
LI.M43.0 myeloid, dendritic cell activation via NFkB (I)
LI.M172 enriched for TF motif TTCNRGNNNNTTC
LI.M24 cell activation (IL15, IL23, TNF)
LI.M160 leukocyte differentiation
LI.M38 chemokines and receptors
LI.M31 cell cycle and growth arrest
LI.M86.0 chemokines and inflammatory molecules in myeloid cells
LI.M13 innate activation by cytosolic DNA sensing
LI.M29 proinflammatory cytokines and chemokines
LI.M78 myeloid cell cytokines, metallopeptidases and laminins
LI.M152.0 TBA (source: B cells)
LI.M195 muscle contraction, SRF targets
LI.M109 receptors, cell migration
LI.M93 TBA
LI.M184.0 TBA
LI.M70.0 TBA
LI.M151 TBA
LI.M10.0 E2F1 targets (Q3)
LI.M4.9 mitotic cell cycle in stimulated CD4 T cells
LI.M128 TBA
LI.M138 enriched for ubiquitination
LI.M37.3 cell division
LI.M143 nuclear pore, transport; mRNA splicing, processing
LI.M250 spliceosome
LI.M245 translation initiation factor 3 complex
LI.M248 TBA
LI.M246 TBA
LI.M57 immuregulation − monocytes, T and B cells
LI.M21 cell adhesion (lymphocyte homing)
LI.M241 TBA
LI.M82 signal transduction, plasma membrane
LI.S9 Memory B cell surface signature
1
0.5
0
−0.5
−1

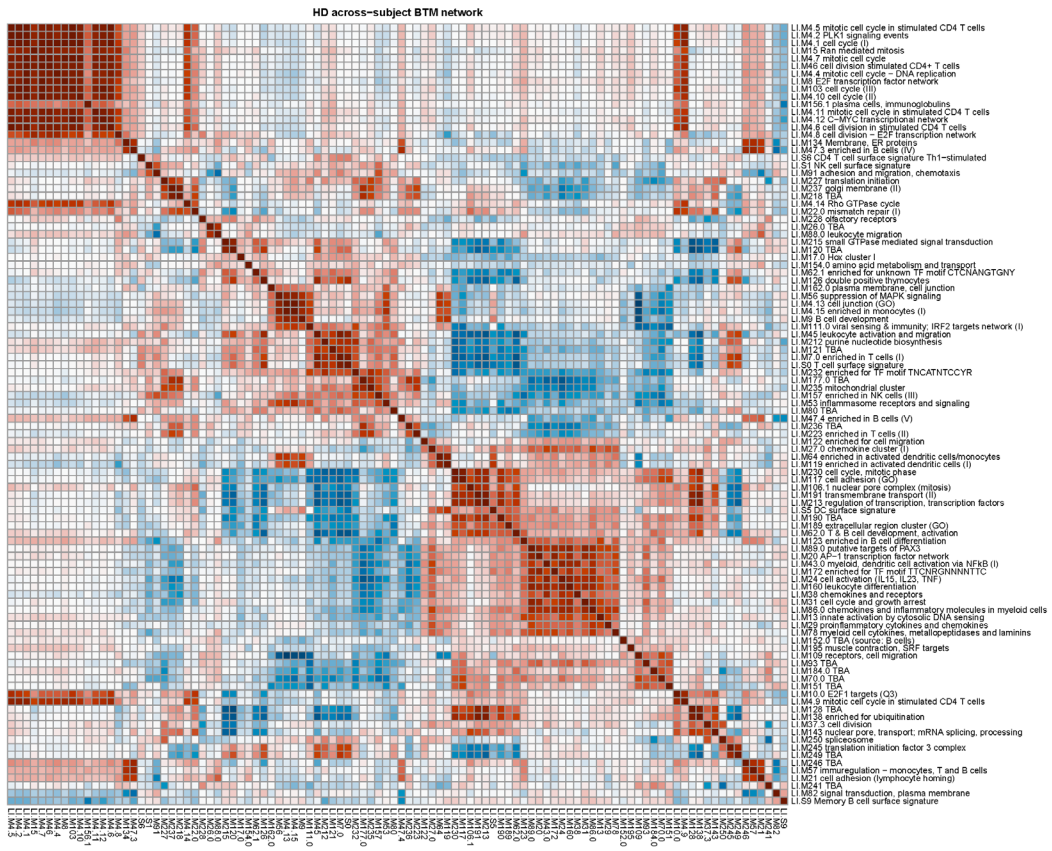
HD across−subject BTM network
LI.M4.5 mitotic cell cycle in stimulated CD4 T cells
LI.M4.2 PLK1 signaling events
LI.M4.1 cell cycle (I)
LI.M15 Ran mediated mitosis
LI.M4.7 mitotic cell cycle
LI.M46 cell division stimulated CD4+ T cells
LI.M4.4 mitotic cell cycle − DNA replication
LI.M6 E2F transcription factor network
LI.M103 cell cycle (III)
LI.M4.10 cell cycle (II)
LI.M156.1 plasma cells, immunoglobulins
LI.M4.11 mitotic cell cycle in stimulated CD4 T cells
LI.M4.12 C−MYC transcriptional network
LI.M4.6 cell division in stimulated CD4 T cells
LI.M4.8 cell division − E2F transcription network
LI.M134 Membrane, ER proteins
LI.M47.3 enriched in B cells (IV)
LI.S6 CD4 T cell surface signature Th1−stimulated
LI.S1 NK cell surface signature
LI.M91 adhesion and migration, chemotaxis
LI.M227 translation initiation
LI.M237 golgi membrane (II)
LI.M218 TBA
LI.M4.14 Rho GTPase cycle
LI.M22.0 mismatch repair (I)
LI.M229 olfactory receptors
LI.M26.0 TBA
LI.M88.0 leukocyte migration
LI.M215 small GTPase mediated signal transduction
LI.M120 TBA
LI.M17.0 Hox cluster I
LI.M154.0 amino acid metabolism and transport
LI.M62.1 enriched for unknown TF motif CTCNANGTGNY
LI.M126 double positive thymocytes
LI.M162.0 plasma membrane, cell junction
LI.M56 suppression of MAPK signaling
LI.M4.13 cell junction (GO)
LI.M4.15 enriched in monocytes (I)
LI.M9 B cell development
LI.M111.0 viral sensing & immunity; IRF2 targets network (I)
LI.M45 leukocyte activation and migration
LI.M212 purine nucleotide biosynthesis
LI.M121 TBA
LI.M7.0 enriched in T cells (I)
LI.S0 T cell surface signature
LI.M232 enriched for TF motif TNCATNTCCYR
LI.M177.0 TBA
LI.M235 mitochondrial cluster
LI.M157 enriched in NK cells (III)
LI.M53 inflammasome receptors and signaling
LI.M80 TBA
LI.M47.4 enriched in B cells (V)
LI.M236 TBA
LI.M223 enriched in T cells (II)
LI.M122 enriched for cell migration
LI.M27.0 chemokine cluster (I)
LI.M64 enriched in activated dendritic cells/monocytes
LI.M119 enriched in activated dendritic cells (I)
LI.M230 cell cycle, mitotic phase
LI.M117 cell adhesion (GO)
LI.M106.1 nuclear pore complex (mitosis)
LI.M191 transmembrane transport (II)
LI.M213 regulation of transcription, transcription factors
LI.S5 DC surface signature
LI.M190 TBA
LI.M189 extracellular region cluster (GO)
LI.M62.0 T & B cell development, activation
LI.M123 enriched in B cell differentiation
LI.M89.0 putative targets of PAX3
LI.M20 AP−1 transcription factor network
LI.M43.0 myeloid, dendritic cell activation via NFkB (I)
LI.M172 enriched for TF motif TTCNRGNNNNTTC
LI.M24 cell activation (IL15, IL23, TNF)
LI.M160 leukocyte differentiation
LI.M38 chemokines and receptors
LI.M31 cell cycle and growth arrest
LI.M86.0 chemokines and inflammatory molecules in myeloid cells
LI.M13 innate activation by cytosolic DNA sensing
LI.M29 proinflammatory cytokines and chemokines
LI.M78 myeloid cell cytokines, metallopeptidases and laminins
LI.M152.0 TBA (source: B cells)
LI.M195 muscle contraction, SRF targets
LI.M109 receptors, cell migration
LI.M93 TBA
LI.M184.0 TBA
LI.M70.0 TBA
LI.M151 TBA
LI.M10.0 E2F1 targets (Q3)
LI.M4.9 mitotic cell cycle in stimulated CD4 T cells
LI.M128 TBA
LI.M138 enriched for ubiquitination
LI.M37.3 cell division
LI.M143 nuclear pore, transport; mRNA splicing, processing
LI.M250 spliceosome
LI.M245 translation initiation factor 3 complex
LI.M248 TBA
LI.M246 TBA
LI.M57 immuregulation − monocytes, T and B cells
LI.M21 cell adhesion (lymphocyte homing)
LI.M241 TBA
LI.M82 signal transduction, plasma membrane
LI.S9 Memory B cell surface signature
1
0.5
0
−0.5
−1

Figure 22. Blood transcription module (BTM) co-expression networks demonstrate similar patterns of co-expression for controls (HC, top) and hemodialysis (HD, bottom), but with weaker edges in HD.
BTM networks are constructed from pairwise Pearson correlations between pairs of BTM eigengenes across subjects and time points before each vaccination dose (V1D0, V2D0) and one week after each vaccination dose (V1D7, V2D7), separately for each group.

Figure 23 displays the percentage of intra-family and inter-family edges with differential co-expression in HD compared to HC ($p < 0.05$, FDR-corrected), separately for each BTM family. Notably, the dendritic cell/antigen presentation (*DC/APC*) BTM family showed the most altered intra-family co-expression, with 30% of intra-family edges demonstrating weakened positive co-expression in HD. Of these, the most weakened edge was between *LI.M43.0 (Myeloid, dendritic cell activation via NfkB (I))* and *LI.S5 (DC surface signature)*. There was also substantial weakening of inter-family positive co-expression pairwise between *DC/APC*, *IFN type I*, and the *Myeloid/Inflamm* family.

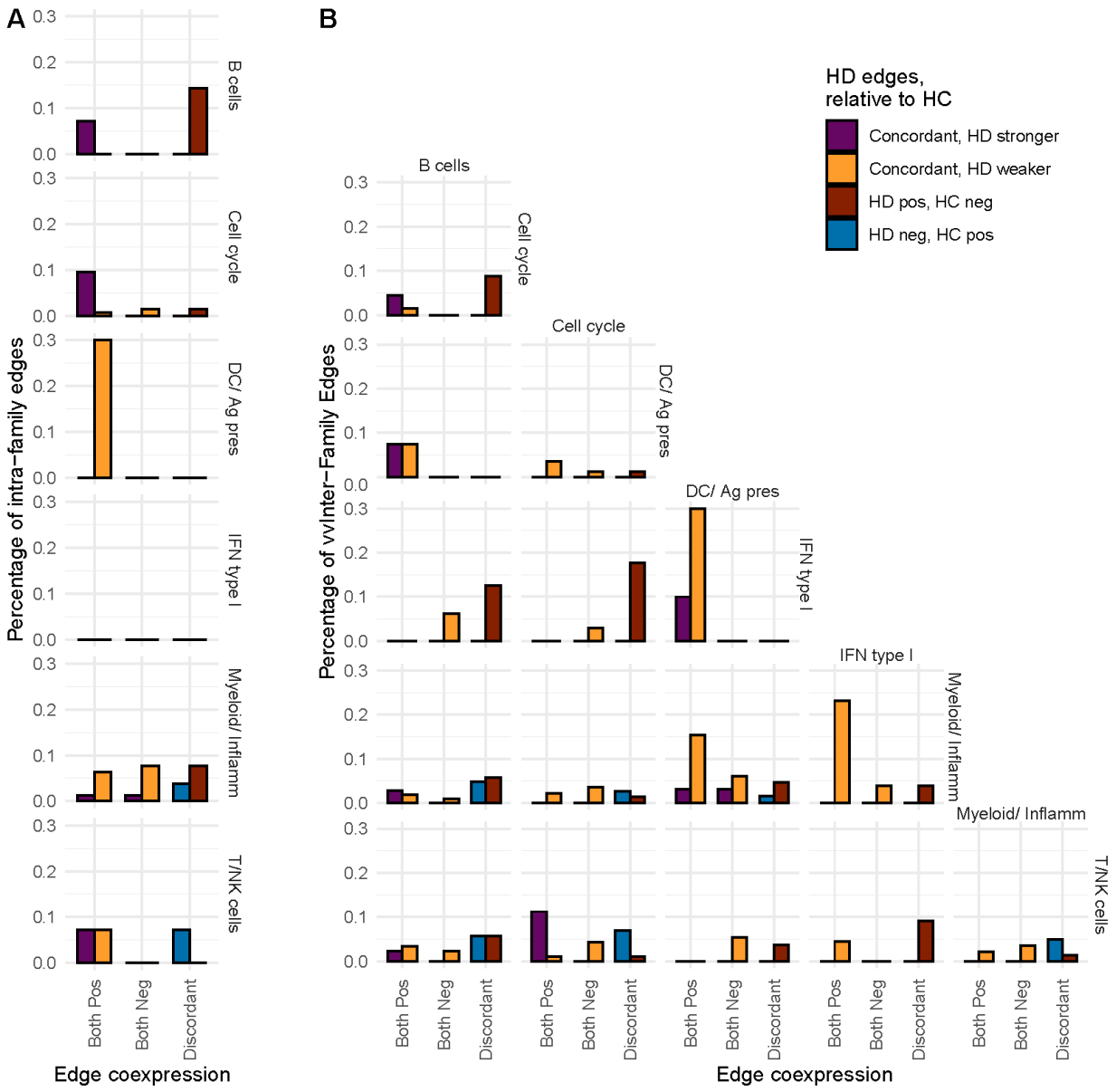

Figure 23. Percentage of all possible edges that are significantly different between controls (HC) and hemodialysis subjects (HD, p < 0.05, FDR), separated by (A) intra-family edges and (B) inter-family edges, pairwise between each set of BTM families.

The number of differentially co-expressed edges between HC and HD that were positively co-expressed in both groups, negatively co-expressed in both, and discordantly co-expressed (opposite signs) was divided by the total number of possible intra-family edges and pairwise inter-family edges.

5.3.2. Single-subject BTM co-expression networks

The single-subject co-expression networks for HC and HD demonstrate appreciable

network structure resembling coarse approximations of their respective group networks (**Figure 24**). Density plots of edge weights across the entire network per subject qualitatively illustrate a weaker bimodal distribution in HD subjects compared to HC (**Figure 25**). This comparison is confirmed statistically with the median edge weight (Fisher Z-value) across all positively coregulated edges being significantly less positive in HD subjects compared to HC ($p < 0.05$) Similarly, the median edge weight across all negatively coregulated edges was significantly less negative in HD subjects compared to HC ($p < 0.05$). These comparisons maintained statistical significance when incorporating SARS-CoV-2 as a covariate

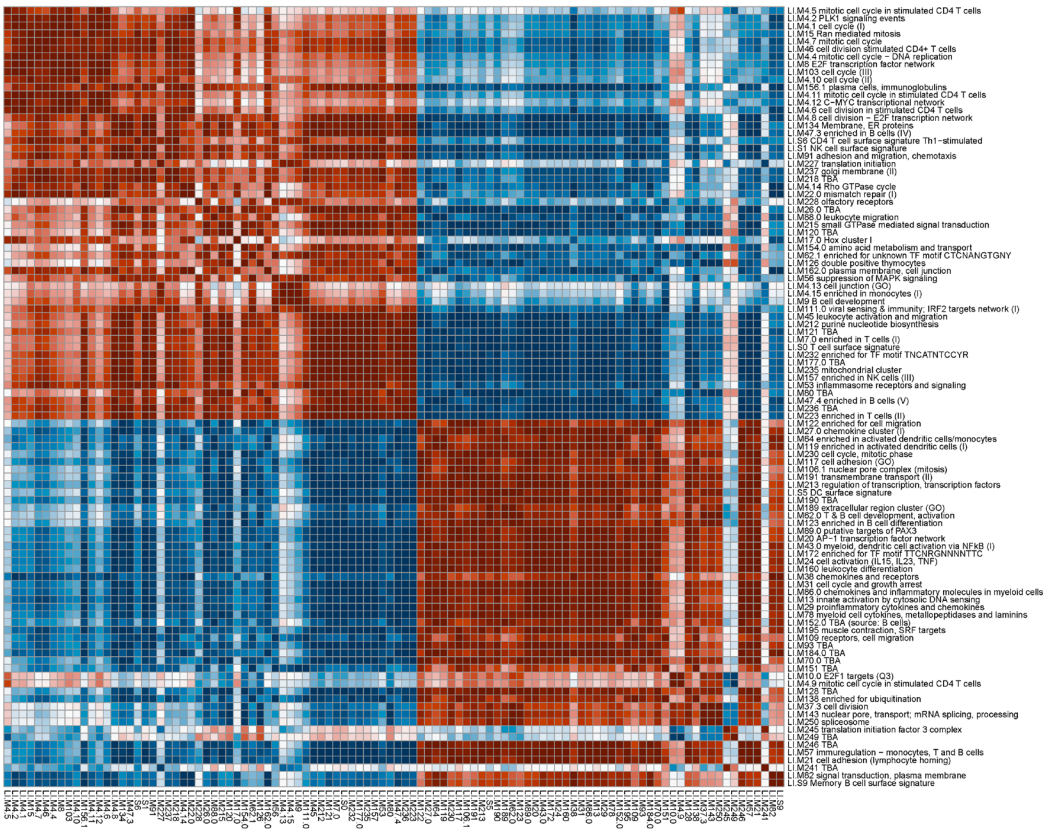
LI.M4.5 mitotic cell cycle in stimulated CD4 T cells
LI.M4.2 PLK1 signaling events
LI.M4.1 cell cycle (I)
LI.M15 Ran mediated mitosis
LI.M4.7 mitotic cell cycle
LI.M46 cell division stimulated CD4+ T cells
LI.M4.4 mitotic cell cycle – DNA replication
LI.M8 E2F transcription factor network
LI.M103 cell cycle (III)
LI.M4.10 cell cycle (II)
LI.M156.1 plasma cells, immunoglobulins
LI.M4.11 mitotic cell cycle in stimulated CD4 T cells
LI.M4.12 C-MYC transcriptional network
LI.M4.6 cell division in stimulated CD4 T cells
LI.M4.8 cell division – E2F transcription network
LI.M134 Membrane, ER proteins
LI.M47.3 enriched in B cells (IV)
LI.S9 CD4 T cell surface signature Th1−stimulated
LI.S1 NK cell surface signature
LI.M91 adhesion and migration, chemotaxis
LI.M227 translation initiation
LI.M237 golgi membrane (II)
LI.M218 TBA
LI.M4.14 Rho GTPase cycle
LI.M22.0 mismatch repair (I)
LI.M228 olfactory receptors
LI.M26.0 TBA
LI.M88.0 leukocyte migration
LI.M215 small GTPase mediated signal transduction
LI.M120 TBA
LI.M17.0 Hox cluster I
LI.M154.0 amino acid metabolism and transport
LI.M62.1 enriched for unknown TF motif CTCNANGTGNY
LI.M126 double positive thymocytes
LI.M162.0 plasma membrane, cell junction
LI.M56 suppression of MAPK signaling
LI.M4.13 cell junction (GO)
LI.M4.15 enriched in monocytes (I)
LI.M9 B cell development
LI.M111.0 viral sensing & immunity; IRF2 targets network (I)
LI.M45 leukocyte activation and migration
LI.M212 purine nucleotide biosynthesis
LI.M121 TBA
LI.M7.0 enriched in T cells (I)
LI.S0 T cell surface signature
LI.M232 enriched for TF motif TNCATNTCCYR
LI.M177.0 TBA
LI.M235 mitochondrial cluster
LI.M157 enriched in NK cells (III)
LI.M53 inflammasome receptors and signaling
LI.M80 TBA
LI.M47.4 enriched in B cells (V)
LI.M236 TBA
LI.M223 enriched in T cells (II)
LI.M122 enriched for cell migration
LI.M27.0 chemokine cluster (I)
LI.M64 enriched in activated dendritic cells/monocytes
LI.M119 enriched in activated dendritic cells (I)
LI.M230 cell cycle, mitotic phase
LI.M117 cell adhesion (GO)
LI.M106.1 nuclear pore complex (mitosis)
LI.M191 transmembrane transport (II)
LI.M213 regulation of transcription, transcription factors
LI.S5 DC surface signature
LI.M190 TBA
LI.M189 extracellular region cluster (GO)
LI.M62.0 T & B cell development, activation
LI.M123 enriched in B cell differentiation
LI.M89.0 putative targets of PAX3
LI.M20 AP−1 transcription factor network
LI.M43.0 myeloid, dendritic cell activation via NFkB (I)
LI.M172 enriched for TF motif TTCNRGNNNTTC
LI.M24 cell activation (IL15, IL23, TNF)
LI.M160 leukocyte differentiation
LI.M38 chemokines and receptors
LI.M31 cell cycle and growth arrest
LI.M86.0 chemokines and inflammatory molecules in myeloid cells
LI.M13 innate activation by cytosolic DNA sensing
LI.M29 proinflammatory cytokines and chemokines
LI.M78 myeloid cell cytokines, metallopeptidases and laminins
LI.M152.0 TBA (source: B cells)
LI.M195 muscle contraction, SRF targets
LI.M109 receptors, cell migration
LI.M93 TBA
LI.M184.0 TBA
LI.M70.0 TBA
LI.M151 TBA
LI.M10.0 E2F1 targets (Q3)
LI.M4.9 mitotic cell cycle in stimulated CD4 T cells
LI.M128 TBA
LI.M138 enriched for ubiquitination
LI.M37.3 cell division
LI.M143 nuclear pore, transport; mRNA splicing, processing
LI.M250 spliceosome
LI.M245 translation initiation factor 3 complex
LI.M249 TBA
LI.M246 TBA
LI.M57 immuregulation − monocytes, T and B cells
LI.M21 cell adhesion (lymphocyte homing)
LI.M241 TBA
LI.M82 signal transduction, plasma membrane
LI.S9 Memory B cell surface signature
1
0.5
0
−0.5
−1

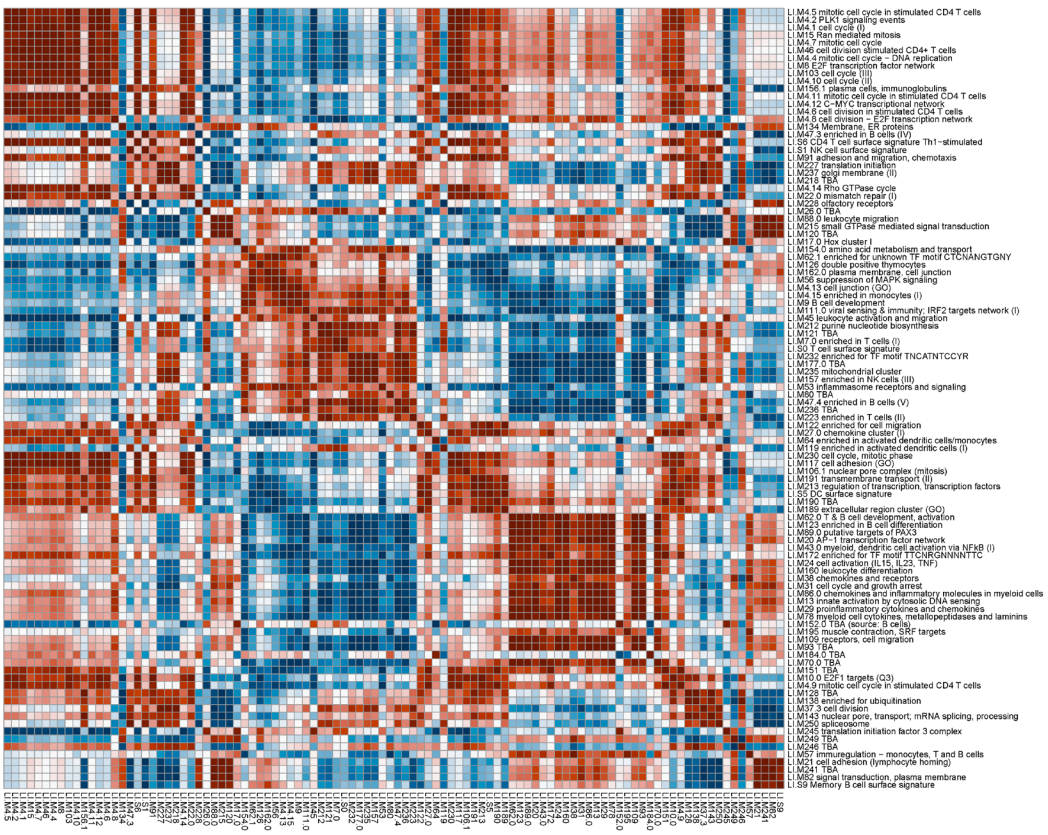
LI.M4.5 mitotic cell cycle in stimulated CD4 T cells
LI.M4.2 PLK1 signaling events
LI.M4.1 cell cycle (I)
LI.M15 Ran mediated mitosis
LI.M4.7 mitotic cell cycle
LI.M46 cell division stimulated CD4+ T cells
LI.M4.4 mitotic cell cycle – DNA replication
LI.M8 E2F transcription factor network
LI.M103 cell cycle (III)
LI.M4.10 cell cycle (II)
LI.M156.1 plasma cells, immunoglobulins
LI.M4.11 mitotic cell cycle in stimulated CD4 T cells
LI.M4.12 C-MYC transcriptional network
LI.M4.6 cell division in stimulated CD4 T cells
LI.M4.8 cell division – E2F transcription network
LI.M134 Membrane, ER proteins
LI.M47.3 enriched in B cells (IV)
LI.S9 CD4 T cell surface signature Th1−stimulated
LI.S1 NK cell surface signature
LI.M91 adhesion and migration, chemotaxis
LI.M227 translation initiation
LI.M237 golgi membrane (II)
LI.M218 TBA
LI.M4.14 Rho GTPase cycle
LI.M22.0 mismatch repair (I)
LI.M228 olfactory receptors
LI.M26.0 TBA
LI.M88.0 leukocyte migration
LI.M215 small GTPase mediated signal transduction
LI.M120 TBA
LI.M17.0 Hox cluster I
LI.M154.0 amino acid metabolism and transport
LI.M62.1 enriched for unknown TF motif CTCNANGTGNY
LI.M126 double positive thymocytes
LI.M162.0 plasma membrane, cell junction
LI.M56 suppression of MAPK signaling
LI.M4.13 cell junction (GO)
LI.M4.15 enriched in monocytes (I)
LI.M9 B cell development
LI.M111.0 viral sensing & immunity; IRF2 targets network (I)
LI.M45 leukocyte activation and migration
LI.M212 purine nucleotide biosynthesis
LI.M121 TBA
LI.M7.0 enriched in T cells (I)
LI.S0 T cell surface signature
LI.M232 enriched for TF motif TNCATNTCCYR
LI.M177.0 TBA
LI.M235 mitochondrial cluster
LI.M157 enriched in NK cells (III)
LI.M53 inflammasome receptors and signaling
LI.M80 TBA
LI.M47.4 enriched in B cells (V)
LI.M236 TBA
LI.M223 enriched in T cells (II)
LI.M122 enriched for cell migration
LI.M27.0 chemokine cluster (I)
LI.M64 enriched in activated dendritic cells/monocytes
LI.M119 enriched in activated dendritic cells (I)
LI.M230 cell cycle, mitotic phase
LI.M117 cell adhesion (GO)
LI.M106.1 nuclear pore complex (mitosis)
LI.M191 transmembrane transport (II)
LI.M213 regulation of transcription, transcription factors
LI.S5 DC surface signature
LI.M190 TBA
LI.M189 extracellular region cluster (GO)
LI.M62.0 T & B cell development, activation
LI.M123 enriched in B cell differentiation
LI.M89.0 putative targets of PAX3
LI.M20 AP−1 transcription factor network
LI.M43.0 myeloid, dendritic cell activation via NFkB (I)
LI.M172 enriched for TF motif TTCNRGNNNTTC
LI.M24 cell activation (IL15, IL23, TNF)
LI.M160 leukocyte differentiation
LI.M38 chemokines and receptors
LI.M31 cell cycle and growth arrest
LI.M86.0 chemokines and inflammatory molecules in myeloid cells
LI.M13 innate activation by cytosolic DNA sensing
LI.M29 proinflammatory cytokines and chemokines
LI.M78 myeloid cell cytokines, metallopeptidases and laminins
LI.M152.0 TBA (source: B cells)
LI.M195 muscle contraction, SRF targets
LI.M109 receptors, cell migration
LI.M93 TBA
LI.M184.0 TBA
LI.M70.0 TBA
LI.M151 TBA
LI.M10.0 E2F1 targets (Q3)
LI.M4.9 mitotic cell cycle in stimulated CD4 T cells
LI.M128 TBA
LI.M138 enriched for ubiquitination
LI.M37.3 cell division
LI.M143 nuclear pore, transport; mRNA splicing, processing
LI.M250 spliceosome
LI.M245 translation initiation factor 3 complex
LI.M249 TBA
LI.M246 TBA
LI.M57 immuregulation − monocytes, T and B cells
LI.M21 cell adhesion (lymphocyte homing)
LI.M241 TBA
LI.M82 signal transduction, plasma membrane
LI.S9 Memory B cell surface signature
1
0.5
0
−0.5
−1

Figure 24. Single subject co-expression networks resemble respective group networks.
Exemplar single-subject co-expression networks are shown for controls (HC, top) and hemodialysis subjects (HD, bottom). BTM networks are constructed from pairwise Pearson correlations between pairs of BTM eigengenes time points before each vaccination dose (V1D0, V2D0) and one week after each vaccination dose (V1D7, V2D7), separately for each subjects.

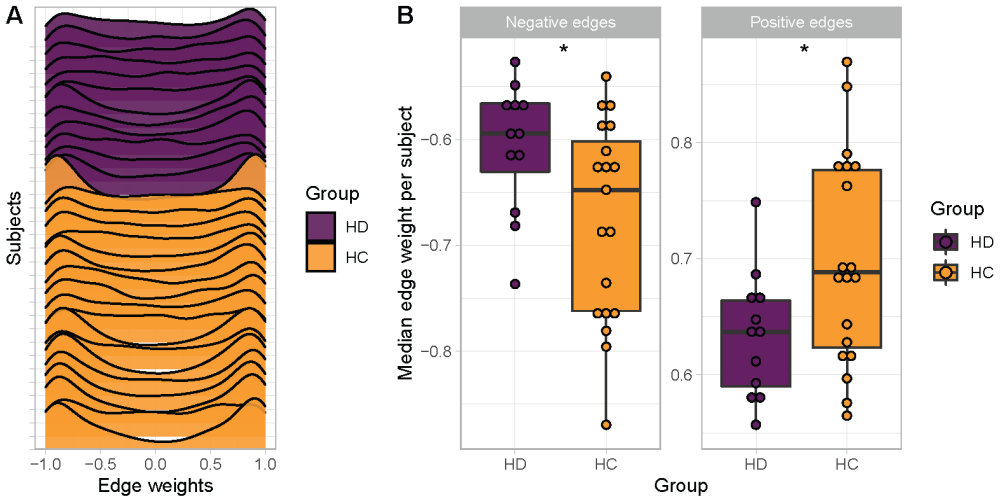

Figure 25. Single-subject co-expression networks demonstrate weaker co-expression in hemodialysis subjects (HD) compared to controls (HC), both for positively and negatively co-expressed blood transcription modules (BTMs).
(A) Density plots of edge weights per subject demonstrating a stronger bimodal distribution in HC subjects compared to HD subjects. (B) Median edge weight across significantly positively co-expressed edges and across significantly negatively co-expressed edges, separately per subject.

Similarly to group-level BTM co-expression networks, the edge differences in single-subject networks were substantially dependent on the BTM family membership of network nodes (BTMs) (**Figure 26**). The *DC/APC* BTM family demonstrated weaker (less positive) inter- and intra-family positive co-expression in HD compared to HC ($p < 0.01$, $p < 0.05$). Like the group-level BTM co-expression networks, the inter-family differences reflected a weakening of positive inter-family regulation pairwise between the *DC/APC*, *IFN type I*, and *Myeloid/Inflamm* families (**Figure 27**). The *DC/APC* BTM family also showed weaker (less negative) inter-family negative co-expression ($p < 0.01$) driven by a weakening of negative co-expression with the *B cell*,

Myeloid/Inflamm, and *T/NK* BTM families. The weakened negative co-expression with the *T/NK* family was the most significantly altered negative edge between all pairs of BTM families ($p < 0.001$). These weakened negative edges are also seen in the group-level BTM co-expression networks (**Figure 23**). The most weakened negative edge between *DC/APC* and *T/NK* from the group network was between *LI.M43.0 (Myeloid, dendritic cell activation via NfkB (I))* and *LI.M7.0 (enriched in T cells (I))*.

The *Myeloid/Inflamm* family demonstrated the most significantly weakened intra-family positive co-expression ($p < 0.0001$). The *T/NK* family was the only BTM family to demonstrate stronger intra-family negative co-expression in HD ($p < 0.05$). Overall, differential co-expression observed between HD and HC single-subject networks is largely reflective of differences observed in the group networks.

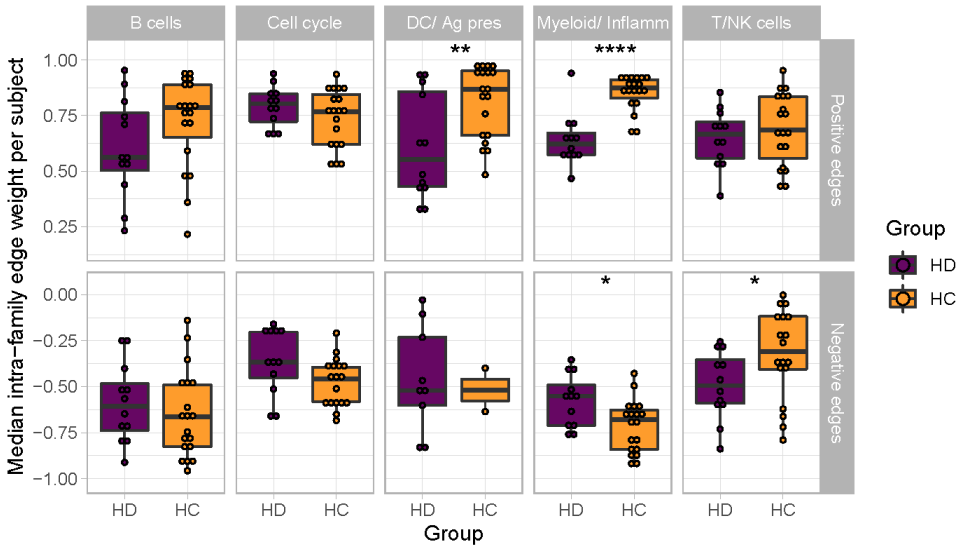

Figure 26. Hemodialysis subjects (HD) demonstrate substantially weaker intra-family positive co-expression within the *Dendritic Cell/Antigen Presentation (DC/APC)* and *Myeloid/Inflammation* blood transcription module (BTM) families.
Median edge strength of intra-family edges is shown for HD and controls, separately for positive edges and negative edges within each BTM family. See Figure S2 for pairwise inter-family median

edge strength between each set of BTM families. *p < 0.05, ** p < 0.01, *** p < 0.001, **** p < 0.0001.

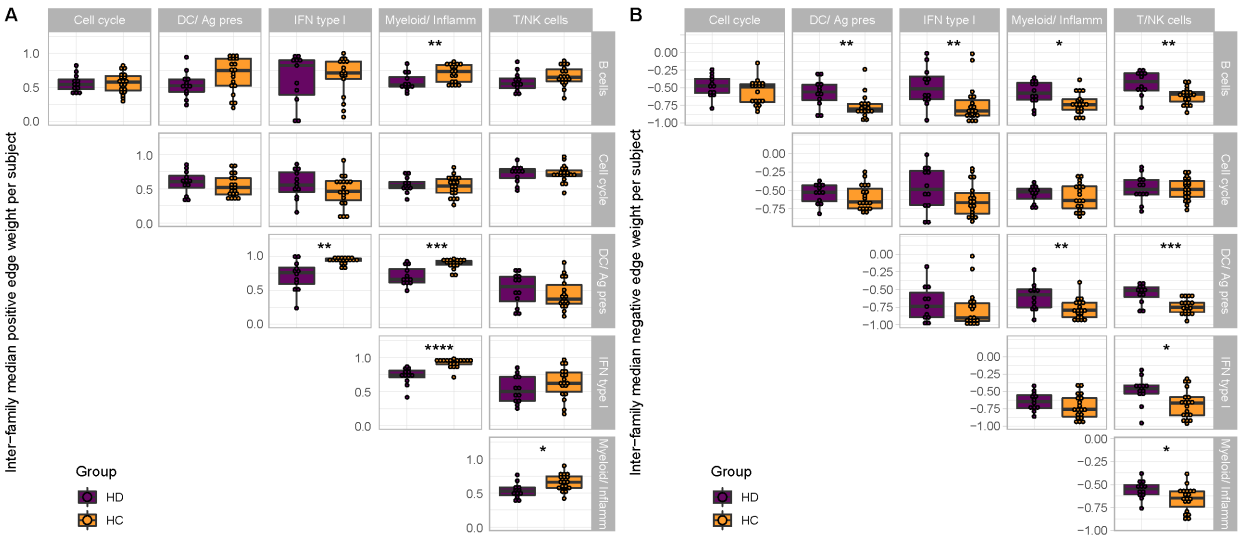

Figure 27. Hemodialysis subjects (HD) demonstrate substantially weaker inter-family positive and negative co-expression between several blood transcription module (BTM) families. Median edge strength of inter-family edges is shown for HD and controls, separately for positive edges and negative edges, pairwise between each BTM family. *p < 0.05, ** p < 0.01, *** p < 0.001, **** p < 0.0001.

5.3.3. PANDA regulatory networks

PANDA analyses demonstrated significant regulatory network differences, with BTM enrichment analysis yielding 35 BTMs with altered signaling [p < 0.05, FDR-adjusted]. 25 BTMs exhibited weakened targeting in HD and 10 exhibited stronger targeting. The top three most differentially targeted BTMs were LI.M161.0 (enriched in NK cells (II)), LI.M43.0 (myeloid, dendritic cell activation via NFkB), and LI.M7.2 (growth factor induced, enriched in nuclear receptor subfamily), all of which exhibited weakened regulation in HD. In LI.M61.0 (enriched in NK cells (II)), the core enrichment genes consist of cell surface receptors on T cells and NK cells. In order of significance, these were TGFBR3, KIR2DS4, CD7 ,IL2RB, S1PR5, KIR2DL3, KIR3DL1,

CD247, and KIR2DL1.

The top 150 most dysregulated edges involving the core enrichment genes are shown in **Figure 28**. The most enriched gene in this BTM, TGFBR3, encodes Type III TGF-beta receptor, which is a central co-receptor for the TGF-beta family required for high affinity binding (Blobe et al. 2001). While most dysregulated gene targets in this BTM exhibit altered targeting primarily by transcription factors (TFs) that function dually as activators and repressors, TGFBR3 demonstrates altered (weaker) targeting predominantly by transcriptional repressors including MECP2 and MBD2, which bind methylated promoter regions of DNA (Lewis et al. 1992; Hendrich and Bird 1998). IL2RB is vital for T-cell mediated immunity and immune tolerance via T regulatory cells (Campbell and Bryceson 2019). Similarly to TGFBR3, IL2RB exhibits weakened regulation by many repressive TFs including MBD2, DNMT1, REST, E2F4, and SMAD2. Interestingly, both TGFBR3 and IL2RB demonstrate isolated decreased at V2D1 in HC compared to V2D0 ($p < 0.001$, FDR-adjusted), but demonstrated no fluctuation across time points for HD. CD7 is expressed by most peripheral T cells and has been shown to act as a costimulatory molecule as well as a trigger for apoptosis of T cells (Lobach et al. 1985; Stillwell and Bierer 2001; Pace et al. 2000; Rappl et al. 2002). KIR2DS4, KIR2DL3, KIR3DL1, and KIR2DL1 encode NK cell receptors that interact with human leukocyte antigen class I molecules (HLA-I). While KIR2DS4 triggers NK cell degranulation upon binding to a conserved bacterial epitope of many human pathogens, KIR2DL3, KIR3DL1, and KIR2DL1 are inhibitory receptors (Sim et al. 2019; Winter et al. 1998). Weakened targeting of LI.M61.0 can thus be broadly characterized as dysregulation of both activating and tolerogenic receptors on T and NK cells

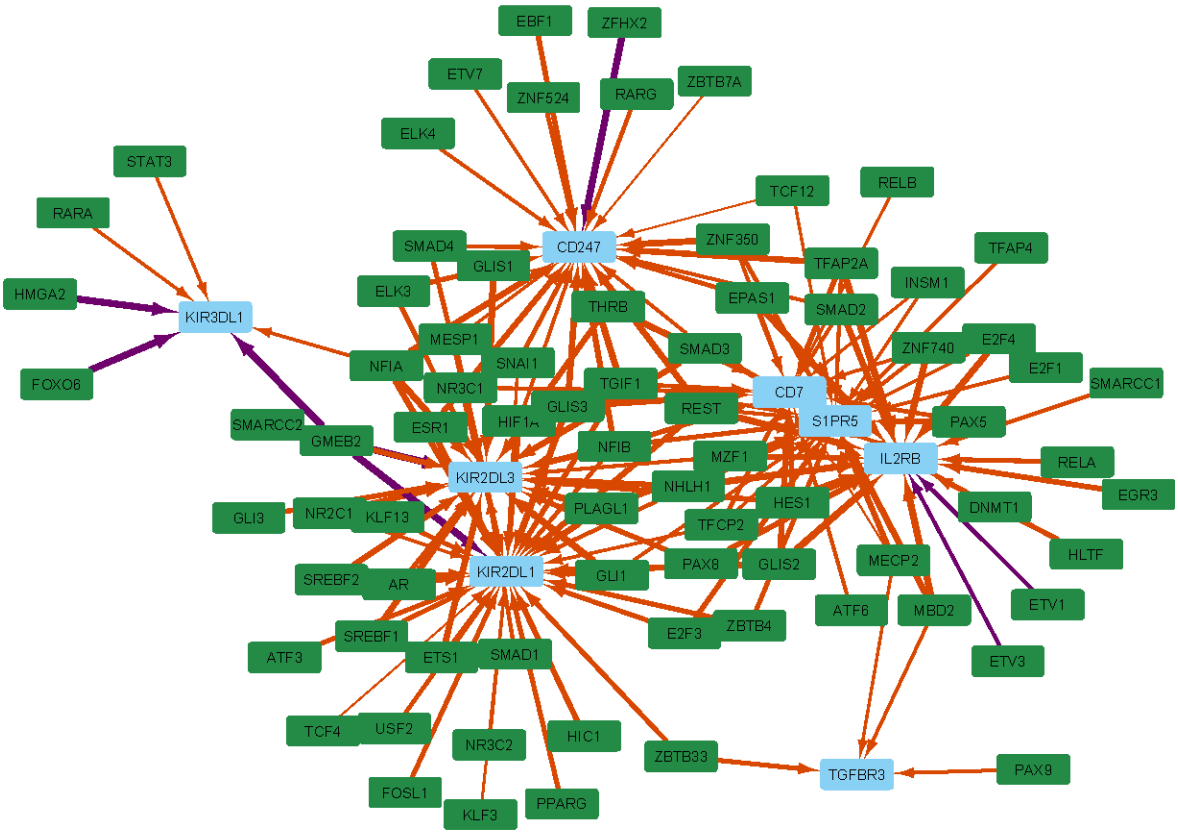

Figure 28. The LI.M61.0 (NK cells (II)) blood transcription module (BTM) is the most significantly dysregulated BTM in the hemodialysis subjects (HD).
The top 150 most dysregulated edges involving the core enrichment genes, which contribute significantly to this enrichment of this BTM, are shown. Green ovals are transcription factors (TFs), blue rectangles are core enriched gene, orange edges are more strongly regulated in controls vs HD, and purple edges are stronger in HD.

The dysregulation of LI.M43.0 (myeloid, dendritic cell activation via NFkB (I)) is driven by significantly altered targeting of core enrichment genes ICAM1, IL23A, NFKBID, VCAM1, EBI3, CD83, BCL3, RELB, TNF, NFKB2, and MAP3K8 (**Figure 29**). These genes represent various players in the NFkB pathway, including TNF, NFKB2, MAP3K8, BCL3, RELB, and NFkB inhibitor NFKBID, as well as cytokines and receptors expressed by dendritic cells including IL23A, EBI3 which heterodimerizes to form IL-27, and CD83. ICAM1 and TNF both exhibit decreased regulation by

several transcriptional repressors including decreased targeting of ICAM by MBD2, DNMT1, and E2Fs, decreased targeting of TNF by ZBTB4, MECP2, TGIF1, ZNF350, and SMAD2.

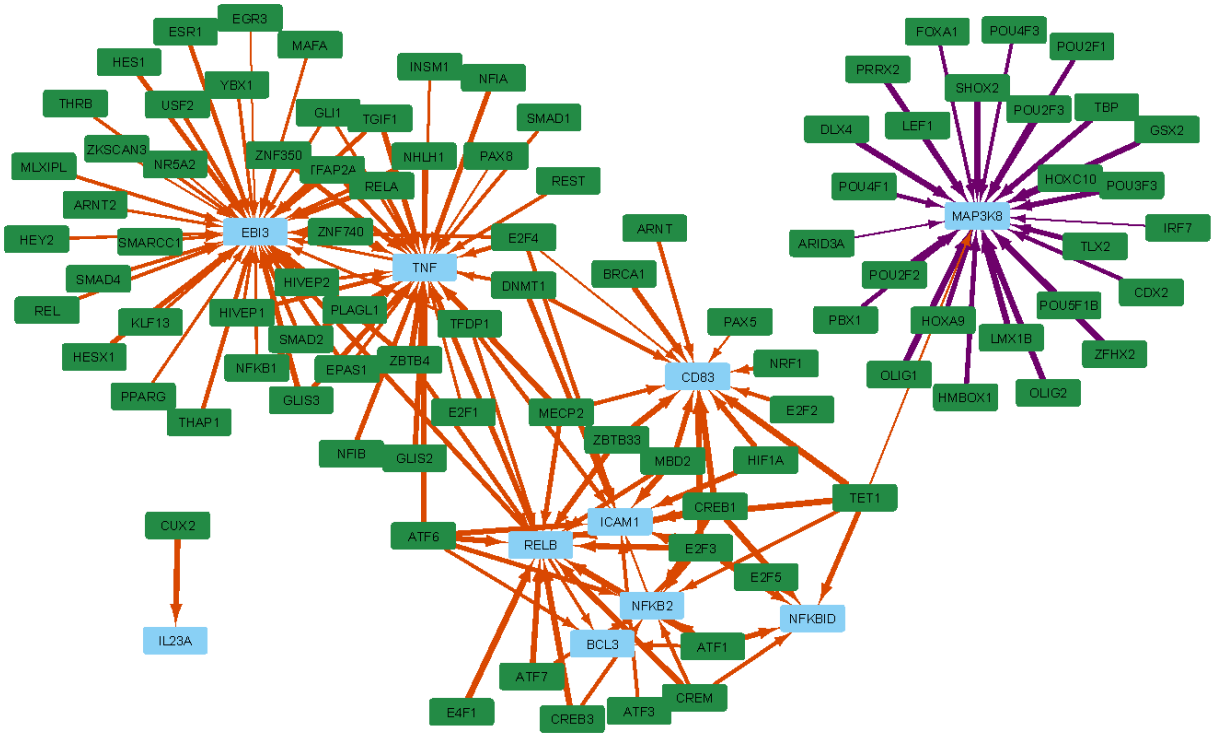

Figure 29. The LI.M43.0 (myeloid, dendritic cell activation via NFkB) blood transcription module (BTM) is the second most significantly dysregulated BTM in the hemodialysis subjects (HD). The top 150 most dysregulated edges involving the core enrichment genes, which contribute significantly to this enrichment of this BTM, are shown. Green ovals are transcription factors (TFs), blue rectangles are core enriched gene, orange edges are more strongly regulated in controls vs HD, and purple edges are stronger in HD.

The dysregulation of LI.M94.0 (growth factor induced, enriched in nuclear receptor subfamily 4) is driven by decreased regulation of NR4A1, PPP1R15A, ID1, CDKN1A (Figure S5), three of which are involved in apoptotic signaling. NR4A1 is a nuclear transcription factor whose translocation to the mitochondria induces apoptosis (Herring, Elison, and Tessem 2019). PPP1R15A is transcribed following stressful growth arrest conditions and DNA-damaging agents,

with protein response correlated with apoptosis (S. Ito et al. 2015). CDKN1A is cyclin-dependent kinase inhibitor that mediates cell cycle arrest and apoptosis (Kleinsimon et al. 2018). The final core enriched gene is Inhibitor of Differentiation 1 (Id1), which is responsible for a switch from DC differentiation to myeloid-derived suppressor cell and Treg expansion, in response to TGF-beta (Papaspyridonos et al. 2015). All of these core enriched genes demonstrate decreased targeting by repressive transcription factors including ZBTB33, MECEP2, MBD2, and DNMT1.

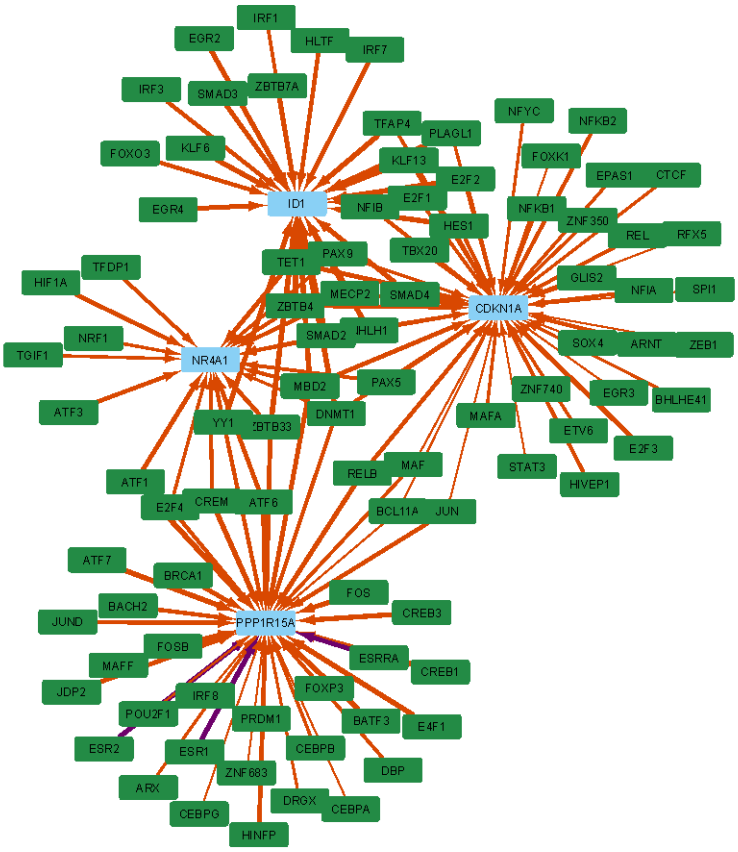

Figure 30. The LI.M94.0 (growth factor induced, enriched in nuclear receptor subfamily 4) blood transcription module (BTM) is the third most significantly dysregulated BTM in the hemodialysis subjects (HD).

The top 150 most dysregulated edges involving the core enrichment genes, which contribute significantly to this enrichment of this BTM, are shown. Green ovals are transcription factors (TFs), blue rectangles are core enriched gene, orange edges are more strongly regulated in

controls vs HD, and purple edges are stronger in HD.

5.4. Discussion

In this study, we elucidate decreasing coupling between immune system components in HD and identify dysregulated blood transcription modules and genes that underlie these altered relationships. While our prior analyses described the time course of transcriptomic responses to the BNT162b2 mRNA COVID-19 vaccine, we treat the vaccination here as an *in vivo* stimulus allowing for broader elucidation of the underlying complex immune dysregulation in ESRD. Importantly, we demonstrate that, by acquiring longitudinal samples of the same subject undergoing vaccination, informative single-subject co-expression networks can be constructed.

Our group co-expression network results demonstrate broadly weakened co-expression in HD compared to HC, representing weaker coupling between different components of the immune system. These differences manifest as both weakened positive and negative co-expression, where strong positive co-expression indicates that when one component is activated the other is also likely to be activated, and strong negative co-expression indicates that when component is activated the other is likely to be repressed. These results were also found at the single-subject level, with weaker median edge weights in HD for positive edges (less positive Fisher-Z values) and for negative edges (less negative Fisher-Z values). These results could represent a global de-sensitization of immune system components due to chronic stimulation by

Group co-expression network analyses demonstrated that the *dendritic cell/antigen presentation* (*DC/APC*) blood transcription module (BTM) family exhibited the largest percentage of intra-family edges with weakened positive co-expression (**Figure 23**). This indicates that many of the BTMs within the *DC/APC* family are less strongly co-activated with one another in HD. This

result was re-capitulated in single-subject co-expression networks, which exhibited significantly weaker median positive co-expression in HD compared to HC ($p < 0.01$) (**Figure 26**). The *DC/APC* family also exhibited significantly altered inter-family edges. The altered positive co-expression was reflective of weaker positive inter-family regulation between (each pair of) the *DC/APC*, *IFN type I*, and *Myeloid/Inflamm* families in both the group and single subject networks (**Figure 23, Figure 27**). The most significantly weakened edge in each of these inter-family relationships involving the *DC/APC* family was *LI.M43.0 (myeloid, dendritic cell activation via NFkB (I))*. This is supported by the weakened regulation of *LI.M43.0 (myeloid, dendritic cell activation via NFkB (I))*, which was the second most dysregulated BTM in our PANDA analysis, with core enrichment genes including NFkB pathway mediators such as TNF, NFkB2, and NFkBID.

These results are consistent with evidence from literature showing significantly decreased numbers of DCs in ESRD which decline further with HD (Kim et al. 2017), as well as impaired maturation of monocytes and dendritic cells (Verkade et al. 2007), and decreased antigen presentation (Satomura et al. 2002; Lim et al. 2007). DC dysfunction in ESRD has been proposed to stem from alterations of pattern recognition receptors (PRRs), leading downstream to impaired T-cell induction (Kato et al. 2008). Various pattern recognition receptor alterations have been reported in the ESRD literature, including both increased and decreased expression of toll-like receptor 4 (TLR4) (Ando et al. 2006; Gollapudi et al. 2010), increased expression of the secreted PRR mannose-binding lectin, and increased expression of major macrophage scavenger receptors SR-A and CD36 (Ando et al. 1996).

In our analysis, tumor necrosis factor (TNF), a proinflammatory cytokine which is upregulated by TLR binding and which is required for activation of NFkB and maturation of DCs

(Hayden and Ghosh 2014; Trevejo et al. 2001), was one of the core enrichment genes in LI.M43.0. Furthermore, our regulatory network analysis demonstrated dysregulation of *LI.M146 (MHC-TLR7-TLR8)* ($p < 0.01$, FDR-adjusted). Interestingly, TLR7 and TLR8 have been shown to induce type 1 interferons (IFNs) in DCs that synergize with the NFkB pathway to activate DCs (Gautier et al. 2005). Taken together, these results reinforce evidence of TLR dysfunction, with a mediating role of type 1 IFN induction, leading to impaired maturation and activation of DCs.

The most significantly dysregulated BTM from our PANDA analysis was *LI.M61.0 (enriched in NK cells (II))*, with core enrichment genes comprising activating and tolerogenic receptors on T cells (TGFBR3, CD7 ,IL2RB, CD247) and NK cells (KIR2DS4, S1PR5, KIR2DL3, KIR3DL1, and KIR2DL1). Weakened regulation of TGFBR3 contributed most significantly to enrichment of this BTM, and encodes a central co-receptor for the TGF-beta family (Blobe et al. 2001). Interestingly, while this receptor is required for high affinity binding, it can also undergo ectodomain shedding, ultimately inhibiting downstream signaling (López-Casillas et al. 1994). In fact, blocking the receptor has been shown to promote TGFβ-dependent induction of Tregs (Ortega-Francisco et al. 2017). The gene therefore plays a dual role in immune activation and tolerance. Interleukin 2 receptor subunit beta (IL2RB), another core enriched gene with weakened regulation from *LI.M61.0*, also plays a critical role in the balance of activation and tolerance via Tregs (Campbell and Bryceson 2019). Weakened regulation of these genes may thus contribute to the disturbed Treg function seen in ESRD (Hendrikx et al. 2009; Ren et al. 2019).

It is of particular note that TGFBR3 and IL2RB exhibited decreased gene expression at only V2D1 in HC ($p < 0.001$, FDR-adjusted), while demonstrating no statistically significance change across time points for HD. Because these gene regulatory networks were constructed from D0

and D7 time points alone, this indicates that these networks are capturing regulatory differences that can predict gene expression changes in unmeasured states.

Our regulatory network results from PANDA further identified regulators of cell survival and apoptosis in ESRD. ESRD literature has demonstrated accelerated apoptosis of neutrophils (Cendoroglo et al. 1999) as well as mixed findings of increased B cell apoptosis in one study (Fernández-Fresnedo et al. 2000) in contrast to increased B-cell survival factors in another study (Pahl et al. 2010). Our results showed weakened regulation of *LI.M94.0 (growth factor induced, enriched in nuclear receptor subfamily 4)*, with differential targeting of four core enriched genes, three of which are involved in apoptotic signaling: nuclear transcription factor NR4A1, PPP1R15A, and CDKN1A. Each of these genes demonstrated weakened targeting by many repressive transcription factors including ZBTB33, MECEP2, MBD2, and DNMT1. It stands to reason that the mixed findings of B cell apoptosis in ESRD stem from context-dependence; Fernández-Fresnedo et al. cultured peripheral blood cells for four days prior to assessing apoptosis, while Pahl et al. assessed apoptosis on freshly isolated cells. It is possible that the weakened repressive regulation of apoptotic regulators such as PPP1R15A and CDKN1A, which are upregulated under conditions of stress, may drive increased B cell apoptosis specifically under conditions of increased stress in ESRD.

Interestingly, many of the enriched core genes in the BTMs with most weakened regulation in HD were differentially targeted by MECP2 and MBD2, including TGFBR3, IL2RB, TNF and all of the core enriched genes in *LI.M94.0 (growth factor induced, enriched in nuclear receptor subfamily 4)*. MECP2 and MBD2 are members of a family of nuclear proteins with a methyl-CpG binding domain (MBD) (Lewis et al. 1992; Hendrich and Bird 1998). While these TFs

traditionally repress transcription from methylated gene promoters, MBD2 has also been reported to function as a demethylase to activate transcription. Interestingly, MBD2 was shown to have a key role in promoting demethylation in a Treg-specific demethylation region, resulting in Foxp3 expression and Treg suppressive function (Wang et al. 2013). This suggests a potential role of altered DNA methylation of peripheral blood in the immune dysregulation of ESRD. In fact, a recent epigenome wide association study identified abnormal DNA methylation of whole blood associated with CKD development (Chu et al. 2017).

There is a wealth of evidence demonstrating TLR-induced alterations of the epigenetic landscape, leading to both increased and decreased expression of TLR-induced genes (Perkins et al. 2016). For example, in macrophages, LPS signaling through TLR4 alters chromatin accessibility at TLR-responsive inflammatory genes including IL-6 (Hargreaves, Horng, and Medzhitov 2009). In support of a mediating role of type 1 IFN in the TLR dysfunction leading to impaired maturation and activation of DCs, type I IFN has also been shown to catalyze methylation of promoters of NF-kB responsive genes (Schliehe et al. 2015). Additionally, oxidative stress has been shown to alter DNA methylation profiles, including in peripheral blood. In fact, oxidative damage to a methyl-CpG site in a methyl binding protein recognition sequence has been shown to substantially reduce binding affinity of MECP2 (Valinluck et al. 2004). It is reasonable that, in addition to altering regulation between immune players, epigenetic mechanisms could independently increase susceptibility of immune subsets to apoptosis.

Results from the single-subject co-expression networks demonstrate that informative single-subject co-expression networks can be directly constructed using vaccination as an *in vivo* immune perturbation. The immune perturbation leads to the high gene expression variance

needed to construct a co-expression network using a small number of samples. The single-subject network results re-capitulate co-expression network differences demonstrated in the group network results. While a small number of subjects are represented in this study, these results are a proof of principle that informative single-subject gene networks can be directly constructed agnostically of group networks. Single-subject networks offer the opportunity to elucidate subtypes of disease or to provide network biomarkers for disease diagnosis, prognosis, or treatment response. While methods have been developed for single-subject network analysis, these networks rely on statistical inference from the impact of a given sample on the aggregate network model (Kuijjer et al. 2019). It should be noted that our single-subject networks represent low resolution networks, with nodes comprised of modules of genes instead of individual genes, which is necessary to enable construction of reliable networks with such few samples per subject. Due to similar constraints, we constructed single subject co-expression networks, but not gene regulatory networks which enable more precise investigation of regulatory relationships. Thus, while single-subject gene networks could yield useful network biomarkers, any investigation into their utility will be necessarily paired with regulatory network methods to provide mechanistic insight.

Overall, we elucidated a complex regulatory interplay in ESRD resulting in simultaneous dampening of immune activation as well as tolerogenic immune responses that can be appreciated on a single-subject level. Our results reinforce prior proposals that TLR dysfunction leads to impaired maturation and activation of DCs. Constitutive stimulation of TLRs may lead to low-grade baseline inflammation, simultaneously resulting in desensitization that impairs the ability of the immune system to mount immunogenic responses. Notably, we also identified

differential gene expression of core dysregulated genes at isolated time points that were not included in gene network construction, indicating that these networks capture regulatory differences that can predict gene expression changes in unmeasured states. These results highlight the importance of studying regulatory interactions to characterize dynamic regulation and dysregulation of the immune system.

6. Conclusions

The overall aim of this thesis was to investigate immune-mediated disease using two different systems vaccinology approaches; one in which we characterized vaccine-conferred immune protection and identified transcriptomic correlates of this protection, and one in which we investigated the broader structure and dynamics of gene dysregulation in immune-mediated disease using vaccination as an *in vivo* stimulus. We applied these approaches to publicly available RNA sequencing data in children at risk for developing asthma, and peripheral blood samples that we collected from healthy controls and immunocompromised patient populations at multiple time points surrounding Covid-19 mRNA vaccination.

First, we showed non-allergen-specific immune network dysregulation in peripheral blood mononuclear cells (PBMCs) of children who later developed a clinical diagnosis of allergic asthma. Using publicly available data, we characterized immune networks of asthmatic predisposition in children at the age of 2, prior to the diagnosis of allergic asthma, who were subsequently diagnosed with asthma at the age of 7. We showed extensive differences of gene co-expression networks and gene regulatory networks in children who developed asthma versus those who did not using RNA sequencing of PBMCs stimulated *in vitro* with tetanus toxoid to elicit an unbiased and broad immune recall response. Moreover, we suggested that these gene network differences prior to asthma diagnosis resulted from altered accessibility of gene targets. In summary, we demonstrated that dysregulated immune states can be appreciated prior to overt clinical symptom presentation using stimulated transcriptomics.

Next, we characterized the BNT162b2 SARS-CoV-2 mRNA vaccine-conferred immune protection from Covid-19 in two immunocompromised patient populations. Individuals with

sarcoidosis demonstrated a significant increase in anti-spike IgG titers and neutralizing function one week after the second vaccination dose that was comparable to controls. However, IgG titers declined significantly back to baseline levels by 6 months. Individuals with end stage renal disease (ESRD) on maintenance hemodialysis (HD) demonstrated a significant increase in IgG titers and neutralizing function at one week after the second vaccination dose, with a small but significant reduction in titers in HD groups ($p < 0.05$). IgG titers remained elevated above baseline at six months in both subject groups. Transcriptomic analyses demonstrated differing time courses of immune response, with predominant T cell activity in controls one week after the first vaccination dose, compared to predominant myeloid cell activity in HD at this time point. HD demonstrated decreased metabolic activity and decreased antigen presentation compared to controls after the second vaccination dose. Additionally, we demonstrated that increased expression of myeloid and T cell activity at two days after the second vaccination dose was predictive of higher antibody development.

We then elucidated decreased coupling between immune system components in HD, and identified dysregulated blood transcription modules and genes that underlie these altered relationships. Our results suggested a role of impaired dendritic cell (DC) activation and maturation through dysregulated toll-like receptor and type I interferon signaling. Our results further suggested altered regulatory T cell function through altered TGF-beta and IL2 receptor signaling. Finally, our regulatory networks suggested decreased regulation of apoptotic regulators NR4A1, PPP1R15A, and CDKN1A by repressive methyl-binding transcriptional repressors that could underlie increased susceptibility to apoptosis in ESRD. Notably, regulatory alterations of TGFBR3 and IL2RB were correlated with decreased gene expression only at one day

after the second vaccination dose in controls (V2D1), while demonstrating no statistically significant change across time points for HD. Because the gene regulatory networks were not constructed using V2D1 data, this indicates that these networks captured regulatory differences that can predict gene expression changes in unmeasured states. This further illustrates the relevance of regulatory network construction in the characterization of dynamic systems.

Our single-subject co-expression networks demonstrated that informative low-resolution single-subject gene expression networks can be directly constructed using vaccination as an *in vivo* immune perturbation. The immune perturbation leads to the high gene expression variance needed to construct a co-expression network using a small number of samples. The single-subject network results re-capitulated co-regulatory network differences demonstrated by the group co-expression network results. While a small number of subjects are represented in this study, these results are a proof of principle that informative single-subject gene networks can be directly constructed agnostically of group networks. Single-subject networks offer the opportunity to elucidate subtypes of disease or to provide network biomarkers for disease diagnosis, prognosis, or treatment response.

The results reported here require experimental validation and extension to larger cohort sizes.

Assessments of chromatin accessibility using ATAC-Seq would enable high level characterization of the epigenetic landscape of PBMCs to determine whether predisposition to atopic phenotypes may indeed be driven by feed-forward mechanisms of altered gene target accessibility. ATAC-Seq could also be used to determine the effect of oxidative stress and repeated endotoxin stimulation on the epigenomic landscape of PBMCs, and whether these result in the regulatory

network changes that we demonstrated in ESRD. Alternatively, given the altered regulation by methyl-CpG binding TFs MECP2 and MBD2 in the ESRD regulatory networks, it would be interesting to determine whether the promoters of genes differentially targeted by these TFs are differentially methylated in ESRD using a DNA methylation profiling method such as Methylated DNA immunoprecipitation (MeDIP). Assessment of specific DNA-protein binding interactions using Chip-seq would offer complementary validation. For example, Chip-seq could be used to determine whether GATA3 demonstrates differential binding at Th1 and Th2 promoters in PBMCs of children that are predisposed to develop allergic phenotypes. It could also be used to validate altered binding of MECP2 or MBD2 at dysregulated gene targets in the PBMCs of individuals with ESRD, or to determine differential binding after exposure of cultured PBMCs to oxidative stress or endotoxins.

It would be of particular interest to assess single-subject co-expression network construction in a large subject cohort to determine if these networks can offer biomarkers for immune-mediated disease diagnosis and prognosis, or elucidate subtypes of disease with heterogeneous etiologies or presentation. For example, sarcoidosis is an autoimmune disease of unclear etiology and heterogenous disease course ranging from acute, self-limited processes to chronic progressive disease with organ failure and death (Swigris et al. 2011). A prior study identified a gene signature including T cell/JAK-STAT pathway genes that differentiated sarcoid patients from controls but had poor predictive accuracy in distinguishing complicated from uncomplicated sarcoidosis (Zhou et al. 2017). Single-subject network characterization of this patient population may help illuminate subtypes of disease or identify biomarkers of outcome or treatment response.

References

1. Aderem, A, and L Hood. 2001. “Immunology in the Post-Genomic Era.” *Nature Immunology* 2 (5): 373–75. https://doi.org/10.1038/87665.
2. Agur, Timna, Naomi Ben-Dor, Shira Goldman, Shelly Lichtenberg, Michal Herman-Edelstein, Dafna Yahav, Benaya Rozen-Zvi, and Boris Zingerman. 2021. “Antibody Response to MRNA SARS-CoV-2 Vaccine among Dialysis Patients - a Prospectivecohort Study.” *Nephrology, Dialysis, Transplantation : Official Publication of the European Dialysis and Transplant Association - European Renal Association*, April. https://doi.org/10.1093/ndt/gfab155.
3. Akinbami, Lara J, Alan E Simon, and Lauren M Rossen. 2016. “Changing Trends in Asthma Prevalence Among Children.” *Pediatrics* 137 (1): 1–7. https://doi.org/10.1542/peds.2015-2354.
4. Altman, Matthew C., Elizabeth Whalen, Alkis Togias, George T. O’Connor, Leonard B. Bacharier, Gordon R. Bloomberg, Meyer Kattan, et al. 2018. “Allergen-Induced Activation of Natural Killer Cells Represents an Early-Life Immune Response in the Development of Allergic Asthma.” *Journal of Allergy and Clinical Immunology*, 1–11. https://doi.org/10.1016/j.jaci.2018.02.019.
5. Anand, Shuchi, Maria E Montez-Rath, Jialin Han, Pablo Garcia, LinaCel Cadden, Patti Hunsader, Russell Kerschmann, et al. 2021. “Antibody Response to COVID-19 Vaccination in Patients Receiving Dialysis.” *MedRxiv : The Preprint Server for Health Sciences*. https://doi.org/10.1101/2021.05.06.21256768.
6. Anderson, P, C Nagler-Anderson, C O’Brien, H Levine, S Watkins, H S Slayter, M L Blue, and S F Schlossman. 1990. “A Monoclonal Antibody Reactive with a 15-KDa Cytoplasmic Granule-Associated Protein Defines a Subpopulation of CD8+ T Lymphocytes.” *Journal of Immunology (Baltimore, Md. : 1950)* 144 (2): 574–82.
7. Ando, M, I Lundkvist, J Bergström, and B Lindholm. 1996. “Enhanced Scavenger Receptor Expression in Monocyte-Macrophages in Dialysis Patients.” *Kidney International* 49 (3): 773–80. https://doi.org/10.1038/ki.1996.107.
8. Ando, M, A Shibuya, K Tsuchiya, T Akiba, and K Nitta. 2006. “Reduced Expression of Toll-like Receptor 4 Contributes to Impaired Cytokine Response of Monocytes in Uremic Patients.” *Kidney International* 70 (2): 358–62. https://doi.org/10.1038/sj.ki.5001548.
9. Arunachalam, Prabhu S, Madeleine K D Scott, Thomas Hagan, Chunfeng Li, Yupeng Feng, Florian Wimmers, Lilit Grigoryan, et al. 2021. “Systems Vaccinology of the BNT162b2 MRNA Vaccine in Humans.” *Nature* 596 (7872): 410–16. https://doi.org/10.1038/s41586-021-03791-x.
10. Ascoli, Christian, Yue Huang, Cody Schott, Benjamin A. Turturice, Ahmed Metwally, David L. Perkins, and Patricia W. Finn. 2018. “A Circulating MicroRNA Signature Serves as a Diagnostic and Prognostic Indicator in Sarcoidosis.” *American Journal of Respiratory Cell and Molecular Biology* 58 (1): 40–54. https://doi.org/10.1165/rcmb.2017-0207OC.
11. Asher, M Innes, Stephen Montefort, Bengt Björkstén, Christopher K W Lai, David P Strachan, Stephan K Weiland, and Hywel Williams. 2006. “Worldwide Time Trends in the Prevalence

of Symptoms of Asthma, Allergic Rhinoconjunctivitis, and Eczema in Childhood: ISAAC Phases One and Three Repeat Multicountry Cross-Sectional Surveys." *Lancet (London, England)* 368 (9537): 733–43. https://doi.org/10.1016/S0140-6736(06)69283-0.

12. Attias, Philippe, Hamza Sakhi, Philippe Rieu, Arvish Soorkia, David Assayag, Sabrina Bouhroum, Patrice Nizard, and Khalil el Karoui. 2021. "Antibody Response to the BNT162b2 Vaccine in Maintenance Hemodialysis Patients." *Kidney International*. https://doi.org/10.1016/j.kint.2021.04.009.
13. Baden, Lindsey R, Hana M El Sahly, Brandon Essink, Karen Kotloff, Sharon Frey, Rick Novak, David Diemert, et al. 2021. "Efficacy and Safety of the MRNA-1273 SARS-CoV-2 Vaccine." *The New England Journal of Medicine* 384 (5): 403–16. https://doi.org/10.1056/NEJMoa2035389.
14. Barnes, Peter J. 2008. "The Cytokine Network in Asthma and Chronic Obstructive Pulmonary Disease." *The Journal of Clinical Investigation* 118 (11): 3546–56. https://doi.org/10.1172/JCI36130.
15. Baughman, R P, S Field, U Costabel, R G Crystal, D A Culver, M Drent, M A Judson, and G Wolff. 2016. "Sarcoidosis in America. Analysis Based on Health Care Use." *Ann Am Thorac Soc* 13 (8): 1244–52. https://doi.org/10.1513/AnnalsATS.201511-760OC.
16. Baughman, R P, E E Lower, M Buchanan, P Rottoli, M Drent, J Sellares, M Terwiel, et al. 2020. "Risk and Outcome of COVID-19 Infection in Sarcoidosis Patients: Results of a Self-Reporting Questionnaire." *Sarcoidosis Vasc Diffuse Lung Dis* 37 (4): e2020009. https://doi.org/10.36141/svdld.v37i4.10726.
17. Biswas, Subhra K, and Eduardo Lopez-Collazo. 2009. "Endotoxin Tolerance: New Mechanisms, Molecules and Clinical Significance." *Trends in Immunology* 30 (10): 475–87. https://doi.org/10.1016/j.it.2009.07.009.
18. Blobe, G C, W P Schiemann, M C Pepin, M Beauchemin, A Moustakas, H F Lodish, and M D O'Connor-McCourt. 2001. "Functional Roles for the Cytoplasmic Domain of the Type III Transforming Growth Factor Beta Receptor in Regulating Transforming Growth Factor Beta Signaling." *The Journal of Biological Chemistry* 276 (27): 24627–37. https://doi.org/10.1074/jbc.M100188200.
19. Braun, Roman Othmar, Livia Brunner, Kurt Wyler, Gaël Auray, Obdulio García-Nicolás, Sylvie Python, Beatrice Zumkehr, et al. 2018. "System Immunology-Based Identification of Blood Transcriptional Modules Correlating to Antibody Responses in Sheep." *NPJ Vaccines* 3: 41. https://doi.org/10.1038/s41541-018-0078-0.
20. Breton, Carrie V, Hyang-Min Byun, Made Wenten, Fei Pan, Allen Yang, and Frank D Gilliland. 2009. "Prenatal Tobacco Smoke Exposure Affects Global and Gene-Specific DNA Methylation." *American Journal of Respiratory and Critical Care Medicine* 180 (5): 462–67. https://doi.org/10.1164/rccm.200901-0135OC.
21. Bunyavanich, Supinda, and Eric E Schadt. 2015. "Systems Biology of Asthma and Allergic Diseases: A Multiscale Approach." *The Journal of Allergy and Clinical Immunology* 135 (1): 31–42. https://doi.org/10.1016/j.jaci.2014.10.015.

22. Campbell, Tessa M, and Yenan T Bryceson. 2019. “IL2RB Maintains Immune Harmony.” *The Journal of Experimental Medicine* 216 (6): 1231–33. https://doi.org/10.1084/jem.20190546.
23. Carnesecchi, Julie, Gianluca Sigismondo, Katrin Domsch, Clara Eva Paula Baader, Mahmoud-Reza Rafiee, Jeroen Krijgsveld, and Ingrid Lohmann. 2020. “Multi-Level and Lineage-Specific Interactomes of the Hox Transcription Factor Ubx Contribute to Its Functional Specificity.” *Nature Communications* 11 (1): 1388. https://doi.org/10.1038/s41467-020-15223-x.
24. Cendoroglo, M, B L Jaber, V S Balakrishnan, M Perianayagam, A J King, and B J Pereira. 1999. “Neutrophil Apoptosis and Dysfunction in Uremia.” *Journal of the American Society of Nephrology : JASN* 10 (1): 93–100. https://doi.org/10.1681/ASN.V10193.
25. Chang, Shaojing, and Thomas M Aune. 2007. “Dynamic Changes in Histone-Methylation ‘marks’ across the Locus Encoding Interferon-Gamma during the Differentiation of T Helper Type 2 Cells.” *Nature Immunology* 8 (7): 723–31. https://doi.org/10.1038/ni1473.
26. Chaussabel, Damien, Charles Quinn, Jing Shen, Pinakeen Patel, Casey Glaser, Nicole Baldwin, Dorothee Stichweh, et al. 2008. “A Modular Analysis Framework for Blood Genomics Studies: Application to Systemic Lupus Erythematosus.” *Immunity* 29 (1): 150–64. https://doi.org/10.1016/j.immuni.2008.05.012.
27. Chen, Shifu, Yanqing Zhou, Yaru Chen, and Jia Gu. 2018. “Fastp: An Ultra-Fast All-in-One FASTQ Preprocessor.” *Bioinformatics (Oxford, England)* 34 (17): i884–90. https://doi.org/10.1093/bioinformatics/bty560.
28. Chu, Audrey Y, Adrienne Tin, Pascal Schlosser, Yi-An Ko, Chengxiang Qiu, Chen Yao, Roby Joehanes, et al. 2017. “Epigenome-Wide Association Studies Identify DNA Methylation Associated with Kidney Function.” *Nature Communications* 8 (1): 1286. https://doi.org/10.1038/s41467-017-01297-7.
29. Cosío, Borja G, Buphinder Mann, Kazuhiro Ito, Elen Jazrawi, Peter J Barnes, K Fan Chung, and Ian M Adcock. 2004. “Histone Acetylase and Deacetylase Activity in Alveolar Macrophages and Blood Mononocytes in Asthma.” *American Journal of Respiratory and Critical Care Medicine* 170 (2): 141–47. https://doi.org/10.1164/rccm.200305-659OC.
30. Drakesmith, Hal, Sant-Rayn Pasricha, Ioav Cabantchik, Chaim Hershko, Guenter Weiss, Domenico Girelli, Nicole Stoffel, et al. 2021. “Vaccine Efficacy and Iron Deficiency: An Intertwined Pair?” *The Lancet. Haematology* 8 (9): e666–69. https://doi.org/10.1016/S2352-3026(21)00201-5.
31. Ducharme, Francine M, Sze M Tse, and Bhupendrasinh Chauhan. 2014. “Diagnosis, Management, and Prognosis of Preschool Wheeze.” *Lancet (London, England)* 383 (9928): 1593–1604. https://doi.org/10.1016/S0140-6736(14)60615-2.
32. Dureault, A, C Chapelon, L Biard, F Domont, L Savey, B Bodaghi, V Pourcher, M R Rigon, P Cacoub, and D Saadoun. 2017. “Severe Infections in Sarcoidosis: Incidence, Predictors and Long-Term Outcome in a Cohort of 585 Patients.” *Medicine (Baltimore)* 96 (49): e8846. https://doi.org/10.1097/MD.0000000000008846.
33. Eizenberg-Magar, Inbal, Jacob Rimer, Irina Zaretsky, David Lara-Astiaso, Shlomit Reich-Zeliger, and Nir Friedman. 2017. “Diverse Continuum of CD4(+) T-Cell States Is Determined by Hierarchical Additive Integration of Cytokine Signals.” *Proceedings of the National*

Academy of Sciences of the United States of America 114 (31): E6447–56. https://doi.org/10.1073/pnas.1615590114.
34. Eleftheriadis, Theodoros, Georgia Antoniadi, Vassilios Liakopoulos, Charalambos Kartsios, and Ioannis Stefanidis. 2007. "Disturbances of Acquired Immunity in Hemodialysis Patients." *Seminars in Dialysis* 20 (5): 440–51. https://doi.org/10.1111/j.1525-139X.2007.00283.x.
35. Ettou, Sandrine, Youngsook L Jung, Tomoya Miyoshi, Dhawal Jain, Ken Hiratsuka, Valerie Schumacher, Mary E Taglienti, Ryuji Morizane, Peter J Park, and Jordan A Kreidberg. 2020. "Epigenetic Transcriptional Reprogramming by WT1 Mediates a Repair Response during Podocyte Injury." *Science Advances* 6 (30): eabb5460. https://doi.org/10.1126/sciadv.abb5460.
36. Feng, F, M P Thompson, B E Thomas, E R Duffy, J Kim, S Kurosawa, J Y Tashjian, Y Wei, C Andry, and D J Stearns-Kurosawa. 2019. "A Computational Solution to Improve Biomarker Reproducibility during Long-Term Projects." *PLoS One* 14 (4): e0209060. https://doi.org/10.1371/journal.pone.0209060.
37. Fernández-Fresnedo, G, M A Ramos, M C González-Pardo, A L de Francisco, M López-Hoyos, and M Arias. 2000. "B Lymphopenia in Uremia Is Related to an Accelerated in Vitro Apoptosis and Dysregulation of Bcl-2." *Nephrology, Dialysis, Transplantation : Official Publication of the European Dialysis and Transplant Association - European Renal Association* 15 (4): 502–10. https://doi.org/10.1093/ndt/15.4.502.
38. Ferrara, Francesca, and Nigel Temperton. 2018. "Pseudotype Neutralization Assays: From Laboratory Bench to Data Analysis." *Methods and Protocols* 1 (1). https://doi.org/10.3390/mps1010008.
39. Foster, Simmie L, Diana C Hargreaves, and Ruslan Medzhitov. 2007. "Gene-Specific Control of Inflammation by TLR-Induced Chromatin Modifications." *Nature* 447 (7147): 972–78. https://doi.org/10.1038/nature05836.
40. Fotin-Mleczek, M, K M Duchardt, C Lorenz, R Pfeiffer, S Ojkic-Zrna, J Probst, and K J Kallen. 2011. "Messenger RNA-Based Vaccines with Dual Activity Induce Balanced TLR-7 Dependent Adaptive Immune Responses and Provide Antitumor Activity." *J Immunother* 34 (1): 1–15. https://doi.org/10.1097/CJI.0b013e3181f7dbe8.
41. Friedman, M A, J R Curtis, and K L Winthrop. 2021. "Impact of Disease-Modifying Antirheumatic Drugs on Vaccine Immunogenicity in Patients with Inflammatory Rheumatic and Musculoskeletal Diseases." *Ann Rheum Dis* 80 (10): 1255–65. https://doi.org/10.1136/annrheumdis-2021-221244.
42. Gaucher, Denis, René Therrien, Nadia Kettaf, Bastian R Angermann, Geneviève Boucher, Abdelali Filali-Mouhim, Janice M Moser, et al. 2008. "Yellow Fever Vaccine Induces Integrated Multilineage and Polyfunctional Immune Responses." *The Journal of Experimental Medicine* 205 (13): 3119–31. https://doi.org/10.1084/jem.20082292.
43. Gautier, Grégory, Martine Humbert, Florence Deauvieau, Mathieu Scuiller, John Hiscott, Elizabeth E M Bates, Giorgio Trinchieri, Christophe Caux, and Pierre Garrone. 2005. "A Type I Interferon Autocrine-Paracrine Loop Is Involved in Toll-like Receptor-Induced Interleukin-

12p70 Secretion by Dendritic Cells." *The Journal of Experimental Medicine* 201 (9): 1435–46. https://doi.org/10.1084/jem.20041964.

44. Gern, James E, Cynthia M Visness, Peter J Gergen, Robert A Wood, Gordon R Bloomberg, George T O'Connor, Meyer Kattan, et al. 2009. "The Urban Environment and Childhood Asthma (URECA) Birth Cohort Study: Design, Methods, and Study Population." *BMC Pulmonary Medicine* 9 (May): 17. https://doi.org/10.1186/1471-2466-9-17.
45. Ghadiani, Mohammad H, Shahin Besharati, Nouraddin Mousavinasab, and Mojgan Jalalzadeh. 2012. "Response Rates to HB Vaccine in CKD Stages 3-4 and Hemodialysis Patients." *Journal of Research in Medical Sciences : The Official Journal of Isfahan University of Medical Sciences* 17 (6): 527–33.
46. Glass, Kimberly, Curtis Huttenhower, John Quackenbush, and Guo Cheng Yuan. 2013. "Passing Messages between Biological Networks to Refine Predicted Interactions." *PLoS ONE* 8 (5). https://doi.org/10.1371/journal.pone.0064832.
47. Glass, Kimberly, John Quackenbush, Dimitrios Spentzos, Benjamin Haibe-Kains, and Guo-Cheng Yuan. 2015. "A Network Model for Angiogenesis in Ovarian Cancer." *BMC Bioinformatics* 16 (April): 115. https://doi.org/10.1186/s12859-015-0551-y.
48. Gollapudi, P, J-W Yoon, S Gollapudi, M V Pahl, and N D Vaziri. 2010. "Leukocyte Toll-like Receptor Expression in End-Stage Kidney Disease." *American Journal of Nephrology* 31 (3): 247–54. https://doi.org/10.1159/000276764.
49. Gotuzzo, Eduardo, Sergio Yactayo, and Erika Córdova. 2013. "Efficacy and Duration of Immunity after Yellow Fever Vaccination: Systematic Review on the Need for a Booster Every 10 Years." *The American Journal of Tropical Medicine and Hygiene* 89 (3): 434–44. https://doi.org/10.4269/ajtmh.13-0264.
50. Granata, Simona, Gianluigi Zaza, Simona Simone, Gaetano Villani, Dominga Latorre, Paola Pontrelli, Massimo Carella, Francesco Paolo Schena, Giuseppe Grandaliano, and Giovanni Pertosa. 2009. "Mitochondrial Dysregulation and Oxidative Stress in Patients with Chronic Kidney Disease." *BMC Genomics* 10 (August): 388. https://doi.org/10.1186/1471-2164-10-388.
51. Grunewald, J, J C Grutters, E V Arkema, L A Saketkoo, D R Moller, and J Muller-Quernheim. 2019. "Sarcoidosis." *Nat Rev Dis Primers* 5 (1): 45. https://doi.org/10.1038/s41572-019-0096-x.
52. Grupper, Ayelet, Nechama Sharon, Talya Finn, Regev Cohen, Meital Israel, Amir Agbaria, Yoav Rechavi, et al. 2021. "Humoral Response to the Pfizer BNT162b2 Vaccine in Patients Undergoing Maintenance Hemodialysis." *Clinical Journal of the American Society of Nephrology : CJASN* 16 (7): 1037–42. https://doi.org/10.2215/CJN.03500321.
53. Gunawardhana, L P, P G Gibson, J L Simpson, H Powell, and K J Baines. 2014. "Activity and Expression of Histone Acetylases and Deacetylases in Inflammatory Phenotypes of Asthma." *Clinical and Experimental Allergy : Journal of the British Society for Allergy and Clinical Immunology* 44 (1): 47–57. https://doi.org/10.1111/cea.12168.

54. Hargreaves, Diana C, Tiffany Horng, and Ruslan Medzhitov. 2009. “Control of Inducible Gene Expression by Signal-Dependent Transcriptional Elongation.” *Cell* 138 (1): 129–45. https://doi.org/10.1016/j.cell.2009.05.047.
55. Hashemzadeh, K, M Fatemipour, S Zahra Mirfeizi, M Jokar, Z Shariati Sarabi, M R Hatef Fard, H Rafatpanah, and M Khodashahi. 2021. “Serum B Cell Activating Factor (BAFF) and Sarcoidosis Activity.” *Arch Rheumatol* 36 (1): 72–79. https://doi.org/10.46497/ArchRheumatol.2021.8013.
56. Hawkins, C, G Shaginurova, D A Shelton, J D Herazo-Maya, K A Oswald-Richter, J E Rotsinger, A Young, et al. 2017. “Local and Systemic CD4(+) T Cell Exhaustion Reverses with Clinical Resolution of Pulmonary Sarcoidosis.” *J Immunol Res* 2017: 3642832. https://doi.org/10.1155/2017/3642832.
57. Hayden, Matthew S, and Sankar Ghosh. 2014. “Regulation of NF-KB by TNF Family Cytokines.” *Seminars in Immunology* 26 (3): 253–66. https://doi.org/10.1016/j.smim.2014.05.004.
58. Hendrich, B, and A Bird. 1998. “Identification and Characterization of a Family of Mammalian Methyl-CpG Binding Proteins.” *Molecular and Cellular Biology* 18 (11): 6538–47. https://doi.org/10.1128/MCB.18.11.6538.
59. Hendrikx, Thijs K, Eveline A F J van Gurp, Wendy M Mol, Wenda Schoordijk, Varsha D K D Sewgobind, Jan N M Ijzermans, Willem Weimar, and Carla C Baan. 2009. “End-Stage Renal Failure and Regulatory Activities of CD4+CD25bright+FoxP3+ T-Cells.” *Nephrology, Dialysis, Transplantation : Official Publication of the European Dialysis and Transplant Association - European Renal Association* 24 (6): 1969–78. https://doi.org/10.1093/ndt/gfp005.
60. Herring, Jacob A, Weston S Elison, and Jeffery S Tessem. 2019. “Function of Nr4a Orphan Nuclear Receptors in Proliferation, Apoptosis and Fuel Utilization Across Tissues.” *Cells* 8 (11). https://doi.org/10.3390/cells8111373.
61. Hosokawa, Hiroyuki, Tomoaki Tanaka, Miki Kato, Kenta Shinoda, Hiroyuki Tohyama, Asami Hanazawa, Yuuki Tamaki, et al. 2013. “Gata3/Ruvbl2 Complex Regulates T Helper 2 Cell Proliferation via Repression of Cdkn2c Expression.” *Proceedings of the National Academy of Sciences of the United States of America* 110 (46): 18626–31. https://doi.org/10.1073/pnas.1311100110.
62. Hunninghake, G W, U Costabel, M Ando, R Baughman, J F Cordier, R du Bois, A Eklund, et al. 1999. “ATS/ERS/WASOG Statement on Sarcoidosis. American Thoracic Society/European Respiratory Society/World Association of Sarcoidosis and Other Granulomatous Disorders.” *Sarcoidosis Vasc Diffuse Lung Dis* 16 (2): 149–73.
63. Ito, Kazuhiro, Gaetano Caramori, Sam Lim, Tim Oates, K Fan Chung, Peter J Barnes, and Ian M Adcock. 2002. “Expression and Activity of Histone Deacetylases in Human Asthmatic Airways.” *American Journal of Respiratory and Critical Care Medicine* 166 (3): 392–96. https://doi.org/10.1164/rccm.2110060.
64. Ito, Sachiko, Yuriko Tanaka, Reina Oshino, Keiko Aiba, Suganya Thanasegaran, Naomi Nishio, and Ken-ichi Isobe. 2015. “GADD34 Inhibits Activation-Induced Apoptosis of Macrophages

through Enhancement of Autophagy." *Scientific Reports* 5 (February): 8327. https://doi.org/10.1038/srep08327.
65. Jahn, Michael, Johannes Korth, Oliver Dorsch, Olympia Evdoxia Anastasiou, Burkhard Sorge-Hädicke, Bartosz Tyczynski, Anja Gäckler, et al. 2021. "Humoral Response to SARS-CoV-2-Vaccination with BNT162b2 (Pfizer-BioNTech) in Patients on Hemodialysis." *Vaccines* 9 (4). https://doi.org/10.3390/vaccines9040360.
66. Johansen, Kirsten L, Glenn M Chertow, David T Gilbertson, Charles A Herzog, Areef Ishani, Ajay K Israni, Elaine Ku, et al. 2022. "US Renal Data System 2021 Annual Data Report: Epidemiology of Kidney Disease in the United States." *American Journal of Kidney Diseases : The Official Journal of the National Kidney Foundation*. https://doi.org/10.1053/j.ajkd.2022.02.001.
67. Kalantar-Zadeh, Kamyar, Deborah L Regidor, Charles J McAllister, Beckie Michael, and David G Warnock. 2005. "Time-Dependent Associations between Iron and Mortality in Hemodialysis Patients." *Journal of the American Society of Nephrology : JASN* 16 (10): 3070–80. https://doi.org/10.1681/ASN.2005040423.
68. Kato, Sawako, Michal Chmielewski, Hirokazu Honda, Roberto Pecoits-Filho, Seiichi Matsuo, Yukio Yuzawa, Anders Tranaeus, Peter Stenvinkel, and Bengt Lindholm. 2008. "Aspects of Immune Dysfunction in End-Stage Renal Disease." *Clinical Journal of the American Society of Nephrology*. American Society of Nephrology. https://doi.org/10.2215/CJN.00950208.
69. Kernan, Kate F, and Joseph A Carcillo. 2017. "Hyperferritinemia and Inflammation." *International Immunology* 29 (9): 401–9. https://doi.org/10.1093/intimm/dxx031.
70. Kim, Ji Ung, Miyeon Kim, Sinae Kim, Tam Thanh Nguyen, Eunhye Kim, Siyoung Lee, Soohyun Kim, and Hyunwoo Kim. 2017. "Dendritic Cell Dysfunction in Patients with End-Stage Renal Disease." *Immune Network* 17 (3): 152–62. https://doi.org/10.4110/in.2017.17.3.152.
71. Kitano, Hiroaki. 2002. "Computational Systems Biology." *Nature* 420 (6912): 206–10. https://doi.org/10.1038/nature01254.
72. Klein, Brianna J, Lianhua Piao, Yuanxin Xi, Hector Rincon-Arano, Scott B Rothbart, Danni Peng, Hong Wen, et al. 2014. "The Histone-H3K4-Specific Demethylase KDM5B Binds to Its Substrate and Product through Distinct PHD Fingers." *Cell Reports* 6 (2): 325–35. https://doi.org/10.1016/j.celrep.2013.12.021.
73. Kleinsimon, Susann, Enya Longmuss, Jana Rolff, Sebastian Jäger, Angelika Eggert, Catharina Delebinski, and Georg Seifert. 2018. "GADD45A and CDKN1A Are Involved in Apoptosis and Cell Cycle Modulatory Effects of ViscumTT with Further Inactivation of the STAT3 Pathway." *Scientific Reports* 8 (1): 5750. https://doi.org/10.1038/s41598-018-24075-x.
74. Klingler, J, S Weiss, V Itri, X Liu, K Y Oguntuyo, C Stevens, S Ikegame, et al. 2020. "Role of IgM and IgA Antibodies in the Neutralization of SARS-CoV-2." *MedRxiv*. https://doi.org/10.1101/2020.08.18.20177303.
75. Koc, Mehmet, Ahmet Toprak, Hakki Arikan, Zekaver Odabasi, Yesim Elbir, Aysin Tulunay, Ebru Asicioglu, et al. 2011. "Toll-like Receptor Expression in Monocytes in Patients with Chronic Kidney Disease and Haemodialysis: Relation with Inflammation." *Nephrology, Dialysis, Transplantation : Official Publication of the European Dialysis and Transplant*

Association - European Renal Association 26 (3): 955–63. https://doi.org/10.1093/ndt/gfq500.

76. Kudryavtsev, I, M Serebriakova, A Starshinova, Y Zinchenko, N Basantsova, A Malkova, L Soprun, et al. 2020. “Imbalance in B Cell and T Follicular Helper Cell Subsets in Pulmonary Sarcoidosis.” *Sci Rep* 10 (1): 1059. https://doi.org/10.1038/s41598-020-57741-0.
77. Kuijjer, Marieke Lydia, Matthew George Tung, GuoCheng Yuan, John Quackenbush, and Kimberly Glass. 2019. “Estimating Sample-Specific Regulatory Networks.” *IScience* 14 (April): 226–40. https://doi.org/10.1016/j.isci.2019.03.021.
78. Labi, Verena, Miriam Erlacher, Stephan Kiessling, Claudia Manzl, Anna Frenzel, Lorraine O’Reilly, Andreas Strasser, and Andreas Villunger. 2008. “Loss of the BH3-Only Protein Bmf Impairs B Cell Homeostasis and Accelerates Gamma Irradiation-Induced Thymic Lymphoma Development.” *The Journal of Experimental Medicine* 205 (3): 641–55. https://doi.org/10.1084/jem.20071658.
79. Langfelder, Peter, and Steve Horvath. 2008. “WGCNA: An R Package for Weighted Correlation Network Analysis.” *BMC Bioinformatics* 9 (December): 559. https://doi.org/10.1186/1471-2105-9-559.
80. Lewis, J D, R R Meehan, W J Henzel, I Maurer-Fogy, P Jeppesen, F Klein, and A Bird. 1992. “Purification, Sequence, and Cellular Localization of a Novel Chromosomal Protein That Binds to Methylated DNA.” *Cell* 69 (6): 905–14. https://doi.org/10.1016/0092-8674(92)90610-o.
81. Li, Shuzhao, Nadine Rouphael, Sai Duraisingham, Sandra Romero-Steiner, Scott Presnell, Carl Davis, Daniel S Schmidt, et al. 2014. “Molecular Signatures of Antibody Responses Derived from a Systems Biology Study of Five Human Vaccines.” *Nature Immunology* 15 (2): 195–204. https://doi.org/10.1038/ni.2789.
82. Li, Xin, Ling Liu, Shangda Yang, Nan Song, Xing Zhou, Jie Gao, Na Yu, et al. 2014. “Histone Demethylase KDM5B Is a Key Regulator of Genome Stability.” *Proceedings of the National Academy of Sciences of the United States of America* 111 (19): 7096–7101. https://doi.org/10.1073/pnas.1324036111.
83. Liberzon, Arthur, Chet Birger, Helga Thorvaldsdóttir, Mahmoud Ghandi, Jill P Mesirov, and Pablo Tamayo. 2015. “The Molecular Signatures Database (MSigDB) Hallmark Gene Set Collection.” *Cell Systems* 1 (6): 417–25. https://doi.org/10.1016/j.cels.2015.12.004.
84. Lim, W H, S Kireta, E Leedham, G R Russ, and P T Coates. 2007. “Uremia Impairs Monocyte and Monocyte-Derived Dendritic Cell Function in Hemodialysis Patients.” *Kidney International* 72 (9): 1138–48. https://doi.org/10.1038/sj.ki.5002425.
85. Lin, Danjuan, Gregory C Ippolito, Rui-Ting Zong, James Bryant, Janet Koslovsky, and Philip Tucker. 2007. “Bright/ARID3A Contributes to Chromatin Accessibility of the Immunoglobulin Heavy Chain Enhancer.” *Molecular Cancer* 6 (March): 23. https://doi.org/10.1186/1476-4598-6-23.
86. Liu, Yuanbin, Gary Fiskum, and David Schubert. 2002. “Generation of Reactive Oxygen Species by the Mitochondrial Electron Transport Chain.” *Journal of Neurochemistry* 80 (5): 780–87. https://doi.org/10.1046/j.0022-3042.2002.00744.x.

87. Lobach, D F, L L Hensley, W Ho, and B F Haynes. 1985. “Human T Cell Antigen Expression during the Early Stages of Fetal Thymic Maturation.” *Journal of Immunology (Baltimore, Md. : 1950)* 135 (3): 1752–59.
88. Longlune, Nathalie, Marie Béatrice Nogier, Marcel Miedougé, Charlotte Gabilan, Charles Cartou, Bruno Seigneuric, Arnaud del Bello, et al. 2021. “High Immunogenicity of a Messenger RNA-Based Vaccine against SARS-CoV-2 in Chronic Dialysis Patients.” *Nephrology, Dialysis, Transplantation : Official Publication of the European Dialysis and Transplant Association - European Renal Association* 36 (9): 1704–9. https://doi.org/10.1093/ndt/gfab193.
89. López-Casillas, F, H M Payne, J L Andres, and J Massagué. 1994. “Betaglycan Can Act as a Dual Modulator of TGF-Beta Access to Signaling Receptors: Mapping of Ligand Binding and GAG Attachment Sites.” *The Journal of Cell Biology* 124 (4): 557–68. https://doi.org/10.1083/jcb.124.4.557.
90. Love, Michael I., Wolfgang Huber, and Simon Anders. 2014. “Moderated Estimation of Fold Change and Dispersion for RNA-Seq Data with DESeq2.” *Genome Biology* 15 (12): 1–21. https://doi.org/10.1186/s13059-014-0550-8.
91. Love, Michael I, Charlotte Soneson, Peter F Hickey, Lisa K Johnson, N Tessa Pierce, Lori Shepherd, Martin Morgan, and Rob Patro. 2020. “Tximeta: Reference Sequence Checksums for Provenance Identification in RNA-Seq.” *PLoS Computational Biology* 16 (2): e1007664. https://doi.org/10.1371/journal.pcbi.1007664.
92. Ma, H, W Zeng, H He, D Zhao, D Jiang, P Zhou, L Cheng, Y Li, X Ma, and T Jin. 2020. “Serum IgA, IgM, and IgG Responses in COVID-19.” *Cell Mol Immunol* 17 (7): 773–75. https://doi.org/10.1038/s41423-020-0474-z.
93. Maeda, K, N Higashi-Kuwata, N Kinoshita, S Kutsuna, K Tsuchiya, S I Hattori, K Matsuda, et al. 2021. “Neutralization of SARS-CoV-2 with IgG from COVID-19-Convalescent Plasma.” *Sci Rep* 11 (1): 5563. https://doi.org/10.1038/s41598-021-84733-5.
94. Mahil, S K, K Bechman, A Raharja, C Domingo-Vila, D Baudry, M A Brown, A P Cope, et al. 2021. “The Effect of Methotrexate and Targeted Immunosuppression on Humoral and Cellular Immune Responses to the COVID-19 Vaccine BNT162b2: A Cohort Study.” *Lancet Rheumatol* 3 (9): e627–37. https://doi.org/10.1016/S2665-9913(21)00212-5.
95. Manansala, M, A Chopra, R P Baughman, R Novak, E E Lower, D A Culver, P Korsten, W P Drake, M A Judson, and N Sweiss. 2021. “COVID-19 and Sarcoidosis, Readiness for Vaccination: Challenges and Opportunities.” *Front Med (Lausanne)* 8: 672028. https://doi.org/10.3389/fmed.2021.672028.
96. Martinez, F D, A L Wright, L M Taussig, C J Holberg, M Halonen, and W J Morgan. 1995. “Asthma and Wheezing in the First Six Years of Life. The Group Health Medical Associates.” *The New England Journal of Medicine* 332 (3): 133–38. https://doi.org/10.1056/NEJM199501193320301.
97. MATUMOTO, M. 1949. “A Note on Some Points of Calculation Method of LD50 by Reed and Muench.” *The Japanese Journal of Experimental Medicine* 20 (2): 175–79.

98. Matusali, G, G Sberna, S Meschi, G Gramigna, F Colavita, D Lapa, M Francalancia, et al. 2022. "Differential Dynamics of SARS-CoV-2 Binding and Functional Antibodies upon BNT162b2 Vaccine: A 6-Month Follow-Up." *Viruses* 14 (2). https://doi.org/10.3390/v14020312.
99. Mazzini, L, D Martinuzzi, I Hyseni, L Benincasa, E Molesti, E Casa, G Lapini, et al. 2021. "Comparative Analyses of SARS-CoV-2 Binding (IgG, IgM, IgA) and Neutralizing Antibodies from Human Serum Samples." *J Immunol Methods* 489: 112937. https://doi.org/10.1016/j.jim.2020.112937.
100. Mert, A, M Bilir, R Ozaras, F Tabak, T Karayel, and H Senturk. 2000. "Results of Hepatitis B Vaccination in Sarcoidosis." *Respiration* 67 (5): 543–45. https://doi.org/10.1159/000067471.
101. Mi, Huaiyu, Qing Dong, Anushya Muruganujan, Pascale Gaudet, Suzanna Lewis, and Paul D Thomas. 2010. "PANTHER Version 7: Improved Phylogenetic Trees, Orthologs and Collaboration with the Gene Ontology Consortium." *Nucleic Acids Research* 38 (Database issue): D204-10. https://doi.org/10.1093/nar/gkp1019.
102. Mikhaylova, Lyudmila, Yiming Zhang, Lester Kobzik, and Alexey V Fedulov. 2013a. "Link between Epigenomic Alterations and Genome-Wide Aberrant Transcriptional Response to Allergen in Dendritic Cells Conveying Maternal Asthma Risk." *PloS One* 8 (8): e70387. https://doi.org/10.1371/journal.pone.0070387.
103. Mikhaylova, Lyudmila, Yiming Zhang, Lester Kobzik, and Alexey V. Fedulov. 2013b. "Link between Epigenomic Alterations and Genome-Wide Aberrant Transcriptional Response to Allergen in Dendritic Cells Conveying Maternal Asthma Risk." *PLoS ONE* 8 (8). https://doi.org/10.1371/journal.pone.0070387.
104. Monath, Thomas P, Richard Nichols, W Tad Archambault, Linda Moore, Ron Marchesani, Jason Tian, Robert E Shope, et al. 2002. "Comparative Safety and Immunogenicity of Two Yellow Fever 17D Vaccines (ARILVAX and YF-VAX) in a Phase III Multicenter, Double-Blind Clinical Trial." *The American Journal of Tropical Medicine and Hygiene* 66 (5): 533–41. https://doi.org/10.4269/ajtmh.2002.66.533.
105. Musaelyan, A, S Lapin, V Nazarov, O Tkachenko, B Gilburd, A Mazing, L Mikhailova, and Y Shoenfeld. 2018. "Vimentin as Antigenic Target in Autoimmunity: A Comprehensive Review." *Autoimmun Rev* 17 (9): 926–34. https://doi.org/10.1016/j.autrev.2018.04.004.
106. Nagai, Kei. 2021. "Dysfunction of Natural Killer Cells in End-Stage Kidney Disease on Hemodialysis." *Renal Replacement Therapy* 7 (1): 8. https://doi.org/10.1186/s41100-021-00324-0.
107. Nie, Jianhui, Qianqian Li, Jiajing Wu, Chenyan Zhao, Huan Hao, Huan Liu, Li Zhang, et al. 2020. "Quantification of SARS-CoV-2 Neutralizing Antibody by a Pseudotyped Virus-Based Assay." *Nature Protocols* 15 (11): 3699–3715. https://doi.org/10.1038/s41596-020-0394-5.
108. Ortega-Francisco, Sandra, Marisol de la Fuente-Granada, Evelyn K Alvarez Salazar, Lizbeth Airais Bolaños-Castro, Gabriela Fonseca-Camarillo, Roxana Olguin-Alor, Germán R Alemán-Muench, et al. 2017. "TβRIII Is Induced by TCR Signaling and Downregulated in

FoxP3(+) Regulatory T Cells." *Biochemical and Biophysical Research Communications* 494 (1–2): 82–87. https://doi.org/10.1016/j.bbrc.2017.10.081.

109. Ouyang, W, M Löhning, Z Gao, M Assenmacher, S Ranganath, A Radbruch, and K M Murphy. 2000. "Stat6-Independent GATA-3 Autoactivation Directs IL-4-Independent Th2 Development and Commitment." *Immunity* 12 (1): 27–37. https://doi.org/10.1016/s1074-7613(00)80156-9.

110. Pace, K E, H P Hahn, M Pang, J T Nguyen, and L G Baum. 2000. "CD7 Delivers a Pro-Apoptotic Signal during Galectin-1-Induced T Cell Death." *Journal of Immunology (Baltimore, Md. : 1950)* 165 (5): 2331–34. https://doi.org/10.4049/jimmunol.165.5.2331.

111. Pahl, Madeleine V, Sastry Gollapudi, Lili Sepassi, Pavan Gollapudi, Reza Elahimehr, and Nosratola D Vaziri. 2010. "Effect of End-Stage Renal Disease on B-Lymphocyte Subpopulations, IL-7, BAFF and BAFF Receptor Expression." *Nephrology, Dialysis, Transplantation : Official Publication of the European Dialysis and Transplant Association - European Renal Association* 25 (1): 205–12. https://doi.org/10.1093/ndt/gfp397.

112. Papaspyridonos, Marianna, Irina Matei, Yujie Huang, Maria do Rosario Andre, Helene Brazier-Mitouart, Janelle C Waite, April S Chan, et al. 2015. "Id1 Suppresses Anti-Tumour Immune Responses and Promotes Tumour Progression by Impairing Myeloid Cell Maturation." *Nature Communications* 6 (April): 6840. https://doi.org/10.1038/ncomms7840.

113. Patro, Rob, Geet Duggal, Michael I Love, Rafael A Irizarry, and Carl Kingsford. 2017. "Salmon Provides Fast and Bias-Aware Quantification of Transcript Expression." *Nature Methods* 14 (4): 417–19. https://doi.org/10.1038/nmeth.4197.

114. Payne, Susan, and Complete Ebook Central Academic. 2017. *Viruses : From Understanding to Investigation*. First edit. Boston, Massachusetts: Elsevier.

115. Pegu, Amarendra, Sarah E O'Connell, Stephen D Schmidt, Sijy O'Dell, Chloe A Talana, Lilin Lai, Jim Albert, et al. 2021. "Durability of MRNA-1273 Vaccine-Induced Antibodies against SARS-CoV-2 Variants." *Science (New York, N.Y.)* 373 (6561): 1372–77. https://doi.org/10.1126/science.abj4176.

116. Perkins, Darren J, Mira C Patel, Jorge C G Blanco, and Stefanie N Vogel. 2016. "Epigenetic Mechanisms Governing Innate Inflammatory Responses." *Journal of Interferon & Cytokine Research : The Official Journal of the International Society for Interferon and Cytokine Research* 36 (7): 454–61. https://doi.org/10.1089/jir.2016.0003.

117. Polack, Fernando P, Stephen J Thomas, Nicholas Kitchin, Judith Absalon, Alejandra Gurtman, Stephen Lockhart, John L Perez, et al. 2020. "Safety and Efficacy of the BNT162b2 MRNA Covid-19 Vaccine." *The New England Journal of Medicine* 383 (27): 2603–15. https://doi.org/10.1056/NEJMoa2034577.

118. Popowski, Melissa, Troy D Templeton, Bum-Kyu Lee, Catherine Rhee, He Li, Cathrine Miner, Joseph D Dekker, et al. 2014. "Bright/Arid3A Acts as a Barrier to Somatic Cell Reprogramming through Direct Regulation of Oct4, Sox2, and Nanog." *Stem Cell Reports* 2 (1): 26–35. https://doi.org/10.1016/j.stemcr.2013.12.002.

119. Pulendran, Bali, Shuzhao Li, and Helder I. Nakaya. 2010. “Systems Vaccinology.” *Immunity* 33 (4): 516–29. https://doi.org/10.1016/j.immuni.2010.10.006.
120. Qiu, Weiliang, Feng Guo, Kimberly Glass, Guo Cheng Yuan, John Quackenbush, Xiaobo Zhou, and Kelan G. Tantisira. 2018. “Differential Connectivity of Gene Regulatory Networks Distinguishes Corticosteroid Response in Asthma.” *Journal of Allergy and Clinical Immunology* 141 (4): 1250–58. https://doi.org/10.1016/j.jaci.2017.05.052.
121. Quackenbush, John. 2006. “Microarray Analysis and Tumor Classification.” *The New England Journal of Medicine* 354 (23): 2463–72. https://doi.org/10.1056/NEJMra042342.
122. Querec, Troy D, Rama S Akondy, Eva K Lee, Weiping Cao, Helder I Nakaya, Dirk Teuwen, Ali Pirani, et al. 2009. “Systems Biology Approach Predicts Immunogenicity of the Yellow Fever Vaccine in Humans.” *Nature Immunology* 10 (1): 116–25. https://doi.org/10.1038/ni.1688.
123. Rahman, Anisur, Abhinav Tiwari, Jatin Narula, and Timothy Hickling. 2018. “Importance of Feedback and Feedforward Loops to Adaptive Immune Response Modeling.” *CPT: Pharmacometrics & Systems Pharmacology* 7 (10): 621–28. https://doi.org/10.1002/psp4.12352.
124. Rappl, G, H Abken, J M Muche, W Sterry, W Tilgen, S André, H Kaltner, S Ugurel, H-J Gabius, and U Reinhold. 2002. “CD4+CD7- Leukemic T Cells from Patients with Sézary Syndrome Are Protected from Galectin-1-Triggered T Cell Death.” *Leukemia* 16 (5): 840–45. https://doi.org/10.1038/sj.leu.2402438.
125. Reese, Sarah E., Cheng-Jian Xu, Herman T. den Dekker, Mi Kyeong Lee, Sinjini Sikdar, Carlos Ruiz-Arenas, Simon K. Merid, et al. 2018. “Epigenome-Wide Meta-Analysis of DNA Methylation and Childhood Asthma.” *Journal of Allergy and Clinical Immunology* 6749 (18). https://doi.org/10.1016/j.jaci.2018.11.043.
126. Ren, Tingting, Jingyuan Xiong, Guangliang Liu, Shaoyong Wang, Zhongqi Tan, Bin Fu, Ruilin Zhang, Xuesong Liao, Qirong Wang, and Zonglin Guo. 2019. “Imbalance of Th22/Treg Cells Causes Microinflammation in Uremic Patients Undergoing Hemodialysis.” *Bioscience Reports* 39 (10). https://doi.org/10.1042/BSR20191585.
127. Ruddy, J A, C M Connolly, B J Boyarsky, W A Werbel, L Christopher-Stine, J Garonzik-Wang, D L Segev, and J J Paik. 2021. “High Antibody Response to Two-Dose SARS-CoV-2 Messenger RNA Vaccination in Patients with Rheumatic and Musculoskeletal Diseases.” *Ann Rheum Dis* 80 (10): 1351–52. https://doi.org/10.1136/annrheumdis-2021-220656.
128. Salvagno, G L, B M Henry, G di Piazza, L Pighi, S de Nitto, D Bragantini, G L Gianfilippi, and G Lippi. 2021. “Anti-Spike S1 IgA, Anti-Spike Trimeric IgG, and Anti-Spike RBD IgG Response after BNT162b2 COVID-19 MRNA Vaccination in Healthcare Workers.” *J Med Biochem* 40 (4): 327–34. https://doi.org/10.5937/jomb0-32373.
129. Sandelin, Albin, Wynand Alkema, Pär Engström, Wyeth W Wasserman, and Boris Lenhard. 2004. “JASPAR: An Open-Access Database for Eukaryotic Transcription Factor Binding Profiles.” *Nucleic Acids Research* 32 (Database issue): D91-4. https://doi.org/10.1093/nar/gkh012.

130. Satomura, Atsushi, Morita Endo, Hiroyuki Ohi, Sukemasa Sudo, Isao Ohsawa, Takayuki Fujita, Misao Matsushita, and Teizo Fujita. 2002. “Significant Elevations in Serum Mannose-Binding Lectin Levels in Patients with Chronic Renal Failure.” *Nephron* 92 (3): 702–4. https://doi.org/10.1159/000064089.
131. Saussine, A, A Tazi, S Feuillet, M Rybojad, C Juillard, A Bergeron, V Dessirier, et al. 2012. “Active Chronic Sarcoidosis Is Characterized by Increased Transitional Blood B Cells, Increased IL-10-Producing Regulatory B Cells and High BAFF Levels.” *PLoS One* 7 (8): e43588. https://doi.org/10.1371/journal.pone.0043588.
132. Scherer, Andreas, Oliver P Günther, Robert F Balshaw, Zsuzsanna Hollander, Janet Wilson-McManus, Raymond Ng, W Robert McMaster, Bruce M McManus, and Paul A Keown. 2013. “Alteration of Human Blood Cell Transcriptome in Uremia.” *BMC Medical Genomics* 6 (June): 23. https://doi.org/10.1186/1755-8794-6-23.
133. Schliehe, Christopher, Elizabeth K Flynn, Bojan Vilagos, Udochuku Richson, Savitha Swaminanthan, Berislav Bosnjak, Lisa Bauer, et al. 2015. “The Methyltransferase Setdb2 Mediates Virus-Induced Susceptibility to Bacterial Superinfection.” *Nature Immunology* 16 (1): 67–74. https://doi.org/10.1038/ni.3046.
134. Seyhan, E C, G Gunluoglu, S Altin, E Cetinkaya, S Sokucu, H Uzun, and M Duger. 2012. “Results of Tetanus Vaccination in Sarcoidosis.” *Sarcoidosis Vasc Diffuse Lung Dis* 29 (1): 3–10.
135. Sim, Malcolm J W, Sumati Rajagopalan, Daniel M Altmann, Rosemary J Boyton, Peter D Sun, and Eric O Long. 2019. “Human NK Cell Receptor KIR2DS4 Detects a Conserved Bacterial Epitope Presented by HLA-C.” *Proceedings of the National Academy of Sciences of the United States of America* 116 (26): 12964–73. https://doi.org/10.1073/pnas.1903781116.
136. Smale, Stephen T, and Amanda G Fisher. 2002. “Chromatin Structure and Gene Regulation in the Immune System.” *Annual Review of Immunology* 20: 427–62. https://doi.org/10.1146/annurev.immunol.20.100301.064739.
137. Sonawane, Abhijeet Rajendra, John Platig, Maud Fagny, Cho-Yi Chen, Joseph Nathaniel Paulson, Camila Miranda Lopes-Ramos, Dawn Lisa DeMeo, John Quackenbush, Kimberly Glass, and Marieke Lydia Kuijjer. 2017. “Understanding Tissue-Specific Gene Regulation.” *Cell Reports* 21 (4): 1077–88. https://doi.org/10.1016/j.celrep.2017.10.001.
138. Stenvinkel, Peter, Markus Ketteler, Richard J Johnson, Bengt Lindholm, Roberto Pecoits-Filho, Miguel Riella, Olof Heimbürger, Tommy Cederholm, and Matthias Girndt. 2005. “IL-10, IL-6, and TNF-Alpha: Central Factors in the Altered Cytokine Network of Uremia--the Good, the Bad, and the Ugly.” *Kidney International* 67 (4): 1216–33. https://doi.org/10.1111/j.1523-1755.2005.00200.x.
139. Sterlin, D, A Mathian, M Miyara, A Mohr, F Anna, L Claer, P Quentric, et al. 2021. “IgA Dominates the Early Neutralizing Antibody Response to SARS-CoV-2.” *Sci Transl Med* 13 (577). https://doi.org/10.1126/scitranslmed.abd2223.
140. Stillwell, R, and B E Bierer. 2001. “T Cell Signal Transduction and the Role of CD7 in Costimulation.” *Immunologic Research* 24 (1): 31–52. https://doi.org/10.1385/ir:24:1:31.

141. Su, Ruey-Chyi, Allan B Becker, Anita L Kozyrskyj, and Kent T Hayglass. 2008. “Epigenetic Regulation of Established Human Type 1 versus Type 2 Cytokine Responses.” *The Journal of Allergy and Clinical Immunology* 121 (1): 57-63.e3. https://doi.org/10.1016/j.jaci.2007.09.004.
142. Su, Ruey-Chyi. 2009. “Altered Epigenetic Regulation and Increasing Severity of Bronchial Hyperresponsiveness in Atopic Asthmatic Children.” *The Journal of Allergy and Clinical Immunology*. United States. https://doi.org/10.1016/j.jaci.2009.08.033.
143. Subesinghe, S, K Bechman, A I Rutherford, D Goldblatt, and J B Galloway. 2018. “A Systematic Review and Metaanalysis of Antirheumatic Drugs and Vaccine Immunogenicity in Rheumatoid Arthritis.” *J Rheumatol* 45 (6): 733–44. https://doi.org/10.3899/jrheum.170710.
144. Subramanian, Aravind, Pablo Tamayo, Vamsi K Mootha, Sayan Mukherjee, Benjamin L Ebert, Michael A Gillette, Amanda Paulovich, et al. 2005. “Gene Set Enrichment Analysis: A Knowledge-Based Approach for Interpreting Genome-Wide Expression Profiles.” *Proceedings of the National Academy of Sciences of the United States of America* 102 (43): 15545–50. https://doi.org/10.1073/pnas.0506580102.
145. Sweiss, N J, R Salloum, S Gandhi, M L Alegre, R Sawaqed, M Badaracco, K Pursell, et al. 2010. “Significant CD4, CD8, and CD19 Lymphopenia in Peripheral Blood of Sarcoidosis Patients Correlates with Severe Disease Manifestations.” *PLoS One* 5 (2): e9088. https://doi.org/10.1371/journal.pone.0009088.
146. Swigris, Jeffrey J, Amy L Olson, Tristan J Huie, Evans R Fernandez-Perez, Joshua Solomon, David Sprunger, and Kevin K Brown. 2011. “Sarcoidosis-Related Mortality in the United States from 1988 to 2007.” *American Journal of Respiratory and Critical Care Medicine* 183 (11): 1524–30. https://doi.org/10.1164/rccm.201010-1679OC.
147. Syed, H, C Ascoli, C F Linssen, C Vagts, T Iden, A Syed, J Kron, et al. 2020. “Infection Prevention in Sarcoidosis: Proposal for Vaccination and Prophylactic Therapy.” *Sarcoidosis Vasc Diffuse Lung Dis* 37 (2): 87–98. https://doi.org/10.36141/svdld.v37i2.9599.
148. Tavana, S, H Argani, S Gholamin, S M Razavi, M Keshtkar-Jahromi, A S Talebian, K G Moghaddam, Z Sepehri, T M Azad, and M Keshtkar-Jahromi. 2012. “Influenza Vaccination in Patients with Pulmonary Sarcoidosis: Efficacy and Safety.” *Influenza Other Respir Viruses* 6 (2): 136–41. https://doi.org/10.1111/j.1750-2659.2011.00290.x.
149. Teijaro, John R, and Donna L Farber. 2021. “COVID-19 Vaccines: Modes of Immune Activation and Future Challenges.” *Nature Reviews. Immunology* 21 (4): 195–97. https://doi.org/10.1038/s41577-021-00526-x.
150. Thomas, Paul D, Michael J Campbell, Anish Kejariwal, Huaiyu Mi, Brian Karlak, Robin Daverman, Karen Diemer, Anushya Muruganujan, and Apurva Narechania. 2003. “PANTHER: A Library of Protein Families and Subfamilies Indexed by Function.” *Genome Research* 13 (9): 2129–41. https://doi.org/10.1101/gr.772403.
151. Trevejo, J M, M W Marino, N Philpott, R Josien, E C Richards, K B Elkon, and E Falck-Pedersen. 2001. “TNF-Alpha -Dependent Maturation of Local Dendritic Cells Is Critical for Activating the Adaptive Immune Response to Virus Infection.” *Proceedings of the*

National Academy of Sciences of the United States of America 98 (21): 12162–67. https://doi.org/10.1073/pnas.211423598.

152. Turturice, Benjamin A., Ravi Ranjan, Brian Nguyen, Lauren M. Hughes, Kalista E. Andropolis, Diane R. Gold, Augusto A. Litonjua, Emily Oken, David L. Perkins, and Patricia W. Finn. 2017. "Perinatal Bacterial Exposure Contributes to IL-13 Aeroallergen Response." *American Journal of Respiratory Cell and Molecular Biology* 57 (4): 419–27. https://doi.org/10.1165/rcmb.2017-0027OC.
153. Ungprasert, P, C S Crowson, and E L Matteson. 2017. "Sarcoidosis Increases Risk of Hospitalized Infection. A Population-Based Study, 1976-2013." *Ann Am Thorac Soc* 14 (5): 676–81. https://doi.org/10.1513/AnnalsATS.201610-750OC.
154. Vagts, C, C Ascoli, D R Fraidenburg, R P Baughman, Y Huang, R Edafetanure-Ibeh, S Ahmed, et al. 2021. "Unsupervised Clustering Reveals Sarcoidosis Phenotypes Marked by a Reduction in Lymphocytes Relate to Increased Inflammatory Activity on 18FDG-PET/CT." *Front Med (Lausanne)* 8: 595077. https://doi.org/10.3389/fmed.2021.595077.
155. Valinluck, Victoria, Hsin-Hao Tsai, Daniel K Rogstad, Artur Burdzy, Adrian Bird, and Lawrence C Sowers. 2004. "Oxidative Damage to Methyl-CpG Sequences Inhibits the Binding of the Methyl-CpG Binding Domain (MBD) of Methyl-CpG Binding Protein 2 (MeCP2)." *Nucleic Acids Research* 32 (14): 4100–4108. https://doi.org/10.1093/nar/gkh739.
156. Vargas, Ashley J, John Quackenbush, and Kimberly Glass. 2016. "Diet-Induced Weight Loss Leads to a Switch in Gene Regulatory Network Control in the Rectal Mucosa." *Genomics* 108 (3–4): 126–33. https://doi.org/10.1016/j.ygeno.2016.08.001.
157. Vercelli, Donata. 2016. "Does Epigenetics Play a Role in Human Asthma?" *Allergology International : Official Journal of the Japanese Society of Allergology* 65 (2): 123–26. https://doi.org/10.1016/j.alit.2015.12.001.
158. Verkade, Martijn Anton, Corné Johan van Druningen, Leonard Maria Bernardus Vaessen, Dennis Adriaan Hesselink, Willem Weimar, and Michiel Gerardus Henricus Betjes. 2007. "Functional Impairment of Monocyte-Derived Dendritic Cells in Patients with Severe Chronic Kidney Disease." *Nephrology, Dialysis, Transplantation : Official Publication of the European Dialysis and Transplant Association - European Renal Association* 22 (1): 128–38. https://doi.org/10.1093/ndt/gfl519.
159. Volkova, L D. 1974. "[Clinical Value of the Determination of Isoenzymes of Malate and Lactate Dehydrogenase in the Urine in Chronic Kidney Diseases in Children]." *Pediatriia* 0 (10): 71–73.
160. Walls, A C, Y J Park, M A Tortorici, A Wall, A T McGuire, and D Veesler. 2020. "Structure, Function, and Antigenicity of the SARS-CoV-2 Spike Glycoprotein." *Cell* 181 (2): 281-292 e6. https://doi.org/10.1016/j.cell.2020.02.058.
161. Wang, Liqing, Yujie Liu, Rongxiang Han, Ulf H Beier, Rajan M Thomas, Andrew D Wells, and Wayne W Hancock. 2013. "Mbd2 Promotes Foxp3 Demethylation and T-Regulatory-Cell Function." *Molecular and Cellular Biology* 33 (20): 4106–15. https://doi.org/10.1128/MCB.00144-13.

162. Weighill, Deborah, Marouen Ben Guebila, Kimberly Glass, John Platig, Jen Jen Yeh, and John Quackenbush. 2021. “Gene Targeting in Disease Networks.” *Frontiers in Genetics* 12: 649942. https://doi.org/10.3389/fgene.2021.649942.
163. Williams, John D, Nicholas Topley, Kathrine J Craig, Ruth K Mackenzie, Monika Pischetsrieder, Cristina Lage, and Jutta Passlick-Deetjen. 2004. “The Euro-Balance Trial: The Effect of a New Biocompatible Peritoneal Dialysis Fluid (Balance) on the Peritoneal Membrane.” *Kidney International* 66 (1): 408–18. https://doi.org/10.1111/j.1523-1755.2004.00747.x.
164. Winter, C C, J E Gumperz, P Parham, E O Long, and N Wagtmann. 1998. “Direct Binding and Functional Transfer of NK Cell Inhibitory Receptors Reveal Novel Patterns of HLA-C Allotype Recognition.” *Journal of Immunology (Baltimore, Md. : 1950)* 161 (2): 571–77.
165. Wu, Lizhen, Jian Cao, Wesley L Cai, Sabine M Lang, John R Horton, Daniel J Jansen, Zongzhi Z Liu, et al. 2018. “KDM5 Histone Demethylases Repress Immune Response via Suppression of STING.” *PLoS Biology* 16 (8): e2006134. https://doi.org/10.1371/journal.pbio.2006134.
166. Zaza, Gianluigi, Paola Pontrelli, Giovanni Pertosa, Simona Granata, Michele Rossini, Silvia Porreca, Frank J T Staal, Loreto Gesualdo, Giuseppe Grandaliano, and Francesco Paolo Schena. 2008. “Dialysis-Related Systemic Microinflammation Is Associated with Specific Genomic Patterns.” *Nephrology, Dialysis, Transplantation : Official Publication of the European Dialysis and Transplant Association - European Renal Association* 23 (5): 1673–81. https://doi.org/10.1093/ndt/gfm804.
167. Zeng, Wei-ping. 2013. “‘All Things Considered’: Transcriptional Regulation of T Helper Type 2 Cell Differentiation from Precursor to Effector Activation.” *Immunology* 140 (1): 31–38. https://doi.org/10.1111/imm.12121.
168. Zhou, Tong, Nancy Casanova, Nima Pouladi, Ting Wang, Yves Lussier, Kenneth S Knox, and Joe G N Garcia. 2017. “Identification of Jak-STAT Signaling Involvement in Sarcoidosis Severity via a Novel MicroRNA-Regulated Peripheral Blood Mononuclear Cell Gene Signature.” *Scientific Reports* 7 (1): 4237. https://doi.org/10.1038/s41598-017-04109-6.

Curriculum Vitae

EDUCATION

University of Illinois in Chicago, MD/PhD Program
2016 – Present
MD, expected graduation May 2024
- Passed USMLE Step 1 with a score of 240 in June 2018
- Passed USMLE Step 2 with a score of 253 in July 2023

PhD, Bioengineering (July 2022)
- Thesis: Elucidation of dysregulated immune profiles via vaccine-induced transcriptomics
- Advisors: Patricia Finn, PhD & David Perkins, MD,PhD

University of California in San Francisco
Graduated Aug 2013
M.S. in Biomedical Imaging
MCAT: 38, 14 Biology, 12 Chemistry/Physics, 12 Verbal

Duke University, Pratt School of Engineering, Durham, NC
Graduated May 2011
B.S.E. in Biomedical Engineering
National Merit Scholar

Peggy Payne Academy, gifted magnet program of Tempe Union High School District
Graduated May 2007
McClintock High School, Tempe, AZ
Valedictorian

HONORS & AWARDS

Alpha Omega Alpha Member, awarded in Aug 2023

NIH F30 Individual Predoctoral MD/PhD Fellow, granted by the National Institute of Child Health and Human Development (Aug 2019-Present)
- Awarded grant for research characterizing gene expression and gene regulatory networks in early allergic disease

1st place, American Society of Functional Neuroradiology conference poster competition (March 2016)
- Awarded for 1st author poster "White Matter Microstructure is Associated with Auditory and Tactile Processing in Children with and without Sensory Processing Disorder"

WORK & RESEARCH EXPERIENCE

Chicago Department of Public Health (CDPH), *Data analyst*
Mar 2020 – Aug 2020

- Worked with Dr. Stockton Meyer, an infectious disease physician at UIC, and Dr. Isaac Ghinai, an Epidemic Intelligence Service officer at the CDPH to report incidences of Covid-19 at homeless shelters in Chicago. I built a model characterizing Covid-19 transmission within the largest homeless shelter in the midwest, informing the CDPH testing protocol at homeless shelters across Chicago. This also led to a first-author publication in the CDC journal Emerging Infectious Diseases.

Finn-Perkins Laboratory at UIC, *PhD candidate*
Aug 2018 – Jul 2022

- Led a team of clinicians, graduate students, and undergraduate students to enroll subjects, and collect and process biologic samples in a study of the Covid-19 vaccination in end stage renal disease patients, sarcoidosis patients, and controls. Used R programming language to characterize gene expression response to Covid-19 vaccination in immunocompromised patient populations compared to controls, characterized underlying immune dysregulation in these cohorts
- Characterized gene expression networks and gene regulatory networks in early allergic disease using R programming language
- Developed benchwork laboratory skills including isolation of peripheral blood mononuclear cells, RNA isolation and library preparation for sequencing, and DNA isolation and library preparation for sequencing

Neural Connectivity Laboratory at UCSF, *Research associate*
Oct 2012 - May 2016

- Characterized brain connectivity in neurodevelopmental disorders and in the healthy developing human brain using diffusion MRI and resting state fMRI in the laboratory of Dr. Pratik Mukherjee, leading to multiple publications
- Developed computational skills including FSL, Matlab, and shell scripting for data processing and analysis
- Scripted, filmed, and produced a crowdfunding campaign video for Sensory Processing Disorders research at UCSF

Neural Systems Laboratory at University of Maryland, *Research assistant*
Jul 2011 - Aug 2012

- Conducted research on the neurological basis of auditory perception and memory in the laboratory of Dr. Jonathan Fritz and Dr. Shihab Shamma
- Completed two graduate-level courses in Computational Neuroscience (with a grade of A) and Quantitative Analysis of Biology (with a grade of A+)
- Designed lab website

Barrow Neurological Institute at St. Joseph's Hospital, *Intern* Summers of 2004, 2005, 2006, 2008, 2009

- Conducted research on the structure and expression of nicotinic acetylcholine receptors in Dr. Ronald Lukas's Neurochemistry lab of Alzheimer's Disease

Duke Cognitive Neuroscience Department, *Research Assistant*
Spring 2009- Spring 2010
- Conducted research on a quantitative explanation of the emotional effect of music in Dr. Dale Purves's research laboratory

TEACHING EXPERIENCE

UIC MD/PhD Program Transition Course, *Primary instructor*
Apr 2023
- Developed a week-long transition course and served as one of two primary instructors for PhD students transitioning to their M3 year

UIC Internal Medicine Residency R Bootcamp, *Primary instructor*
Jun-Jul 2020, Sep 2021
- Developed an R programming language multi-week bootcamp curriculum and served as primary instructor for new UIC Innovations and Technology in Medicine (ITIM) track residents.
- Presented on behalf of the ITIM track at Medicine grand rounds April 13, 2021

UCSF Master's in Biomedical Imaging Matlab Bootcamp, *Primary instructor*
Sep 2015-Nov 2015
- Developed a Matlab bootcamp curriculum and served as primary instructor for incoming UCSF Master's students in the Biomedical Imaging program; 26 total hours of instruction

LEADERSHIP & VOLUNTEERING EXPERIENCE

Mobile migrant healthcare team (MMHT), *Run lead, Crowdfunding campaign videographer/produced, Chair of informatics*

May 2023 – Present
- Coordinating teams of physicians, nurses, and medical students to provide healthcare assessments to migrants arriving in Chicago who are living temporarily at police precincts and Chicago O'Hare airport
- Working with Spanish-speaking M1's and M2's to gather HPIs and perform physical exams before presenting to an attending physician, biking to pharmacies to pick up additional medications/supplies during assessment runs
- Filmed and produced a crowdfunding video, raising > $20,000 in funds to provide medications/supplies to migrants
- Chaired the informatics group, overseeing the implementation of a Redcap database for hundred of patient encounters for data analytic purposes, and to track follow-up clinical information, and generate automatic medication/supply inventory lists for our supply team.

Covid-19 Rapid Response Team, *Member*
Jul 2020 – Dec 2020
- Worked with the Rapid Response Team, a collaboration between UIC and Rush physicians, nurses, and students, and the Chicago department of public health (CDPH) to perform Covid-19 testing at homeless shelters and nursing homes during the Covid-19 pandemic

Community Outreach & Intervention Program, *Volunteer*
Oct 2017 – Jun 2018
- Volunteered with a program that provides harm reduction services, helping with pop-up health clinics, and providing harm-reduction education.

UIC College of Medicine Artists, *President* Aug 2017 – May 2018
- Led a medical school student organization dedicated to fostering artistic skills and interests in students. Organized a college-wide talent show and oversaw production of a magazine containing art and poems created by UIC college of medicine students.

PUBLICATIONS

Peer-reviewed journals

Chang YS, Huang K, Lee JM, Vagts CL, Ascoli C, Amin MR, et al. Immune response to the mRNA COVID-19 vaccine in hemodialysis patients: cohort study. medRxiv [Preprint]. 2023 Jan 19:2023.01.19.23284792. doi: 10.1101/2023.01.19.23284792. PMID: 36711520; PMCID: PMC9882629.

Chang YS, Mayer S, Davis ES, Figueroa E, Leo P, Finn PW, Perkins DL. Transmission Dynamics of Large Coronavirus Disease Outbreak in Homeless Shelter, Chicago, Illinois, USA, 2020. Emerg Infect Dis. 2022 Jan;28(1):76-84. doi: 10.3201/eid2801.210780. Epub 2021 Dec 2. PMID: 34856112; PMCID: PMC8714208.

Chang YS, Turturice BA, Schott C, Finn PW, Perkins DL, et al. (2020) Immune network dysregulation precedes diagnosis of asthma. Scientific Reports. *Under Revision.*

Chang YS, Owen JP, Thieu T, Pojman NJ, Bukshpun P, Wakahiro MLJ, et al. (2016) Reciprocal alterations of white matter microstructure in carriers of deletions versus duplications at the 16p11.2 chromosomal locus. Human Brain Mapping. doi: 10.1002/hbm.23211.

Chang YS, Gratiot M, Owen JP, Aitken A, Desai SS, Arnett AB, et al. (2016) White matter microstructure is associate with auditory and tactile processing in children with and without sensory processing disorder. Frontiers in Neuroanatomy. http://dx.doi.org/10.3389/fnana.2015.00169

Chang YS, Owen JP, Pojman NJ, Thieu T, Bukshpun P, Wakahiro MLJ, et al. (2015) White Matter Changes of Neurite Density and Fiber Orientation Dispersion during Human Brain Maturation. PLoS ONE 10(6): e0123656. doi:10.1371/journal.pone.0123656

Chang Y-S, Owen JP, Desai SS, Hill SS, Arnett AB, Harris J, et al. (2014) Autism and Sensory Processing Disorders: Shared White Matter Disruption in Sensory Pathways but Divergent Connectivity in Social-Emotional Pathways. PLoS ONE 9(7): e103038.

Vagts CL, **Chang YS**, Ascoli C, Lee JM, Huang K, Huang Y, et al. Trimer IgG and neutralising antibody response to COVID-19 mRNA vaccination in individuals with sarcoidosis. ERJ Open Res. 2023 Jan 3;9(1):00025-2022. doi: 10.1183/23120541.00025-2022. PMID: 36601311; PMCID: PMC9501840.

Nickles MA, Huang K, **Chang YS**, Tsoukas MM, Sweiss NJ, Perkins DL, Finn PW. Gene Co-expression Networks Identifies Common Hub Genes Between Cutaneous Sarcoidosis and Discoid Lupus Erythematosus. Front Med (Lausanne). 2020 Nov 25;7:606461. doi: 10.3389/fmed.2020.606461. PMID: 33324666; PMCID: PMC7724034.

Ghinai I, Davis ES, Mayer S, Toews KA, Huggett TD, Snow-Hill N, Perez O, Hayden MK, Tehrani S, Landi AJ, Crane S, Bell E, Hermes JM, Desai K, Godbee M, Jhaveri N, Borah B, Cable T, Sami S, Nozicka L, **Chang YS**, et al. Risk Factors for Severe Acute Respiratory Syndrome Coronavirus 2 Infection in Homeless Shelters in Chicago, Illinois-March-May, 2020. Open Forum Infect Dis. 2020 Oct 12;7(11):ofaa477. doi: 10.1093/ofid/ofaa477. PMID: 33263069; PMCID: PMC7665740.

Brandes-Aitken A, Anguera JA, **Chang Y-S**, Demopoulos C, Owen JP, et al. (2019) White Matter Microstructure Associations of Cognitive and Visuomotor Control in Children: A Sensory Processing Perspective. Front. Integr. Neurosci. 12:65.

Langenecker SA, Jenkins LM, Stange JP, **Chang YS**, DelDonno SR et al (2018) Cognitive control neuroimaging measures differentiate between those with and without future recurrence of depression. Neuroimage Clinical 20:1001-1009.

Jenkins LM, Stange JP, Bessette KL, **Chang YS**, Corwin SD et al (2018) Differential engagement of cognitive control regions and subgenual cingulate based upon presence or absence of comorbid anxiety with depression.

Shang Y, Hinkley LB, Cai C, Subramaniam K, **Chang YS** et al. (2018) Functional and Structural Brain Plasticity in Adult Onset Single-Sided Deafness. Front. Hum. Neurosci. 12:474.

Palacios EM, Yuh EL, **Chang YS**, Yue JK, Schnyer DM, et al. (2017) Resting-State Functional Connectivity Alterations Associated with Six-Month Outcomes in Mild Traumatic Brain Injur. J Neurotrauma 34(8):1546-1557.

Palacios EM, Martin AJ, Boss MA, Ezekiel F, **Chang YS**, et al (2016) Toward Precision and Reproducibility of Diffusion Tensor Imaging: A Multicenter Diffusion Phantom and Traveling Volunteer Study. AJNR Am J Neuroradiol 38(3):537-545.

Owen JP, **Chang YS**, Mukherjee P (2015) Edge density imaging: Mapping the anatomic embedding of the structural connectome within the white matter of the human brain. Neuroimage 109:402-417.

Owen JP, **Chang YS**, Pojman NJ, Bukshpun P, Wakahiro ML, et al. (2014) Aberrant white matter microstructure in children with 16p11.2 deletions, J Neurosci 34:6214-6223.

Posters and oral presentations

Chang YS, Turturice BA, Schott C, Finn PW, Perkins DL, et al. (2019) Gene network dysregulation characterizes and predicts susceptibility to atopic phenotypes. **Poster session** at UIC College of Medicine Scholarly Activities Day 2019 March 5; Chicago, IL.

Chang YS, Owen JP, Thieu T, Pojman NJ, Bukshpun P, Wakahiro MLJ, et al. (2015) Reciprocal alterations of white matter microstructure in carriers of deletions versus duplications at the 16p11.2 chromosomal locus. **Oral presentation** at: Human Brain Mapping 2015 June 14-18; Honolulu, HI.

Chang YS, Owen JP, Pojman NJ, Bukshpun P, Wakahiro ML, et al. (2015) Age-related Changes of Neurite Density and Fiber Orientation Dispersion in White Matter during Childhood Brain Maturation. **Poster session** presented at: Human Brain Mapping 2015 June 14-18; Honolulu, HI.

Chang YS, Owen JP, Thieu T, Pojman NJ, Bukshpun P, Wakahiro MLJ, et al. (2015) Reciprocal alterations of white matter microstructure in carriers of deletions versus duplications at the 16p11.2 chromosomal locus. **Poster session** presented at: International Society for Magnetic Resonance in Medicine 2015 May 30 - June 5; Toronto, ON.

Chang YS, Owen JP, Pojman NJ, Bukshpun P, Wakahiro ML, et al. (2015) White matter changes of neurite density and fiber orientation dispersion during human brain maturation. **E-poster session** presented at: International Society for Magnetic Resonance in Medicine 2015 May 30 - June 5; Toronto, ON.

Chang YS, Owen JP, Thieu T, Pojman NJ, Bukshpun P, Wakahiro MLJ, et al. (2015) Reciprocal alterations of white matter microstructure in carriers of deletions versus duplications at the 16p11.2 chromosomal locus. **Oral presentation** at: American Society of Neuroradiology 2015 Apr 25-30; Chicago, IL.

Chang YS, Owen JP, Pojman NJ, Bukshpun P, Wakahiro ML, et al. (2015) Age-related Changes of Neurite Density and Fiber Orientation Dispersion in White Matter during Childhood Brain Maturation. **Oral presentation** at: American Society of Neuroradiology 2015 Apr 25-30; Chicago, IL.

Chang YS, Owen JP, Desai SS, Hill SS, Arnett AB, Harris J, et al. (2014) Differing patterns of white matter connectivity in Autism Spectrum Disorders versus Sensory Processing Disorders. **Oral presentation** at: American Society of Neuroradiology 2014 May 17-22; Montreal, Quebec, Canada.

Cooper S, **Chang YS**, Aguilar JS, Santos RM, Romhany C, Bednarz C, et al. (2023) Mobile Migrant Health Team: Initiative and Care Model. **Poster presentation** at: The Latino Medical Student Association National Conference 2023 Sep 15-16; Atlanta, GA.

Appendix

Copyright permissions from Scientific Reports, ERJ, and MedRXiv:

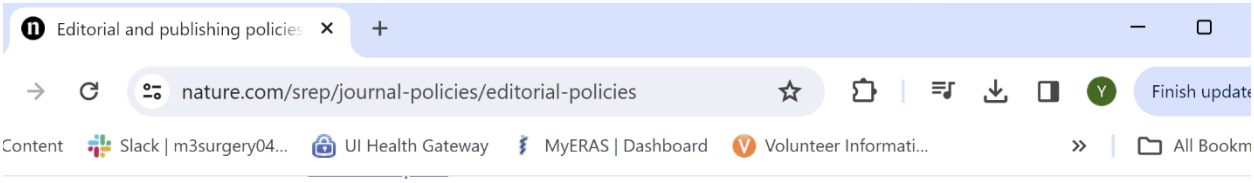

License agreement and author copyright

Scientific Reports does not require authors to assign copyright of their published original research papers to the journal. Articles are published under a CC BY license (Creative Commons Attribution 4.0 International License). The CC BY license allows for maximum dissemination and re-use of open access materials and is preferred by many research funding bodies. Under this license, users are free to share (copy, distribute and transmit) and remix (adapt) the contribution including for commercial purposes, providing they attribute the contribution in the manner specified by the author or licensor (read full legal code).

Visit our open research site for more information about Creative Commons licensing.

ERJ Open Research is built on the following principles.

- Rigorous peer review: manuscripts will be evaluated by an experienced and well-regarded editorial board and reviewers.
- High production values: the ERS in-house technical and production staff will copyedit manuscripts, redraw figures and work with authors to ensure the published paper reflects the hard work that went into their research.
- Open access: all *ERJ Open Research* papers are free to read, share and reuse under the CC-BY or CC-BY-NC licences, provided the source is cited. Publication fees are kept low, with discounts for ERS members and researchers from lower-income countries.
- ERS backing: the European Respiratory Society brings together the leading thinkers in respiratory science and medicine to organise the world's largest respiratory congress, publish a range of journals and books, organise respiratory education and lobby for better respiratory health. *ERJ Open Research* has the strongest possible support.

Immune response to the mRNA COVID-19 vaccine in hemodialysis patients: cohort study

Yi-Shin Chang,[1,2,*] Kai Huang,[1,2,*] Jessica M Lee,[1,3] Christen L Vagts,[1] Christian Ascoli,[1] Md-Ruhul Amin,[1] Mahmood Ghassemi,[1] Claudia M Lora,[1] Russell Edafetanure-Ibeh,[1] Yue Huang,[1] Ruth A Cherian,[1] Nandini Sarup,[1] Samantha R Warpecha,[1] Sunghyun Hwang,[1] Rhea Goel,[1] Benjamin A Turturice,[1,3,4] Cody Schott,[1,3,5] Montserrat Hernandez,[1] Yang Chen,[1,6] Julianne Joregensen,[1,2] Wangfei Wang,[1,2] Mladen Rasic,[1,2] Richard M Novak,[1] Patricia W Finn,[1,2,3,**] and David L Perkins[1,2,6,**]